Aus der

Medizinischen Klinik und Poliklinik I,

Klinikum der Ludwig-Maximilians-Universität München

Vorstand: Prof. Dr. Steffen Massberg

Dissertation

zum Erwerb des Doctor of Philosophy (Ph.D.)

an der Medizinischen Fakultät der

Ludwig-Maximilians-Universität zu München

Macrophage derived complement factor C3 impacts on cardiac remodeling

Lulu Liu

Jilin, China

Mit Genehmigung der Medizinischen Fakultät der
Ludwig-Maximilians-Universität zu München

First evaluator: Prof. Dr. Christian Schulz

Second evaluator: Prof. Dr. Andreas Dendorfer

Third evaluator: Prof. Dr. Christoph Reichel

Fourth evaluator: Prof. Dr. Arthur Liesz

Dean: **Prof. Dr. Thomas Gudermann**

Datum der Verteidigung:

_____26.07.2023_____

Table of content

Abstract

Myocardial infarction (MI) is a common condition with strong impact on mortality and morbidity. Coronary occlusion induces myocardial necrosis triggering inflammatory responses of various cell types, leading to myocardial healing or scar formation. The majority of immune cells in the heart are myeloid cells, which play a role in the pathophysiology of MI. They are attracted by inflammatory mediators such as cytokines and chemokines, and recruited to ischemic myocardium. The notion that the complement system mediates immunological defense and is stimulated by MI is supported by prior research. Robust upregulation of the complement system contributes to the postinfarct inflammation process both directly, e.g. by chemoattracting immune cells, and indirectly, such as by inserting the membrane attack complex (MAC) into damaged cells within ischemic myocardium. Complement component 3 (C3) is a key factor in the complement cascade and massive C3 deposition is found in the ischemic region after MI. Blockage or genetic deficiency of C3 has been shown to reduce ischemic injury. However, the underlying mechanisms have been unclear. We utilized C3-tdTomato knock-in reporter mice to monitor C3 expression in immune cells in health and in response to MI, and characterized its role in postinfarct cardiac inflammation and remodeling. Using flow cytometry we identified profound expression of C3 by circulating myeloid cells already in steady state conditions. While presence of C3 was low in healthy mouse hearts, cardiac resident macrophages upregulated C3 within 48h after myocardial ischemia/reperfusion (I/R) injury. Transplantation of donor bone marrow (BM) cells to lethally irradiated mice demonstrated that BM-independent tissue macrophages, which originated from embryonic hematopoiesis, produce this complement factor whereas only minimal amounts of C3 are taken up from blood circulation. In line with this, circulating myeloid cells of bone marrow donors generate C3 in high abundance in recipient mice lacking serum-derived C3. While macrophage C3 had no significant impact on cardiac remodeling after short-term ischemia, tissue resident macrophage derived C3 impacted on infarct size and cardiac remodeling in mice undergoing chronic infarction. Taken together, we provide a comprehensive characterization of C3 expression in immune cells and decipher the upregulation of C3 in cardiac macrophages upon inflammation, shedding light on the importance of intracellularly

generated C3 and paving the way for future investigations of post-ischemic inflammation.

List of figures

List of abbreviations

AGM	Aorto-gonado-mesonephros
BM	Bone marrow
BMT	Bone marrow transplantation
CD	Cluster of differentiation
CT	Computed tomography
CVF	Cobra venom factor
C3aRA	C3a receptor antagonist
DAMP	Damage-associated molecular pattern
ECM	Extracellular matrix
EDV	End-diastolic volume
EF	Ejection fraction
EMP	Erythro-myeloid progenitor
ER	Endoplasmic rediculum
ESV	End-systolic volume
FDG	Fluorodeoxyglucose
FMO	Fluorescence minus one
GFP	Green fluorescent protein
HSC	Hematopoietic stem cell
IFN	Interferon
IM	Inflammatory monocyte
LAD	Left anterior descending artery
LAD-1	Leukocyte adhesion deficiency type 1
LPS	Lipopolysaccharides
LVMV	Left ventricular metabolic volume
MAC	Membrane attack complex
MBL	Mannose-binding lectin

M-CSF	Macrophage colony-stimulating factor
MFI	Median fluorescence intensity
MHC II	Major histocompatibility complex class II
MI	Myocardial infarction
MI/R	Myocardial ischemia reperfusion
mTOR	Mammalian target of rapamycin
NIM	Non-inflammatory monocyte
PET	Positron emission tomography
ROS	Reactive oxygen species
SCF	Stem cell factor
SV	Stroke volume
TPD	Total perfusion deficit
WGA	Wheat germ agglutinin
WT	Wild type
YS	Yolk sac

1. Introduction

1.1 Myocardial infarction

Cardiovascular disease has remained to be the biggest cause of death in the world. Acute myocardial infarction (MI) thereby represents the most frequent condition underlying cardiovascular death [1-3].

Pathology defines MI as myocardial cell death caused by acute coronary artery occlusion or persistent ischemia. High demand for oxygen and nutrients in cardiomyocytes is blocked or severely reduced, leading to a series of cellular events and production of inflammatory mediators that attract immune cells and activate host defense systems such as the complement cascade. Following MI, damaged cardiac cells are removed by phagocytes and reconstructed as a granulation tissue [4, 5]. Excessive inflammation and adverse cardiac remodeling will eventually result in serious cardiac conditions that are associated with high mortality [6].

In the past decades, percutaneous coronary intervention (PCI) has been implemented to reopen the occluded vessel and reestablish coronary blood flow. This profoundly reduced mortality and morbidity of MI patients. Since a larger number of patients survives the acute event, however, long-term consequences of myocardial ischemia such as adverse remodeling and heart failure have come into focus. In the light of an ageing society, heart failure is expected to rank among the top causes of mortality and morbidity [7]. To improve this condition, an in-depth understanding of the pathological mechanisms of MI and post-infarct remodeling is required to develop novel therapeutic approaches.

1.2 Pathophysiology of post-infarct inflammation and remodeling

Ischemic injury of the heart induces cardiomyocyte death, which is followed by an inflammatory response and the formation of a fibrotic scar to replace the destroyed myocardium. Cardiac repair following MI can be divided into three overlapping

phases: early inflammatory phase, reparative and proliferate phase, and maturation phase [1, 3, 5].

The inflammatory first phase is initiated by the interruption of blood flow in a coronary artery and followed by cellular injury and death in the corresponding myocardium. This in turn leads to an acute inflammatory response to remove necrotic cell debris, which is linked to the production of reactive oxygen species (ROS), generation of damage-associated molecular patterns (DAMPs) and activation of complement system, among various inflammatory pathways. The local release of cytokines and chemokines promotes the recruitment of inflammatory cells to the injured myocardium. They contribute to the degradation and clearance of necrotic tissue and extracellular matrix (ECM) proteins, and release anti-inflammatory mediators, shifting the inflammatory phase to the reparative and proliferative phase [1].

The phagocytosis and removal of apoptotic cells, most prominently inflammatory neutrophils, by macrophages represent as a hallmark of the resolution of inflammation. This process is associated with macrophages polarizing to a M2-like "resolution-mediating" phenotype and is characterized by the release of anti-inflammatory and pro-fibrotic mediators, the latter promoting myofibroblast proliferation and collagen deposition. Altogether, with the aim of preventing myocardium from rupture and limiting partial deterioration of cardiac function, granulation tissue is formed [8].

Following the reparative and proliferative phase, the ECM is crosslinked in the infarct zone to consolidate the forming scar, and the local reparative cells are deactivated to remain in a quiescent state [9].

All these phases are orchestrated by finely regulated balance between pro-inflammatory and anti-inflammatory activity. Timely transition from one phase to next phase is essential to achieve successful heart remodeling and preserve cardiac function. Adverse heart remodeling, compromised cardiac function, and heart failure can occur as a result of excessive activation and prolonging of inflammation or suppression of a repair phase [10].

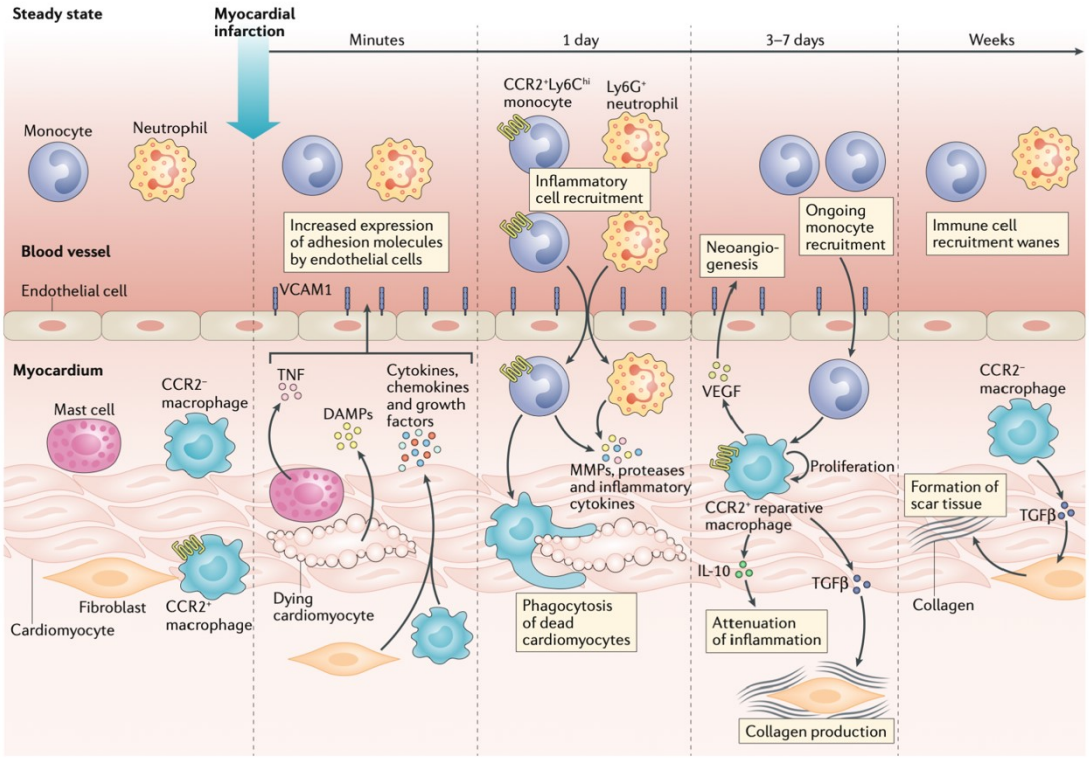

Fig. 1.2.1 Pathophysiological course during myocardial infarction. Reprinted by permission from Springer Nature [10]. Copyright © 2018.

1.3 Immune system engagement in myocardial infarction

Immune cells are present in the myocardium and engaged at all stages of post-MI inflammation, especially monocytes/macrophages and neutrophils. Neutrophils are recruited to the injured myocardium within a few hours, peaking at 24h post-MI. They mainly execute their function by scavenging cellular debris and ECM. In addition, neutrophils generate ROS that directly cause myocardial injury and stimulate the release of pro-inflammatory factors. Neutrophil also secrete cytokines and chemokines that induce further inflammation. Neutrophils are thought to be detrimental in inflammation. However, an increasing body of evidence shows that neutrophils may also play a protective role in myocardial healing, a process that occurs at later stages of post-MI remodeling [6, 11, 12]. Depletion of neutrophils with anti-Ly6G antibody results in reduced monocytes recruitment in the setting of MI and deficiency of altering macrophages to a M2 phenotype, thereby leading to

accumulation of dead cells and failed resolution, inducing more fibrosis and adverse heart remodeling [11].

Mature monocytes are classified in mice as two main subsets by their expression level of Ly6C. Classical Ly6C^{high} monocytes derive from hematopoietic stem cells (HSCs) progenitors and are recruited to the injured site post-MI in a CCR2 (C-C chemokine receptor type 2)-dependent manner, where they differentiate to inflammatory macrophages and release pro-inflammatory cytokines like TNF-α and IL-1β. Both Ly6C^{high} monocytes and inflammatory macrophages originate from Ly6C^{high} monocytes phagocytose necrotic cells and damaged matrix debris in the early inflammatory phase. Non-classical Ly6C^{low} monocytes, in contrast, differentiate from Ly6C^{high} monocytes in a NR4A1 (nuclear receptor subfamily 4 group A member 1) -dependent manner. NR4A1 is a transcription factor that is essential for Ly6C^{low} monocytes development but dispensable for Ly6C^{low} macrophages [13]. These Ly6C^{low} monocytes patrol along the vascular luminal wall and scavenge dead endothelial cells, pathogens, and oxidized lipids in steady state. Resembling murine monocytes, human monocytes also can be divided into two subpopulations: CD14+CD16- monocytes mirror mouse Ly6C^{high} monocytes and CD14^{low}CD16+ monocytes possess similar phenotypic profiles with patrolling monocytes [14, 15].

While neutrophils are thought to be the first effector cells that rapidly respond to MI, a recent study found robust recruitment of patrolling monocytes in infarcted myocardium that outpaced neutrophil recruitment [16]. However, another study found that monocyte infiltration is quickly replaced by neutrophil recruitment, implying that early infiltrated monocytes have an attracting role in drawing neutrophils to the infarct myocardium [17].

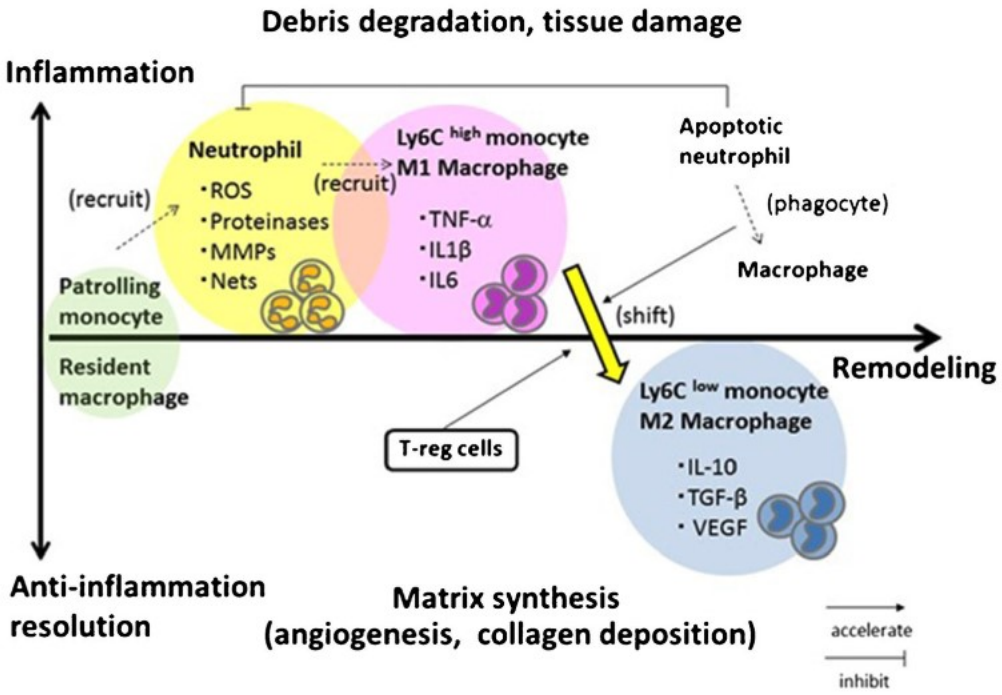

Fig. 1.3.1 Immune cells response post-MI. Reprinted by permission from Springer Nature [18]. Copyright © 2015.

Macrophages were thought to exclusively originate from bone marrow (BM) HSCs derived monocytes. However, fate-mapping studies have shown a distinct origin of tissue macrophages from yolk sac (YS) erythro-myeloid progenitors (EMPs) in the development of embryos at E8.5, prior to the establishment of HSC-derived hematopoiesis, constitute the primitive hematopoiesis. Shortly after the emergence of macrophage progenitors of YS origin, they traffic and colonize the embryo tissues through bloodstream, eventually give rise to most tissue resident macrophage populations, where they self-maintain locally independent of HSCs. Starting at E10.5 in the aorto-gonado-mesonephros (AGM) region, HSCs emerge and constitute the definitive hematopoiesis. Then they migrate and colonize bone marrow at E15, giving rise to the adult HSC pool [19-21].

Specifically, brain microglia develop exclusively from YS EMPs and replenish themselves through local proliferation in steady state. Intestinal macrophages, on the contrary, derive almost completely from constant blood monocytes replenishment in adults. However, most tissue resident macrophages are of mixed origin, such as cardiac macrophages, liver Kupfer cells, epidermal Langerhans cells, and lung alveolar macrophages. They persist into the adulthood but can be replaced by

circulating monocytes under inflammation conditions and in ageing mice [22]. Heidt and colleagues investigated monocytes contribution to macrophages in steady state by parabiosis and irradiation-based chimera. They demonstrate resident heart macrophages are only around 2.7% and 10% replaced by transferred hematopoietic stem cells in parabiosis and chimera model, respectively. Therefore, majority of tissue resident macrophages originate from YS EMPs and are mainly self-renewal by local proliferation [23].

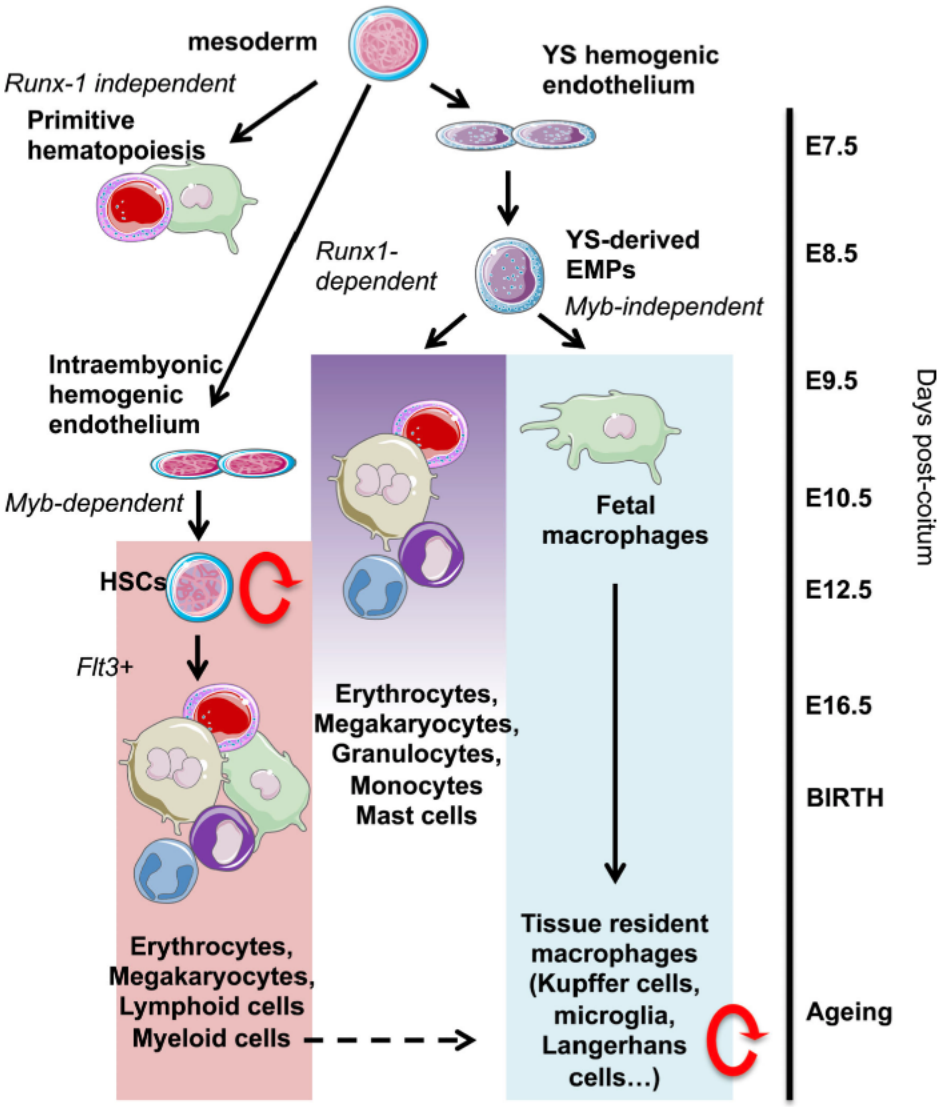

Fig. 1.3.2 Macrophage development throughout lifespan. Reprinted by permission from Springer Nature [20]. Copyright © 2016.

In adult mouse heart, macrophages are classified into 4 subsets on the basis of CCR2 and major histocompatibility complex class II (MHC II) expression, CCR2- MHC

II^{low}, CCR2- MHC II^{high}, CCR2+ MHC II^{low} and CCR2+ MHC II^{high} subsets [24, 25]. The CCR2- MHC II^{low} subsets consist of embryonic-derived macrophages, whereas some CCR2- MHC II^{high} macrophages may partially be replenished by monocytes; both CCR2- populations are regarded as long-lived cells. Whereas CCR2+ macrophages originate solely from circulating monocytes and are short-lived cells [26]. Treatment with different stimulus in macrophages in vitro propose another classification, which propose 2 subsets: classical-activated or inflammatory macrophages termed M1 when treated with LPS or IFNg; and alternative-activated or reparative macrophages termed M2 when treated with IL-4 or IL-10 [27]. CCR2- tissue resident macrophages possess proangiogenic and reparative properties, which may play a significant role in immune surveillance and support host defense in the heart, indicating they are more of M2 phenotype. In contrast, CCR2+ macrophages are more pro-inflammatory and more of M1 phenotype. Moreover, CCR2+ and CCR2- tissue resident macrophages differentially mediate monocyte and neutrophil recruitments and influence monocyte fate decision after myocardial injury, as CCR2+ macrophages promote monocytes and neutrophils infiltration while CCR2-macrophages have the opposite function [28]. During MI, $Ly6C^{high}$ monocytes infiltrate the damaged myocardium and differentiate into M1 macrophages, together execute phagocytosis properties. M2 macrophages take over the responsibility for inflammation resolution when entering to reparative phase through three different main sources: M1>M2 conversion, $Ly6C^{high}$ monocytes differentiation and less $Ly6C^{low}$ monocytes differentiation [27].

1.4 The complement system

The complement system is one of the most important components of the immune system and has been discovered over 100 years ago. It is composed of a variety of circulating and membrane-bound proteins, which have a crucial role in the detection and clearance of pathogens, autoimmunity as well as inflammation [29]. One or more of the three main pathways—classical, alternative, and lectin pathway—can trigger the complement cascade [30, 31]. While mannose-binding lectin (MBL) detecting microbial sugars activates the lectin pathway, the classical pathway is activated by antibodies, C-reactive protein, and C1q on target surfaces. Both the classical and

lectin pathways lead to the generation of C4b2a complex (also known as C3 convertase). The alternative pathway, however, is initiated by hydrolysed C3 ($C3(H_2O)$) spontaneously at a very low rate and forms C3bBb, the fluid-phase C3 convertase [32]. All these three pathways converge at the step of C3 convertase generation and subsequent generation of C5 convertase, leading to the cleavage of C5 and formation of membrane attack complex (MAC) on pathogens or other target membranes [33]. C3 convertase cleave C3 into two fragments, the anaphylatoxin C3a and the opsonin C3b. C5 convertase cleave C5 into the anaphylatoxin C5a and the opsonin C5b. The anaphylatoxin C3a and C5a binds to C3a receptor (C3aR) and C5a receptor (C5aR), respectively. They trigger pro-inflammatory signaling and act as chemoattractants for neutrophils, monocytes, and macrophages trafficking towards inflammation[34]. Once C3b is generated, it not only activates the alternative pathway amplifying complement activation by binding to factor B (fB), but also elicits the opsonization and phagocytosis of targeted pathogens by scavenger cells [33, 35]. C5b assembles with other complement components C6, C7, C8, and C9, causing the formation of the cytotoxic C5b-9 complex, the MAC. The insertion of MAC in targeted membrane disrupts the integrity of pathogen and thereby induces cell lysis and apoptosis. In addition, MAC is capable of activating cytokine production, inflammation, and gene expression [36].

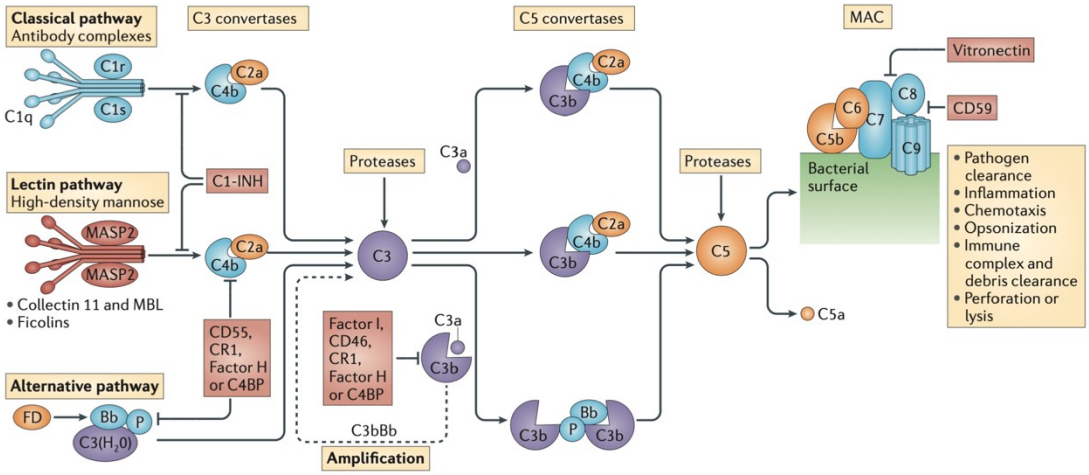

Fig. 1.4.1 Conventional complement activation pathways. Reprinted by permission from Springer Nature [37]. Copyright © 2014.

The pathogenic onset and spread of different inflammatory injuries are significantly aided by the activation of the complement system. Evidence from previous work delineates the important role of MBL pathway in I/R injury. Specific inhibition or blockade of MBL in mice protects against infarction and attenuates ventricular dysfunction following I/R [38-40]. In addition, Chun and colleagues demonstrate circulating fB, which is required for the activation of alternative pathway, plays an essential role in amplifying I/R induced necrosis and damage. $fB^{-/-}$ mice showed diminished C3 deposition and preserved myocardial function compared to WT mice [41]. The engagement of classical pathway in the development of myocardial injury has been under debate. While studies using C1 esterase inhibitor (C1INH) inhibits both classical and lectin pathway show a beneficial effect on I/R injury, other studies using $C1q^{-/-}$ mice observe no cardioprotective capability in mediating I/R [42, 43]. In a nutshell, the activation of MBL pathway during myocardial injury is a key mediator in the pathogenesis whereas alternative pathway mainly executes its function by augmenting the other activation pathways and hence contributing to myocardium damage.

Since complement C3 is a key factor in the complement cascade and involved in all three activation pathways, studies have been carried out to investigate on the role of C3 in ischemic disease. Cobra venom factor (CVF) is an anti-complement protein purified from cobra venom that is analogous to complement C3, allowing for continuous C3 cleavage and C3 depletion [44-46]. Studies using CVF have shown that complement C3 depletion leads to lower C3 deposition in the ischemia area and reduction of pro-inflammatory factors, ultimately protects intestinal mucosal, lung, and cardiac ischemia injury from damage and dysfunction to some extent [47-49]. Thus, depletion of C3 with CVF provides a protective role in the pathological process of MI. C3a receptor antagonist (C3aRA) is also applied to inhibit C3a in the setting of myocardial is chemia/reperfusion (I/R) injury. However, C3aRA has been found to have a strong side effect of neutropenia and it only prevents cardiac injury when it is administrated within the neutropenic time frame, therefore indicating a minimal ability of C3a in mediating I/R injury [50]. Wysoczynski and colleagues examined the function of C3 on scar formation, remodeling and regeneration following chronic MI. They took advantage of C3 knock out mice and found C3 deficiency exacerbates

impaired cardiac function and adverse heart remodeling, demonstrating C3 is essential to preserve myocardial function and regeneration [51].

1.5 Intracellular complement

While liver is a key source of circulating complement components, they are also synthesized by local somatic cells including both immune (such as monocytes, macrophages, neutrophils, T cells and B cells) and non-immune cells (such as astrocytes, mast cells, epithelial cells, and fibroblasts) [29, 37, 52, 53]. Peter Garred proposed a specific term 'complosome' for the complement produced intracellularly. Recent studies have elucidated a crosstalk between complement system and inflammation. Pro-inflammatory cytokines can stimulate and/or augment local complement production. Increases of local complement, in turn, can mediate cytokine production, suggesting bidirectional feedback loops exit in immune response [37].

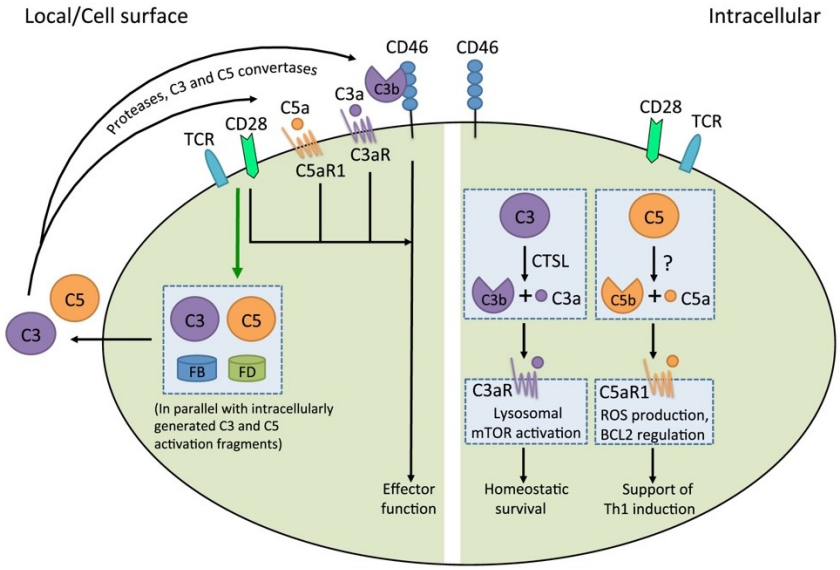

Fig. 1.5.1 Local complement activation. Reprinted by permission from Cell Press [54]. Copyright © 2016 Elsevier Inc.

Claudia Kemper's group demonstrated the activation of intracellular C3 is not limited to engage cell surface C3aR and extracellular space. Besides, intracellular generated C3 can directly bind to C3aR, which is expressed on lysosomes, and be activated within the cytoplasm. Specifically, endogenous C3 cleaved by protease cathepsin L in resting human T cells engages with C3aR, thereby drives basal mammalian target of

rapamycin (mTOR) activation, which is required for sustaining T cell homeostasis [55, 56]. In line with this, patients with leukocyte adhesion deficiency type 1 (LAD-1) present with reduced amount of intracellular C3a generation and impaired immune function. Restoration of intracellular C3a rescues IFN-Y secretion and reduces IL-17 production, which then leads to the normal effector activity. In contrast, patients suffering from arthritis display severer disease with increased accumulation of endogenous C3 produced by T cells [57]. Notably, intracellular C3 is preserved in patients with serum C3-deficiency, indicating that intracellular C3 is uncoupled from the serum-operative complement [55]. Therefore, discovery of the complosome supports the notion that complement not only provides classical immune-related functions but also controls basic cellular processes.

During MI, both myeloid cells and complement C3 are important effector systems. Since in previous studies C3 depletion was associated with adverse outcomes, we hypothesize that myeloid-derived complement C3 could represent a key factor in post-MI inflammation and that manipulation of intracellular C3 may provide therapeutic benefits for the treatment of MI.

2. Material and Methods

2.1 Mice

C3^{tdTomato} reporter mice (*C3-tdT*) were kindly provided by Prof. Claudia Kemper at the National Institute of Health, Bethesda, USA. In brief, IRES-tdTomato cassette was inserted after C3 STOP codon and further flanked by loxP sites, which allowed to monitor C3 expression and be able to delete C3 conditionally by the activation of Cre recombinase [58]. Similarly, *C3aReceptor*^{tdTomato}(*C3aR-tdT*) reporter mice was kindly provided by Prof. Jörg Köhl at University of Lübeck, Germany [59]. *Rank*^{Cre} *(also known as Tnfrsf11a*^{Cre}*)* [60], *LysM*^{Cre} mice [61] were purchased from the Jackson laboratory. *Mrp8*^{cre} mice [62] were provided by Prof. Andrés. Hidalgo, CNIC Madrid, Spain. Cell specific knock-out mice were generated by crossing *Cre*-driven promoter mice and reporter mice. In specific, *Rank*^{cre}*, LysM*^{cre}*, Mrp8*^{cre} mice were crossed with homozygous *C3-tdT* mice to deplete C3 in tissue resident macrophages (*Rank*$^{\Delta C3}$), BM derived myeloid cells (*LysM*$^{\Delta C3}$) and neutrophils (*Mrp8*$^{\Delta C3}$), respectively. *Rank*^{cre} *mice* were also cross-mated with *C3aR-tdT* mice to deplete C3aR expressed by tissue resident macrophages (*Rank*$^{\Delta C3aR}$). *CD45.1* (Ly5.1) mice were received from the JAX company, and were used as BM recipients or donors as indicated. PCR genotyping was performed according to manufactory protocols as previously described. All mice mentioned above were used at least 8 weeks old for baseline experiments and 12 weeks old for injury model.

All experiments had been approved by licences from the Government of Bavaria (Regierung von Oberbayern) according to German legislation.

2.2 Methods

2.2.1 Timed mating

Mice at the age of 10-20 weeks were included for timed mating. *C3-tdT*$^{fl/+}$ and *C57BL/6*（*WT*）mice were mated in the evening and separated the next day early morning. To

estimate embryonic development, the midday of the vaginal plug formed was considered as embryonic day 0.5 (E0.5). At E10.5 and E16.5, female mice were sacrificed, and embryos were collected one by one with careful disinfection to avoid contamination.

2.2.2 BM transplantation

To create chimerism, conventional irradiation was carried out to abrogate hematopoietic cells of recipient mice and therefore enabled the reconstitution of the hematopoietic system, which was engrafted with BM from donor mice. In detail, recipient mice were subjected to 6.5 Gy whole-body irradiation twice (at least 4 hours apart). Femur, tibia, and humerus of donor mice were harvested and flushed with PBS. Following filtration and centrifugation, donor hematopoietic stem cells were collected and suspended with PBS. $1.0*10^7$ cells in the volume of 200ul were transplanted intravenously to the recipient mice right after the second irradiation.

Efficiency of chimerism was checked in peripheral blood 6 weeks after BM transplantation by flow cytometry. Over 90% of blood cells derived from donor origin was considered to be efficient, however, blood chimerism typically was > 95%. Then 2 months later the mice that successfully achieved replacement of BM cells were utilized to perform further experiments. Prophylactic antibiotic in the drinking water were given to mice before the administration of irradiation and continued for 1 month after transplantation.

2.2.3 Myocardial Ischemia-reperfusion (I/R) and chronic myocardial infarction (MI) model

Mice were used at the age of 12-30 weeks. Anesthesia was induced by 5% isoflurane inhalation and followed by intraperitoneal injection of Fentanyl (0.05mg/kg), midazolam (5.0mg/kg) and medetomidine (0.5mg/kg). Mice were subsequently placed on a heating mat to keep body temperature. To visualize the trachea, an incision was made on the cervical skin along the body vertical axis. Mice were intubated with an endotracheal tube (metal cannula 19G) via larynx (MiniVent Ventilator model No. 845, Harvard Apparatus®) and ventilation volume was 200ul cycling at a frequency of

150/min. The skin incision was sutured with single staples (7-0 Prolene, Ethicon, Norderstedt). The chest wall was opened between the 2nd and 3rd rib and retracted with 5-0 suture (5-0 Prolene, Ethicon, Norderstedt) upwards and downwards to expose the left ventricle as well as left auricle. To induce ischemia injury, left anterior descending artery (LAD) was located and a double knot was made around the artery 1-2mm from the tip of the left auricle with an 8-0 suture (8-0 Prolene). For reperfusion injury, a placeholder was placed on the top of LAD within the double knot and then tightened the knot to fully block bloodstream. The placeholder consisted of a 30G cannula and polyethylene tube. The successfully ligation was confirmed by myocardial blanching and arrhythmia. 60 mis later, the place holder was removed, and the knot was cut open to release the occlusion and resulted in the reperfusion injury. For chronic MI, the LAD was ligated without re-opening. Then 5-0 suture was used to close the chest cavity, 7-0 suture was used to close the muscle layer and skin. Mice were given 0.1mg/kg Buprenorphine subcutaneously as an analgesic treatment, three times per day for 3 days. Thereafter, mice were sacrificed, and organs were harvested at different time points depending on experimental needs.

2.2.4 Tissue collection and processing for flow cytometry

For embryonic tissues, pregnant females were sacrificed by cervical dislocation after inhalational isoflurane anaesthesia on desired days. The uterus was taken out and placed on Petri dishes containing 4°C phosphate-buffered saline (PBS, Invitrogen) separately. Embryos were separated from placenta and then euthanized immediately by cervical dislocation with scissors. At E10.5, yolk sac (YS) and embryo proper (EP) were separated and collected under dissecting microscope. At E16.5, embryo blood, heart, liver, lung, and brain were harvested. To note, disinfection of instruments between embryos were mandatory because of litter mates' different genotypes. Genotyping of embryos was conducted as previously described by collecting a piece of tissue. *C3-tdT*$^{fl/+}$ embryos were served as positive reporters and the others were controls.

For adult tissues, mice were anaesthetized as described above. Then blood was collected by cardiac puncture in the 2nd intercostal space with a 2ml syringe (BD Discardit™, USA) prefilled with (for plasma collection) or without (for serum

collection) 100ul of ACD (Acid citrate dextrose) buffer. Subsequently, the abdominal and chest cavity were quickly opened, and an incision for liver was made. The mice were then perfused with 20ml ice-cold PBS through intracardiac injection. After perfusion, liver was dissected out and kept in a 15ml falcon containing PBS. Aorta from aorta arch to the branch of iliac artery was harvested after removal of intestine, colon, lung, and connective tissues under a dissecting microscope. Then heart, liver, brain, and femur were collected. Infarcted hearts were divided into remote area (proximal LAD supply area) and ischemia area (distal LAD supply area).

To obtain suspension of single cells for flow cytometry, embryo tissues were incubated in enzymatic mix composed of 1mg/ml Collagenase D (Roche, Burgess Hill, UK), 60U/ml Desoxyribonuclease (DNAse I, Sigma-Aldrich), 2.4mg/ml Dispase (Sigma-Aldrich), 3% fetal bovine serum (Invitrogen, Paisley, UK) and PBS at 37°C for 30 mins. Adult tissues were weighed and cut up into pieces with scalpels and forceps. Then the tissues were transferred to 50ml falcons containing specific enzymatic mix for specific tissues and incubated at 37°C for 30 mins in a shaking machine (Thermomixer comfort, Eppendorf, Hamburg). For the heart, the enzymatic mix contained 10mg/ml Collagenase I (Sigma Aldrich), 10mg/ml Collagenase XI (Sigma Aldrich), 10mg/ml Hyaluronidase (Sigma Aldrich), and 100U/ml DNAse I. For the liver and brain, 1mg/ml Collagenase D, 100U/ml DNAse I, 2.4mg/ml Dispase, and PBS were used. For the aorta, 20mg/ml Collagenase II (Worthington Biochemical Corporation) and 20mg/ml Elastase (Worthington Biochemical Corporation) were mixed in PBS to digest aorta for 15 mins. Thereafter the adventitia was separated from intima and medium.

After enzymatic digestion, tissues were mashed through a 70µm cell strainer and cells were collected in 15ml falcons. Following centrifugation (4°C, 350g, 5 mins), the pellets were first resuspended and blocked with Fc block (CD32/CD16 purified monoclonal antibody that diluted in flow cytometry buffer (PBS 1X, 0.5% BSA, 2mM ETDA) for 15 mins and then incubated with antibodies for 30 mins. For the BM, both ends of femur were cut open and flushed with PBS by using a 5ml syringe and 26G needle. 3 ml of ammonium chloride lysis buffer was added to 100ul ACD-treated blood and BM to get rid of erythrocytes for 5 mins and this process was stopped by adding 6ml PBS. Followed by a second erythrocytolysis and centrifugation (4°C, 320g, 5

mins), cells were resuspended in Fc block and then incubated with antibodies as mentioned before. All procedures were conducted on ice.

2.2.5 Flow cytometry

Surface-stained cells were thoroughly washed and centrifuged at 350g for 5 mins, and they were then resuspended in flow cytometry buffer. Flow cytometry data was recorded on a BD Fortessa® flow cytometer and gating strategy is depicted below. Data were analysed using FlowJo® (version 10.0.8r1).

2.2.6 Immunohistology

As to the purpose of histological analysis, hearts were perfused with 20ml ice-old PBS and followed by organs harvesting. Organs were then fixed in 4% PFA (Formaldehyde Solution Methanol-free, Thermofisher Scientific) for 30 mins at 4°C, incubated in 30% sucrose (Sigma Aldrich®)-solution overnight, and thereafter embedded in Tissue-Tek (Sakura Finetek Germany GmbH) and kept at -80°C freezer. To obtain different levels of heart slices, 12µm thickness of heart cryoscetions were made with a cryotome machine (CryoStar NX70, Thermo Fisher Scientific) and 50µm interval was acquired between every 6 cuts.

For immunofluorescence staining, heart samples were fixed with 4% PFA for 10 mins, washed with PBS and permeabilization was accomplished with 0.5% Triton X-100 for 10 mins. Following 1h blocking with 10% goat/donkey serum at room temperature, samples were then incubated with primary antibodies (see Table 1) for 2h-overnight. Afterwards, secondary antibodies (see Table 1) were applied after washing and incubated for another 1h. WGA-Alexa Fluro 647 conjugated antibody (Wheat Germ Agglutinin, ThermoFisher Scientific) was used together with the secondary antibody when there was the need for labeling fibrotic tissue. Hoechst 33342 was added to visualize nuclei. Finally, samples were washed again and covered with Fluorescence Mounting Medium and coverslips.

Slides were analyzed with fluorescence microscope Axio Imager M2 (Carl Zeiss®) and fibrotic area was assessed using ZEN Imaging and ImageJ software. Images were taken by confocal microscope (LSM 880, Carl Zeiss) with Airyscan processing. The extend

of tissue fibrosis was calculated as ratio of WGA positive area to whole heart area by an independent researcher in a blind manner using Image J software.

2.2.7 Generation of Hoxb8 cell line derived from BM

Hoxb8 progenitor cells were established as previously described [63, 64]. In brief, to generate virus-containing supernatant, HEK-293T cells were transfected with retroviral backbone pMSCVneo-ER-Hoxb8 and in parallel, pCL-Eco packaging vectors facilitated by Lipofectamine 2000. The supernatant of these cells that contained virus was collected 48h after the transfection and placed at -80°C for later use. Next, in order to harvest BM cells, 8–12 week-old mice were sacrificed and BM were collected as described before. BM progenitor cells were then transduced with the retrovirus we prepared before to bring in estrogen-regulated Hoxb8 and cultured in a so-called "proliferation medium", which was consisted of RPMI 1640, 10% FCS, 1% penicillin/streptomycin, 1μM β-estradiol, 30 μM 2-Mercapto-Ethanol, and 6% SCF-containing supernatant. 4 weeks later the transduction, the stable immortalized ER- Hoxb8 multipotent progenitor cells were successfully generated.

2.2.8 Differentiation of Hoxb8 progenitors into macrophages

To stimulate the differentiation of Hoxb8 progenitors into macrophages, the progenitors were washed twice with PBS to deactivate Hoxb8 and suppled with "differentiation medium" that containing same as proliferation medium except for β-estradiol. $5*10^5$ cells were seeded in 10cm cell culture dish and 10 ng/ml M-CSF that enabled the differentiation process were added to the medium. During the differentiation step, the medium was dispensed every 2 days and 5 days later, macrophages were used for desired experiment.

2.2.9 In vivo PET imaging

Non-invasive in vivo imaging of the remodeling heart was carried out using a small animal PET/CT scanner (Nanoscan PET-MRI, Mediso, Hungary) at day 6 and day 30 after I/R, as previously described [65]. We investigated C3-tdT mice and mouse models

with cell-specific conditional C3 deletion. Following anesthesia with 2.5% isoflurane and pure oxygen, the mice were placed in a heating pad and then maintained the anesthetic state with 1.5% isoflurane. Approximately 20MBq of radiotracer 18F-FDG was administrated with an intravenous catheter via tail vein and transferred to a mouse-specific holder to enable PET/CT scan. ECG electrodes were placed on the mice and ECG was recorded with a dedicated physiological monitoring system (BioVet, Australia). 30 mins later, a whole-body CT scan was performed immediately for PET image reconstruction. A three-dimensional PET acquisition was initiated right after the CT scan and lasted for 15 min. Mice remained under anesthetic during the entire scanning process.

PET images were analyzed using the Inveon Research workplace in a blinded manner (Siemens Medical Solutions, Knoxville, TN) as described previously [65]. The infarct size was associated with reduced 18F-FDG accumulation and myocardial viability, which could be measured as a percentage of the left ventricular surface area and represented by total perfusion deficit (TPD). We set a threshold of infarct size in mice undergoing permanent LAD ligation, considering an infarct area of < 20% of the left ventricle mass as insufficient injury, and in that respective case mice were not subjected to further analysis and quantification. The percentage of the injected dose per gram (%ID/g) and left ventricular metabolic volume (LVMV) were assessed from static images. The parameters of left ventricular function including EDV, ESV, SV, and EF were also estimated from ECG-gated images using QGS® (Cedars-Sinai, USA), as described previously.

2.2.10 Statistics

GraphPad Prism 9 was used for data analysis. All data were presented as mean ± standard deviation (SD). Normal distribution was assessed by Shapiro-Wilk normality test. For groups with normally distributed data, unpaired's t test and one-way ANOVA was performed for 2-group and 3-group comparison, respectively. A Welch's correction was applied when SDs were significantly different ($P<0.05$). For groups that did not follow Gaussian distribution, nonparametric Mann-Whitney test or Kruskal-Wallis test was carried out as indicated. The differences between groups were considered to be significant with $P<0.05$.

2.3 Materials

Table 1 Antibodies and Reagents

Antibody	Clone	Fluorescence	Company	Catalog number
Flow cytometry				
CD45	30-F11	PerCP-Cy5.5	BioLegend	103132
CD45.1	A20	FITC	BioLegend	110706
CD45.2	104	APC-Cy7	BD Biosciences	560694
CD45.2	104	PerCP-Cy5.5	BioLegend	109828
CD11b	M1/70	PE-Cy7	BD Biosciences	552850
F4/80	BM8	BV421	BioLegend	123132
CD64	X54-5/7.1	APC	BioLegend	139306
Ly6G	1A8	BV605	BioLegend	127639
CD3	17A2	APC-Cy7	BioLegend	100222
CD19	1D3/CD19	FITC	BioLegend	152404
Gr-1	RB6-8C5	PerCP-Cy5.5	BioLegend	108428
CD115	AFS98	BV421	BioLegend	135513
CD16/CD32	2.4G2	uncoupled	BD Biosciences	553142
MHC II	M5/114.15.2	BV510	BioLegend	107635
Ly6C	H1.4	BV510	BioLegend	128033
Podoplanin	8.1.1	BV421	BioLegend	127423
CD11c	N418	APC-Cy7	BioLegend	117324
TER-119	TER-119	APC-Cy7	BioLegend	116223
CD31	390	APC-Cy7	BioLegend	102439
Immunohistology				
Complement C3	11H9	Unconjugated	Novus Biologicals	NB200-540
Complement C3	Polyclonal	Unconjugated	Thermo Fisher	PA5-21349
GM130	Clone 35	Unconjugated	BD Transduction Laboratories	610822

Rab7A	Rab7-117	Unconjugated	GeneTex	GTX16196
EEA1	Polyclonal	Unconjugated	abcam	ab2900
Calnexin	Polyclonal	Unconjugated	abcam	ab22595
CD68	FA-11	Unconjugated	Bio-Rad	MCA1957
tdTomato	Polyclonal	Unconjugated	LSBio	LS-C340696
Isotype IgG2a, k	eBR2a	Unconjugated	Invitrogen	14-4321-82
goat anti-rabbit	Polyclonal	Alexa Fluor 488	Invitrogen	A-11034
goat anti-rat	Polyclonal	Alexa Fluor 594	Invitrogen	31220
goat anti-mouse	Polyclonal	Alexa Fluor 488	Invitrogen	A-11001
donkey anti-goat	Polyclonal	Alexa Fluor 594	Invitrogen	PA1-28659
WGA		Alexa Fluor 647	Thermo Fisher	W32466
Hoechst 33342		Blue fluorescence	Thermo Fisher	H3570
Other reagents and materials				
RPMI 1640 Medium		Sigma Aldrich		R8758
FBS		BIO-SELL		S0615
penicillin/streptomycin		Sigma Aldrich		P4333
2-Mercapto-Ethanol		Sigma Aldrich		M3148
M-CSF		Immuno Tools		12344115
Tissue-Tek Cryomold Standard		Sakura Finetek		4557
Mounting medium		Dako North America Inc., USA		S3023
Saponin		Carl Roth		4185.1
Albumin Fraction V		Carl Roth		8076.4
Triton X-100		Sigma-Aldrich		T8787
Tween20		Sigma-Aldrich		P1379
Sucrose		Sigma-Aldrich		S1888
16% Formaldehyde		Thermo Fisher		28908

3. Results

3.1 C3 is produced by macrophages in vitro

To investigate whether macrophages have the capacity to produce C3, we established cultured macrophages from Hoxb8-immortalized hematopoietic progenitors of wildtype (WT) mice. To localize C3 in macrophages and their subcellular structures, we stained C3 and intracellular compartment markers, and then investigated their localization by confocal microscope. We identified C3 in Golgi, endoplasmic reticulum (ER) and ER derived secondary vesicles, indicating that C3 is produced by macrophages (**Fig. 3.1.1**).

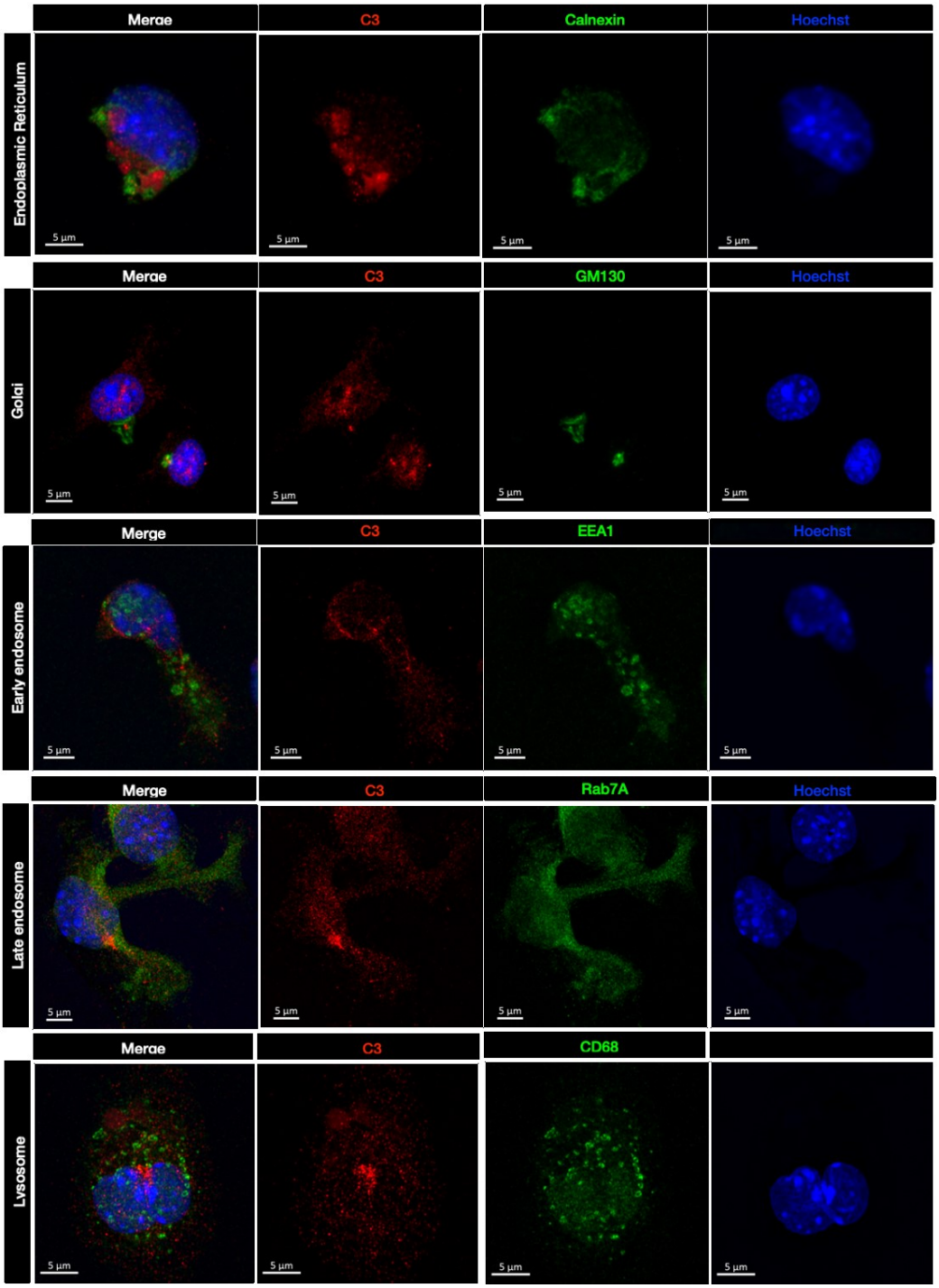

Fig. 3.1.1 C3 production in macrophages. Representative immunofluorescence staining images of BM derived Hoxb8 macrophages with subcellular compartments. Scale bar, 5µM. x63 magnification assessed by confocal microscope. Calnexin, endoplasmic reticulum marker; GM130, Golgi marker; EEA1, early endosomal vesicle marker; Rab7A, late endosomal vesicle marker; CD68, lysosomal marker.

3.2 C3 production by myeloid cells in vivo

To determine the quantitative expression of C3 in immune cells, we took advantage of C3-tdTomato knock-in reporter mice (*C3-tdT*), which enabled the labeling of C3 protein with tomato signal and allows for the quantification of C3 [57]. In brief, C3 gene of Bl6 background mice is monitored by inserting an IRES-tdTomato cassette downstream of C3 and this C3-tdTomato sequence is flanked by *loxP* sites (Fig. 3.2.1). Consequently, this C3-tdT reporter mice could later be cross-mated with Cre-driven cell-specific mice and conditionally deplete C3 by the activation of Cre recombinase [66].

As a first step, we aimed to characterize C3-tdT expression in immune cells of blood circulation and tissues. Representative gating strategies are shown in **Fig. 3.2.1**. A first screen by flow cytometry demonstrated the high abundance of C3-tdT in myeloid cells, both monocytes and neutrophils, with more than 90% of tomato labeling in BM and blood. Lower than 3% of lymphocytes (CD19+ B cells and CD3+ T cells) were present with tomato labeling in the BM whereas tomato positive blood lymphocytes were less than 1% (**Fig. 3.2.2**).

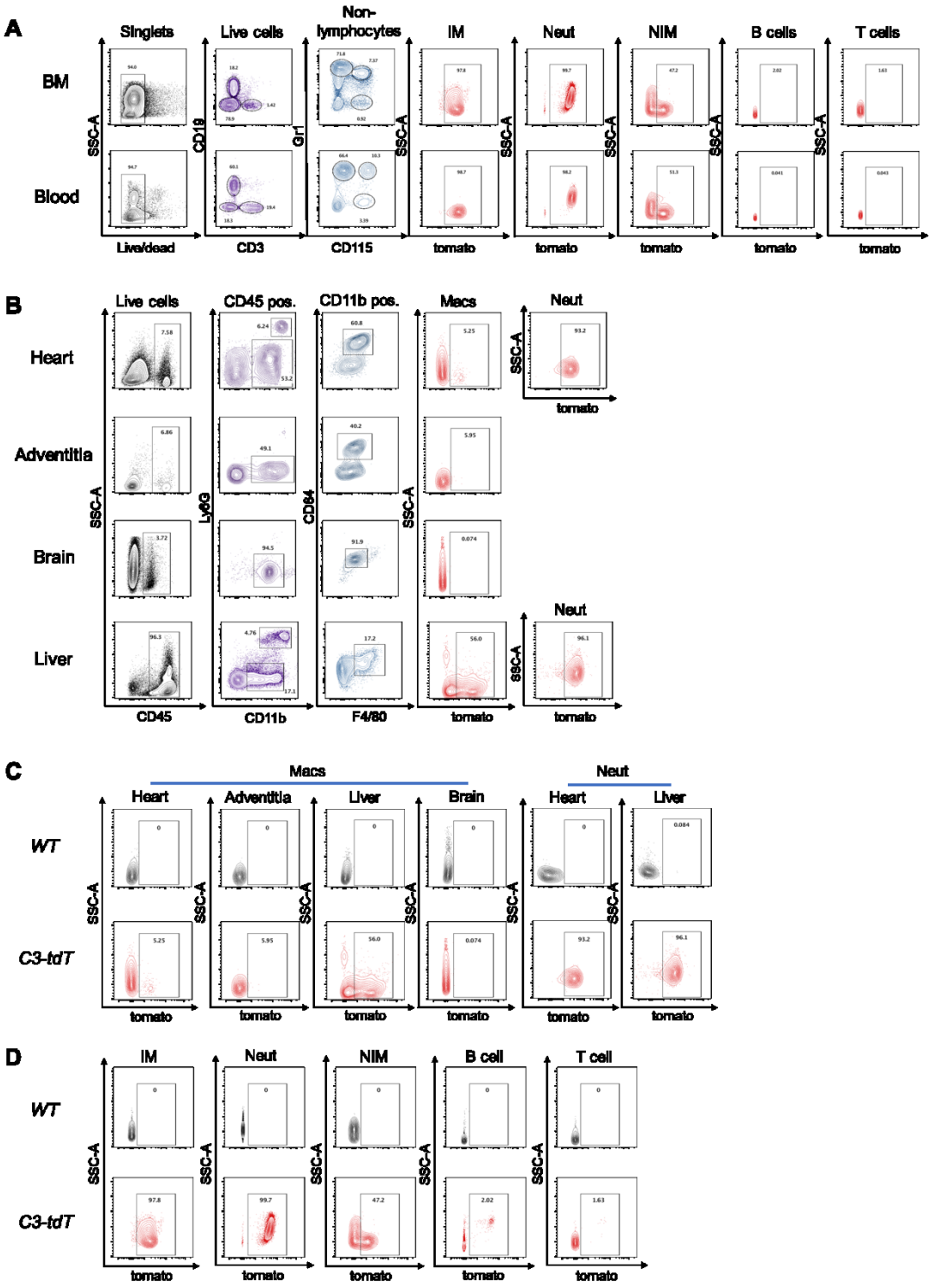

Fig. 3.2.1 Representative gating strategy for flow cytometry. C3-tdT expression in **A)** immune cells in the circulation (Upper, BM; Lower, blood) and **B)** tissue macrophages (Macs) and neutrophils (Neut) among different tissues. Circulating cells was first gated on singlets, live cells and gated on CD3 and CD19 lymphocytes. Within non-lymphocytes population, neutrophils were identified as $CD115Gr1^{+}$. Classical, inflammatory (IM) and non-inflammatory (NIM) monocytes were separated according to Gr1 expression, IM were identified as $CD115^{+}Gr1^{+}$ and NIM were

$CD115^{+}Gr1$. For tissue macrophages and neutrophils, they were identified as $CD45^{+}CD11b^{+}F4/80^{+}CD64^{+}$ and $CD45^{+}CD11b^{high}Ly6G^{+}$, respectively. *WT* mice were used as FMO control for setting an accurate gating for tomato signal in **C)** tissues and **D)** BM.

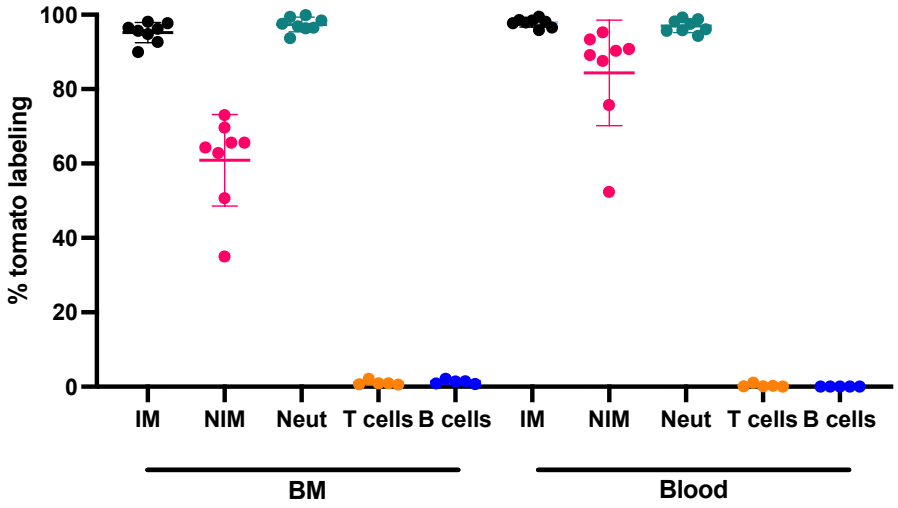

Fig. 3.2.2 C3 is present in circulating myeloid cells in steady state. Percentage quantification of C3-tdT expression in immune cells in the circulation; analyzed by flow cytometry (n=8, values shown were mean±SD).

We further characterized C3-tdT expression in tissue macrophages and neutrophils. In steady state, only some macrophages (~10%) expressed C3-tdT in the heart and adventitia, and around 40% of liver Kupffer cells. In contrast, brain microglia showed no expression of C3-tdT. Consistently with neutrophils in the circulation, the percentage of intrinsic tomato expressing neutrophils in both heart and liver appeared to be the highest (>90%) (**Fig. 3.2.3**).

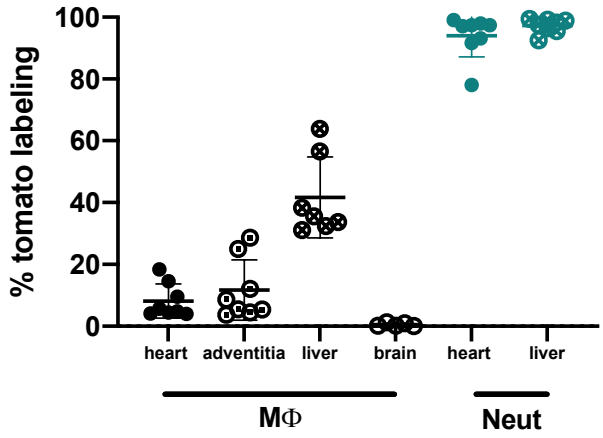

Fig. 3.2.3 C3 expression in tissue macrophages and neutrophils in steady state. Percentage quantification of C3-tdT expression in immune cells in tissues; analyzed by flow cytometry (n=5-8, values shown are mean±SD).

3.3 Myeloid derived C3 during embryonic development

In previous studies, tissue macrophages have been found to originate from two distinct progenitors, yolk sac (YS) progenitors (also known as erythron-myeloid progenitors, EMP) and hematopoietic stem cells. It has been reported that EMPs appear at E8.25, migrate to embryo and give rise to tissue resident macrophages at a peak of E10.5, and complete by E12.5. Whereas HSCs arise at E10.5, eventually migrate to BM and persist hematopoiesis in the adulthood [19, 21].

Thus, we aimed to address the macrophage C3 expression pattern during embryo development. We carried out timed mating of heterozygous *C3-tdT* reporter mice with *WT* mice and collected embryos at two different stages of embryonic development, E10.5 and E16.5. At E10.5, there was no C3-tdT expression in F4/80^{+}CD64^{+} macrophages, neither in YS nor the embryo proper (**Fig. 3.3.1**). Additionally, we did not find any expression in embryonic neutrophils as well. As the complement system has a prominent role in immune defense against invading pathogens and damaged host cells, it is reasonable that we could not detect C3 expression at this early stage of embryo development.

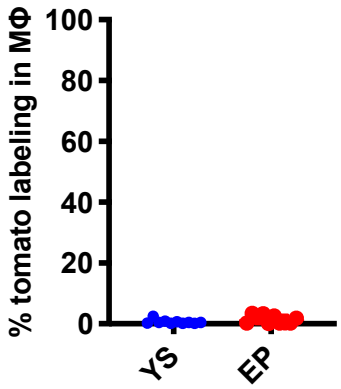

Fig. 3.3.1 C3 is undetectable in myeloid cells at early embryonic development. E10.5. YS, yolk sac. EP, embryo proper. n=10. Error bars, mean±SD.

At E16.5, the embryo is approaching the time of birth and macrophage populations are acquiring a more mature phenotype [60]. In line with this, we indeed identified expression of C3-tdT in myeloid immune cells of both circulation and tissues. Over 70% of blood monocytes expressed C3-tdT. The percentage of C3-tdT expression in macrophages and neutrophils of embryo tissues was similar to that of adult tissues. A large proportion of neutrophils expressed C3-tdT in healthy conditions. Further, C3-tdT was more present in F4/80^{low} macrophages rather than F4/80^{hi} macrophages, indicating that C3 was more of BM hematopoietic origin in steady state (**Fig. 3.3.2**).

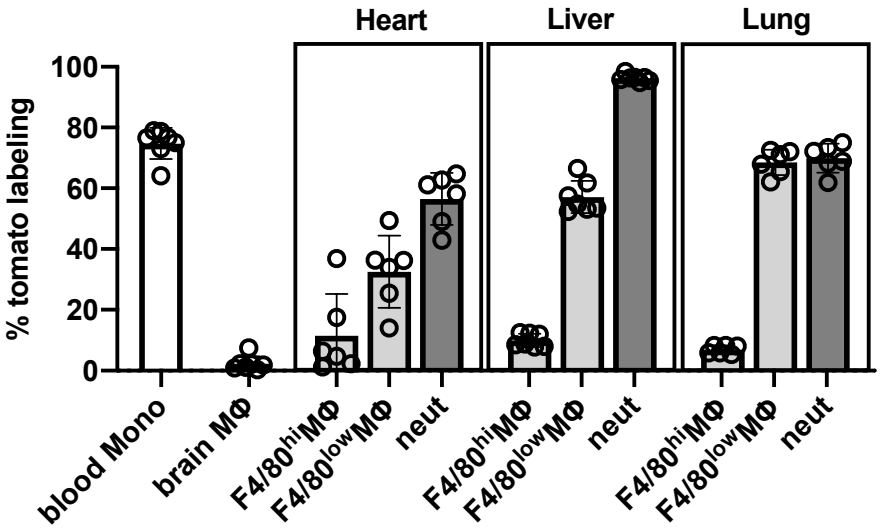

Fig. 3.3.2 C3 is produced in myeloid cells at late embryonic development. E16.5. n=6-7. Error bars, mean±SD.

3.4 Induction of C3 after I/R

3.4.1 Upregulation of C3 expression in cardiac macrophages after I/R

It is well known that activation of complement system is engaged in the process of I/R and increased C3 deposition is found in infarcted hearts [67, 68]. We therefore carried out myocardial ischemia reperfusion model on *C3-tdT* reporter mice, to investigate the response of circulating myeloid cells and tissue resident macrophages in post-I/R injury. We performed LAD ligation for 60mins and reperfused heart for 6h and 48h, respectively. Compared to steady state conditions, we found no response regarding C3 expression in cardiac macrophages at 6h reperfusion. However, with 48h reperfusion time, not only the percentage but also the intensity of C3-tdT expression in cardiac macrophages was significantly increased. This induction of C3-tdT was paralleled with the increased number of macrophages in the ischemic heart (**Fig. 3.4.1**).

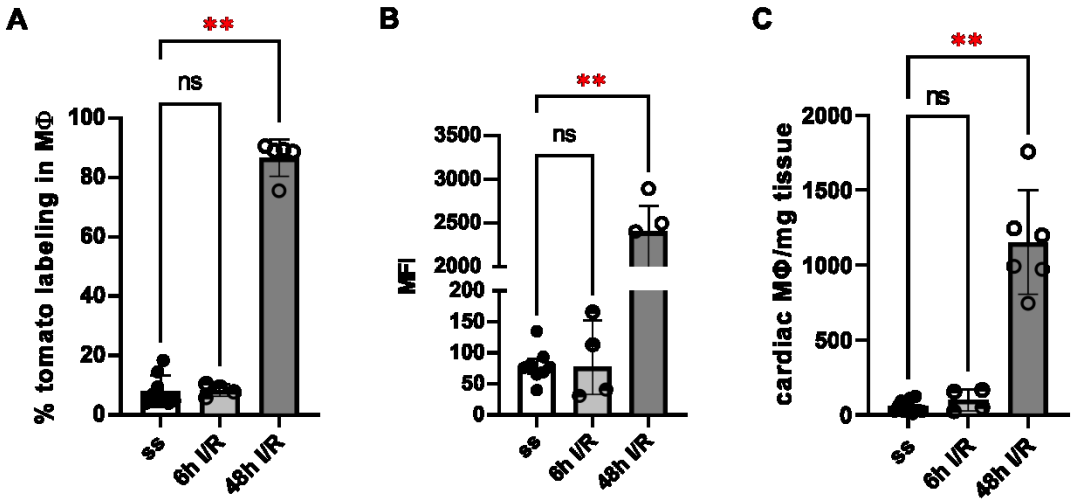

Fig. 3.4.1 Increased C3 in cardiac macrophages 48h after I/R. A) Percentage and **B)** MFI of tomato labeling in cardiac macrophages. **C)** Absolute number of macrophages in ischemic myocardium. Error bar, mean±SD. One-way ANOVA was performed. **p<0.01.

Neutrophils in the heart showed nearly hundred percent of C3-tdT expression in steady state. After I/R, a significant raise was still detected in the percentage of C3

expressing neutrophils in the ischemia area with both 6h and 48h reperfusion. However, the intensity of C3-tdT (MFI) in neutrophils was unaltered after injury at both time points (**Fig. 3.4.2**). Once ischemia occurred, neutrophils were among the first immune cells attracted by inflammatory signals within few hours to ischemic area. This process was later followed by monocyte recruitment to the heart [69]. In the I/R model, neutrophil numbers in the injured myocardium increased 6h after the onset of reperfusion, and neutrophils continued to be recruited for up to 4 days (**Fig. 3.4.3**). This indicated that neutrophils provide C3 mainly through their recruitment into the injured heart rather than by upregulation of C3 production.

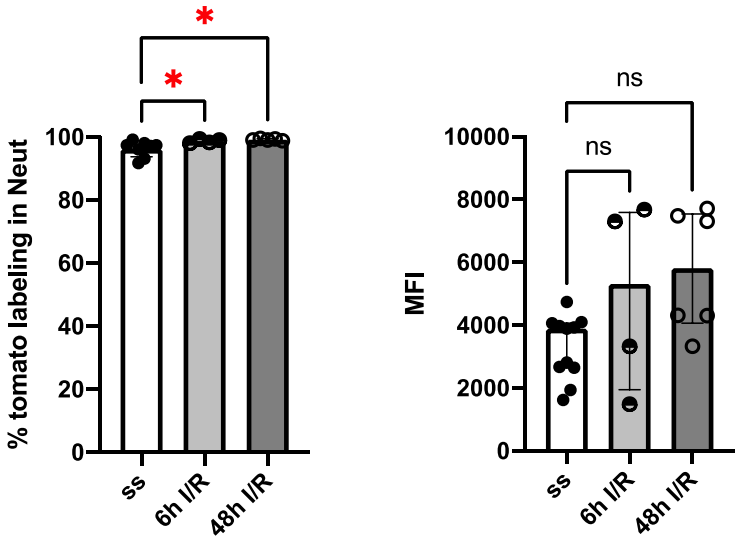

Fig. 3.4.2 Neutrophils are recruited to ischemic myocardium after I/R. Percentage (**left**) and MFI (**right**) of C3-tdT expression in neutrophils in cardiac ischemic area. Error bar, mean±SD. One-way ANOVA was performed. *p<0.05.

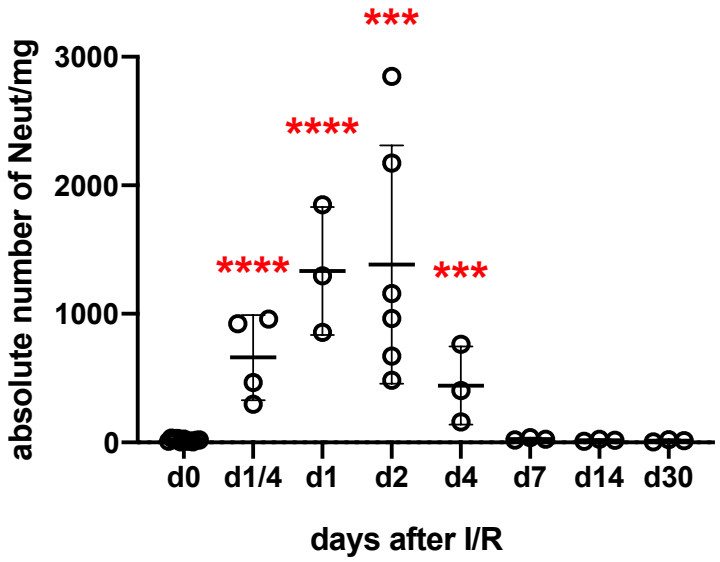

Fig. 3.4.3 Kinetics of neutrophils recruitment following I/R. Absolute number of neutrophils in ischemic myocardium quantified by total neutrophil number (defined as $Ly6G^{+}CD11b^{hi}$ cells by flow cytometry) per mg heart tissue (weighed before tissue digestion). Error bar, mean±SD. Unpaired t-test between each time point post-I/R and steady state was performed. ***p<0.001; ****p<0.0001.

Moreover, the induction of C3 expressing cardiac macrophages was not limited to ischemic area. We could also perceive the increment of tomato positive macrophages in the remote area after 48h reperfusion. No difference of C3 expressing neutrophils could be found between ischemia area and remote area after I/R (**Fig. 3.4.4**), underlining the fast recruitment of neutrophils and their broad distribution in the heart after I/R.

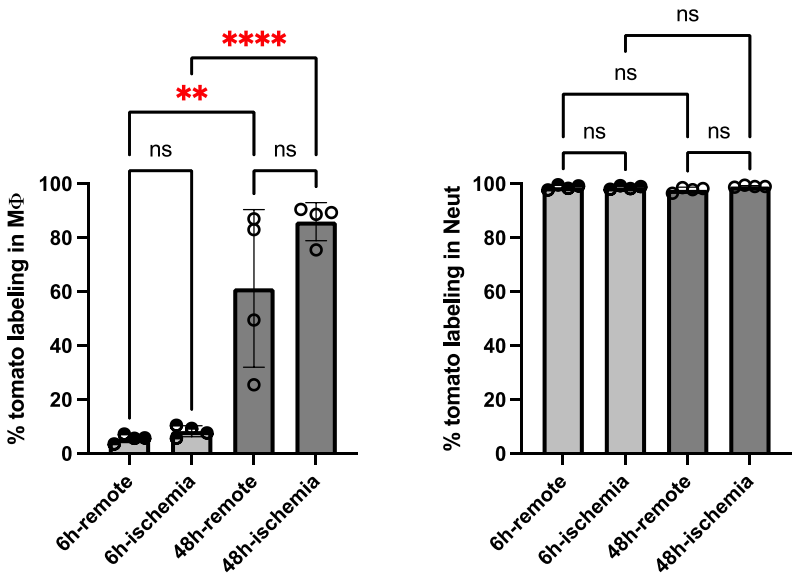

Fig. 3.4.4 The induction of C3 in cardiac macrophages is not limited to ischemic myocardium. Comparison of C3-tdT expression in macrophages (**left**) and neutrophils (**right**) between ischemia area and remote area, after both 6h and 48h reperfusion. Error bar, mean±SD. One-way ANOVA was performed. **p<0.01; ****p<0.0001.

Meanwhile, we evaluated C3-tdT expression in circulating myeloid cells in BM and blood. No difference could be detected in both inflammatory and non-inflammatory monocytes at both time points. A minor reduction of C3 expressing neutrophils was measured in BM after 6h reperfusion, but not in the blood (**Fig. 3.4.5**). C3-tdT intensity did not change in circulating myeloid cells (**Fig. 3.4.6**), indicating that the intrinsic C3 signal was stable. This was in contrast to the induction of C3 production in cardiac macrophages after I/R.

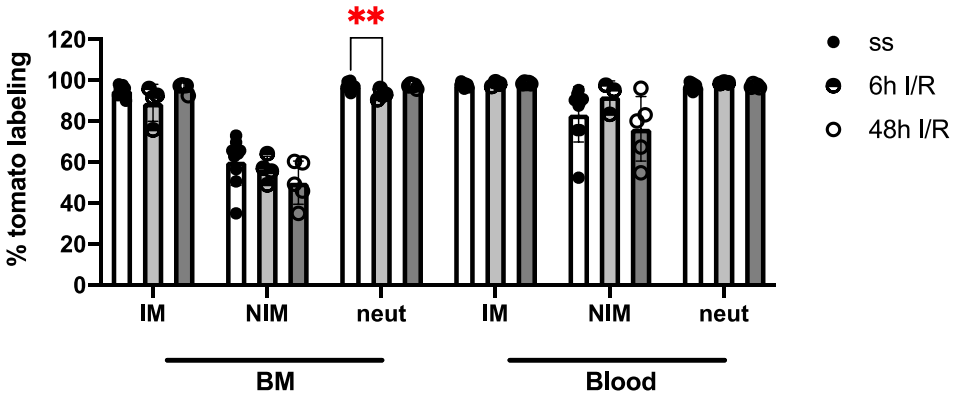

Fig. 3.4.5 Percentage of C3 expression in myeloid cells in the circulation. Error bar, mean±SD. One-way ANOVA was performed. **p<0.01.

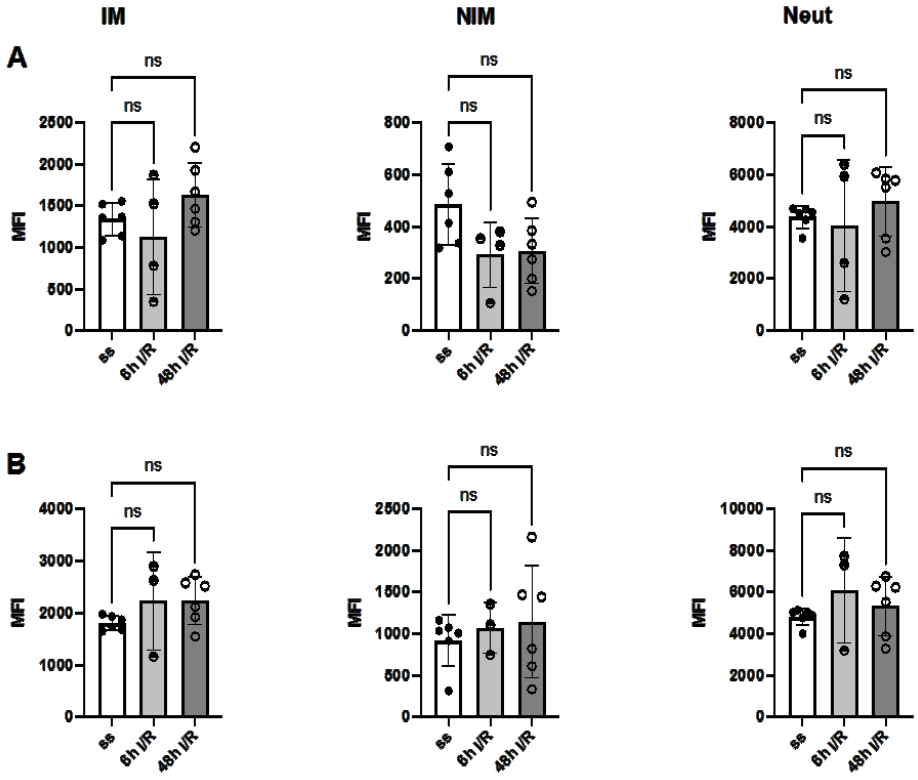

Fig. 3.4.6 Intensity of C3 in circulating myeloid cells in steady state and after I/R. **A)** BM; **B)** blood. Error bar, mean±SD. One-way ANOVA was performed.

To further investigate C3 deposition after I/R, we injected Mfge8-GFP before we sacrificed mice at the time point of 6h reperfusion. Previous studies have demonstrated the bridging property of Mfge8 protein to recognize phosphatidylserine of apoptotic cells and its capacity to bind to phagocytic macrophages [70]. Therefore,

we took advantage of this signature of Mfge8 and utilized a GFP conjugated Mfge8 to facilitate the labeling of apoptosis at early stage of infarction. We found that C3 (labeled in red) was colocalized with macrophages (labeled in grey) and corresponding to apoptotic area (labeled in green) (**Fig. 3.4.7**).

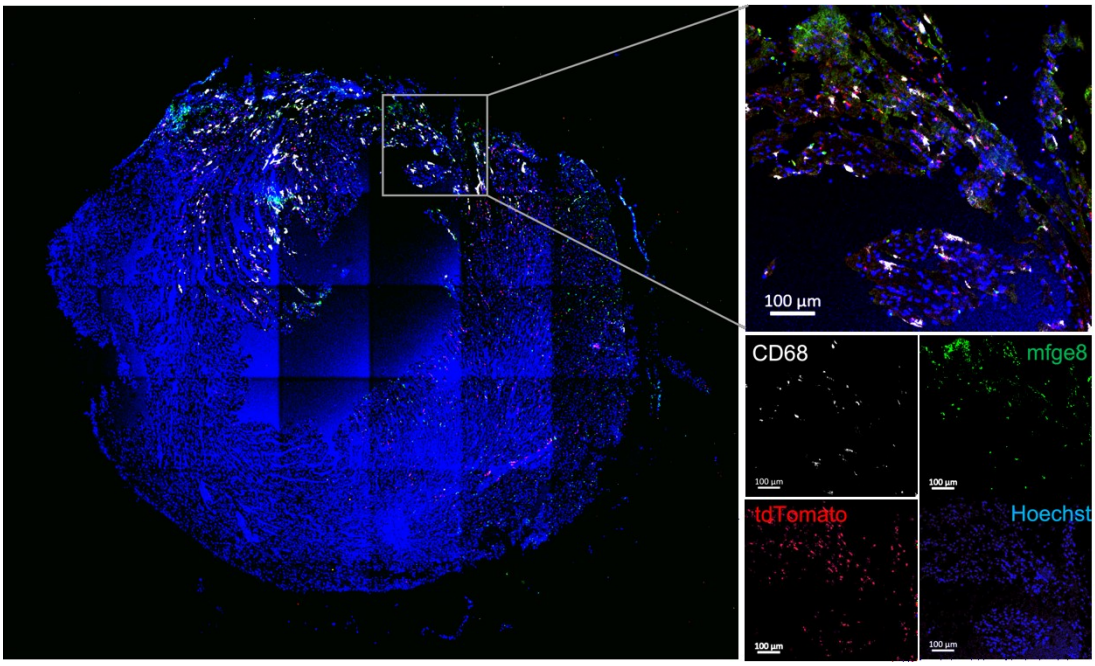

Fig. 3.4.7 Immunofluorescence staining of apoptosis in the heart after I/R for 6h.

Representative immunofluorescence staining images of colocalization of C3-tdT and cardiac macrophages in ischemic area. X20 magnification checked by confocal microscope. CD68, macrophage marker; Mfge8-GFP, apoptotic cell marker. Scale bar, 100µm.

3.4.2 Minor contribution of C3 from cardiac non-immune cells

The heart is composed of 25-35% myocytes and 65-75% non-myocytes, of which 60% are endothelial cells, approximately 20% fibroblasts, and 5-10% immune cells [71]. Evidencing from previous studies, C3 is also synthesized by endothelial cells and fibroblasts [72, 73]. Therefore, we evaluated tomato labeling on CD45 population in *C3-tdT* reporter mice in steady state and underwent I/R. Our results showed that only minor fractions of non-leukocytes in the heart expressed C3 under baseline condition. When exposed to I/R, C3 expression in non-immune cells did not increase (**Fig. 3.4.8**).

This suggested that non-immune cells played a minor role in contributing C3 after I/R.

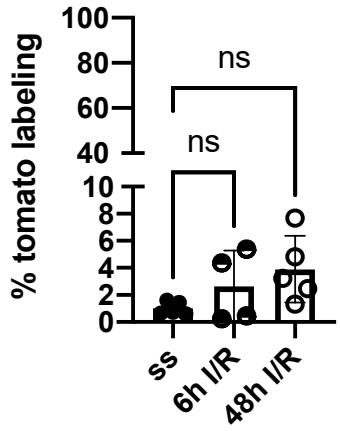

Fig. 3.4.8 Expression of C3 in non-leukocytes in the heart. Tomato labeling in CD45 population gated from live cells. Error bar, mean±SD. One-way ANOVA was performed.

3.4.3 C3 production in non-cardiovascular tissue macrophages following systemic inflammation

In response to myocardial infarction, a variety of immune cells are engaged in the inflammatory process and tissue remodeling. Thereby, a broad variety of pro/anti-inflammatory molecules are being produced and released to the circulation. This may contribute to systemic inflammation after I/R and could yield secondary complications in remote organs. Thus, we investigated whether C3 was also induced in remote tissue macrophages. We first measured C3 production in brain microglia and liver Kupfer cells. However, Kupfer cells did not alter C3 expression in response to cardiac I/R, as neither the percentage of C3 expressing Kupfer cells nor C3-tdT intensity changed in this scenario. In addition, brain microglia did not express C3-tdT in steady state or be induced after I/R, indicating that brain microglia was probably protected from blood-brain barrier and would not be affected by peripheral inflammation (**Fig. 3.4.9**).

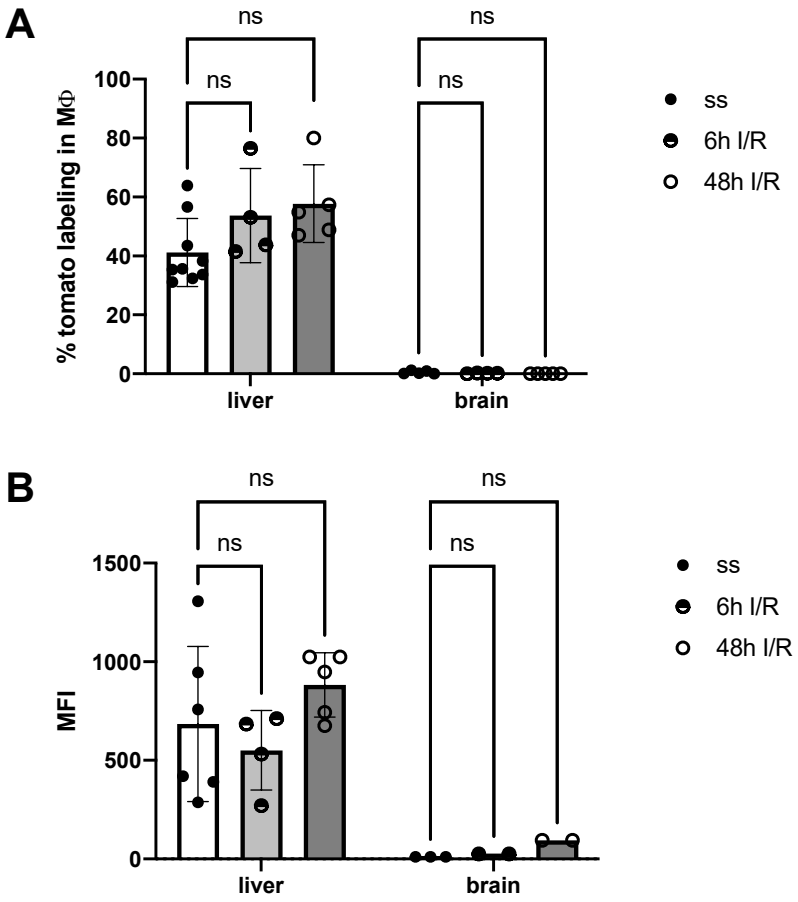

Fig. 3.4.9 Macrophage C3 expression in non-cardiovascular tissue do not respond to systemic inflammation triggered by I/R. Comparison of **A)** percentage and **B)** MFI of C3-tdT expression in tissue macrophages in steady state and after injury. Error bar, mean±SD. One-way ANOVA was performed.

3.4.4 Induction of C3 in arterial macrophages after I/R

Interestingly, we found that arterial macrophages responded to myocardial infarction with 30% increase in macrophages expressing C3 48h after reperfusion (**Fig. 3.4.10**). The induction of C3 in arterial macrophages was likely caused by monocyte recruitment or local proliferation, as the median intensity did not differ. This was in line with a previous finding that myocardial infarction will mobilize HSC cells depart from their BM niche and give rise to an increase of monocytes/macrophages in atherosclerotic plaques after being subjected to MI [74].

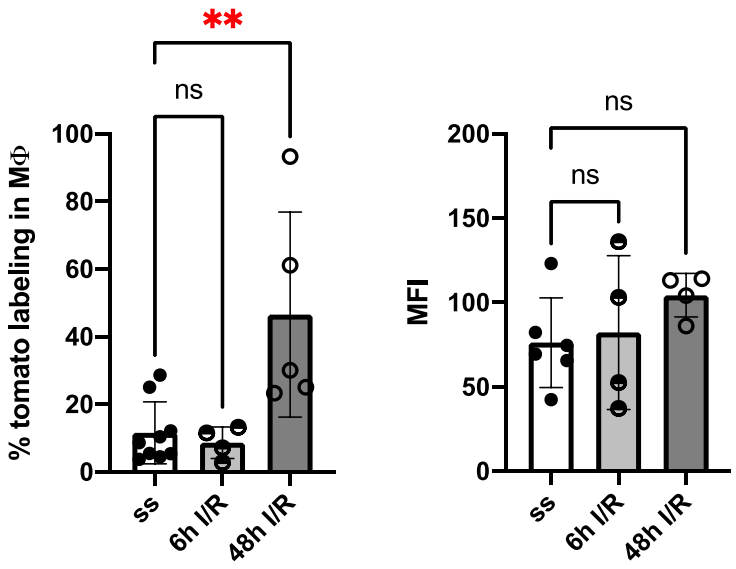

Fig. 3.4.10 Infiltration of C3 expressing arterial monocytes/macrophages after I/R. Comparison of percentage (**left**) and MFI (**right**) of C3-tdT expression in arterial macrophages in steady state and after injury. Error bar, mean±SD. One-way ANOVA was performed. **p<0.01

3.5 Assessment of C3 origin

Given the different origins of C3 outlined above, we set up whole body irradiation and BM transplantation (BMT) with congenic mice. For determination of C3 that was produced by BM derived myeloid cells, we collected BM from *C3-tdT* reporter mice (CD45.2 genetic background) and transplanted BM cells into *CD45.1* mice. This resulted in BM replacement in *CD45.1* recipient mice by CD45.2 HSCs carrying the tdT signal. Vice versa, to evaluate the contribution of serum complement to C3 levels in circulating myeloid cells as well as to assess C3-production by embryo-derived resident macrophages, we transplanted BM cells harvested from *CD45.1* mice to *C3-tdT* reporter mice, thus mostly eliminating tdT signals derived from BM (**Fig. 3.5.1**).

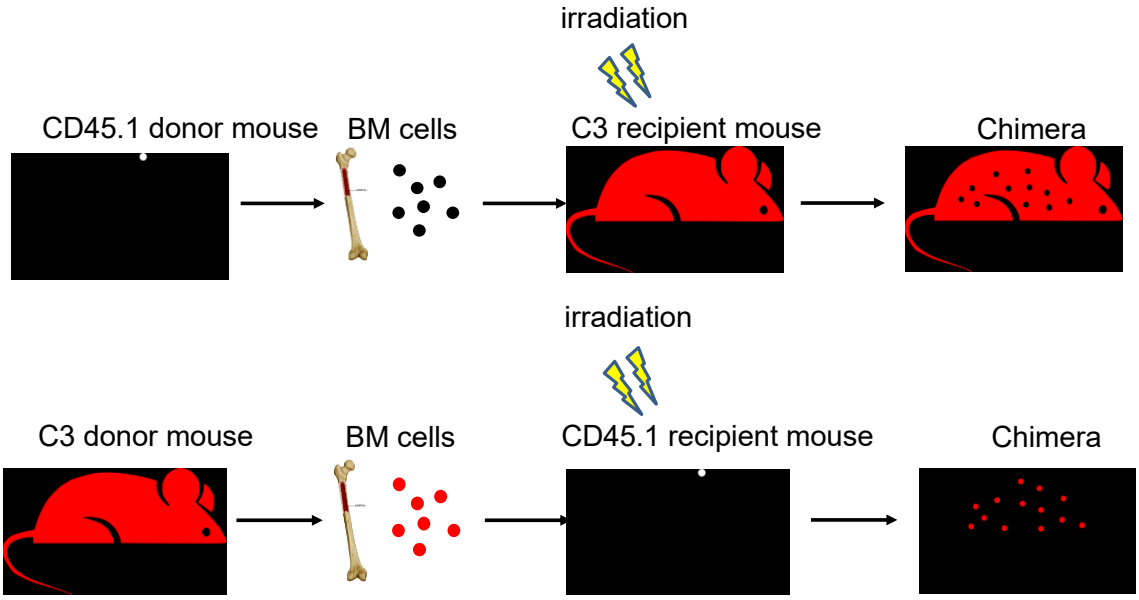

Fig. 3.5.1 Schematic illustration of BM transplantation after lethal irradiation.

We first collected blood samples from recipient mice and assessed the chimerism efficiency by flow cytometry. Successful reconstitution was defined by over 90% cells were repopulated from donor HSCs after BMT for 6 weeks (**Fig. 3.5.2**).

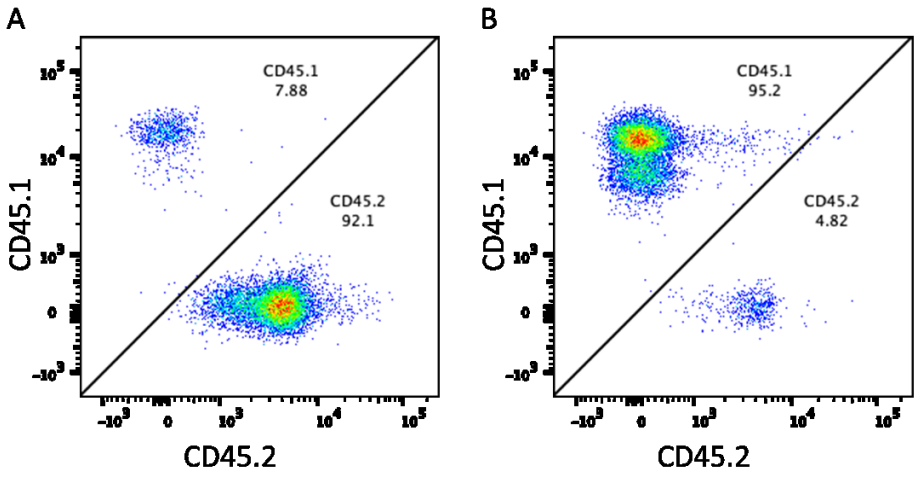

Fig. 3.5.2 Chimerism efficiency after BMT. Representative chimerism evaluated by flow cytometry. **A)** *C3-tdT* reporter mice were served as donor; *CD45.1* mice were served as recipients; **B)** *CD45.1* mice were served as donor; *C3-tdT* mice were recipients.

3.5.1 C3 contribution by BM HSCs

2 months after reconstitution with *C3-tdT* BM, flow cytometry was carried out to measure the production of C3-tdT by BM derived myeloid cells in steady state and C3-tdT regulation after I/R.

As shown in **Fig. 3.5.3**, tomato labeling was confined to CD45.2^{+} circulating myeloid cells in both steady state and after I/R injury. Worth mentioning, non-labelled CD45.1^{+} blood cells did not take up C3 from extracellular sources, neither in steady state and nor after I/R. Moreover, C3-tdT expression was exclusively detected in CD45.2 donor derived macrophages and neutrophils in the ischemic myocardium. Although macrophages and neutrophils were being mobilized in high abundance in response to acute I/R injury, no uptake of C3-tdT could be observed in CD45.1^{+} recipient derived macrophages and neutrophils. These results indicated that myeloid cells produced C3 in a cell-intrinsic manner and independently of serum complement, and that C3 was not transferred between myeloid cells.

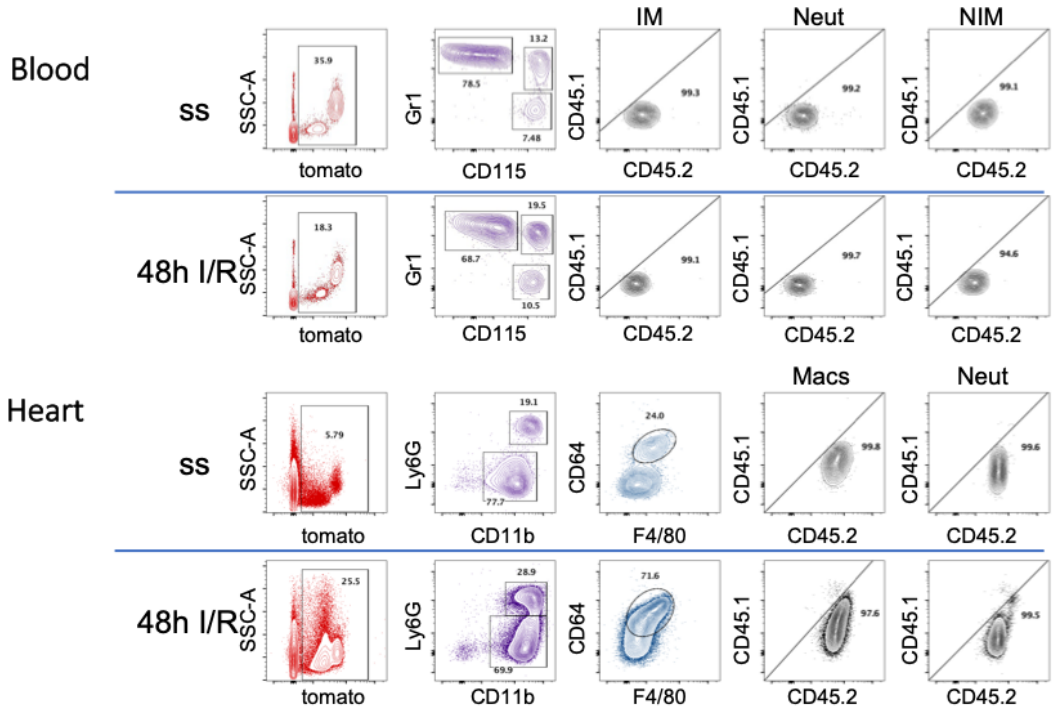

Fig. 3.5.3 No transfer of C3-tdT between myeloid cells. First gated on tomato positive cells. Within this population, gated on neutrophils and monocytes and evaluated the contribution of CD45.1 and CD45.2 origin.

We further characterized C3-tdT expression by CD45.2$^+$ myeloid cells that originated from donor HSCs and evaluated the contribution of myeloid cell derived C3 to the upregulation in cardiac macrophages after I/R. The gating strategy is shown as **Fig. 3.5.4**. We found that C3-tdT was expressed by CD45.2$^+$ blood myeloid cells to the same extent (percentage) as in non-irradiated *C3-tdT* reporter mice. When we induced I/R in these chimeric mice, we found no changes in the percentage of C3-tdT expressing CD45.2$^+$ blood myeloid cells after injury (**Fig. 3.5.5 A**), and no detectable upregulation of C3-tdT expression in myeloid cells as shown in intensity either, although we could see a significant induction of C3 expression in blood inflammatory monocytes (**Fig.3.5.5 C**). In contrast, no C3-tdT expression could be detected in CD45.1$^+$ recipient myeloid cells in the circulation under baseline condition and even post-I/R. (**Fig.3.5.5 B**)

In analogy to myeloid cells in the circulation, we detected a similar C3-tdT expression pattern in CD45.2$^+$ macrophages and neutrophils among different tissues as that in *C3-tdT* reporter mice in steady state. Notably, C3-tdT production in CD45.2$^+$ cardiac macrophages was strongly increased after I/R, indicating that BM derived cells can upregulate C3 without the input from extracellular sources. In addition, a larger proportion of arterial macrophages from CD45.2$^+$ population expressed C3-tdT post-I/R injury, which was reminiscent of our earlier studies in C3-tdT reporter mice. This further illustrated that monocytes were most likely the major contributor to the upregulation of C3-tdT in arterial macrophages. On the contrary, no upregulation of C3 was observed in liver Kupfer cells within the CD45.2$^+$ population (**Fig. 3.5.6 A and B**). Furthermore, tissue macrophages or neutrophils derived from CD45.1 donor cells did not take up C3-tdT after I/D, either (**Fig. 3.5.6 C**).

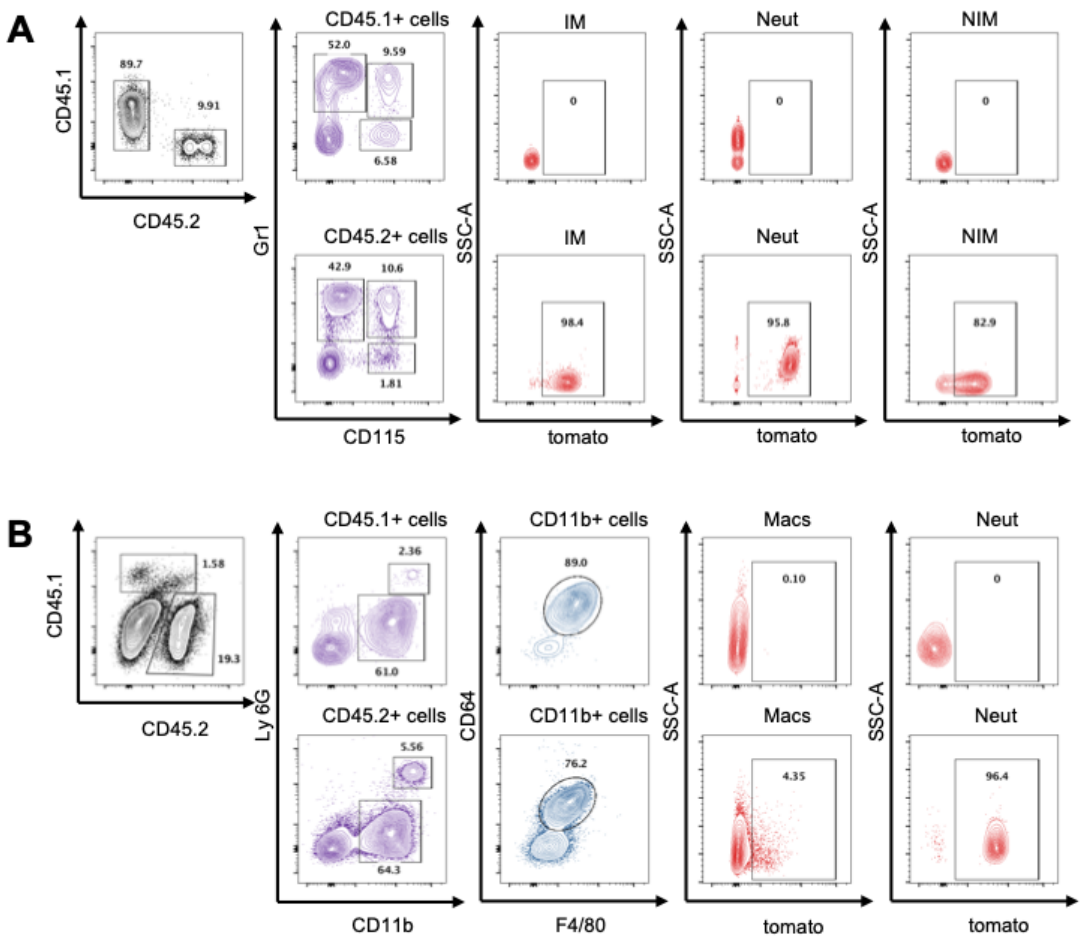

Fig. 3.5.4 Representative gating strategy for chimera mice. Data shown were obtained from **A)** blood and **B)** heart in CD45.1 recipient mice in steady state.

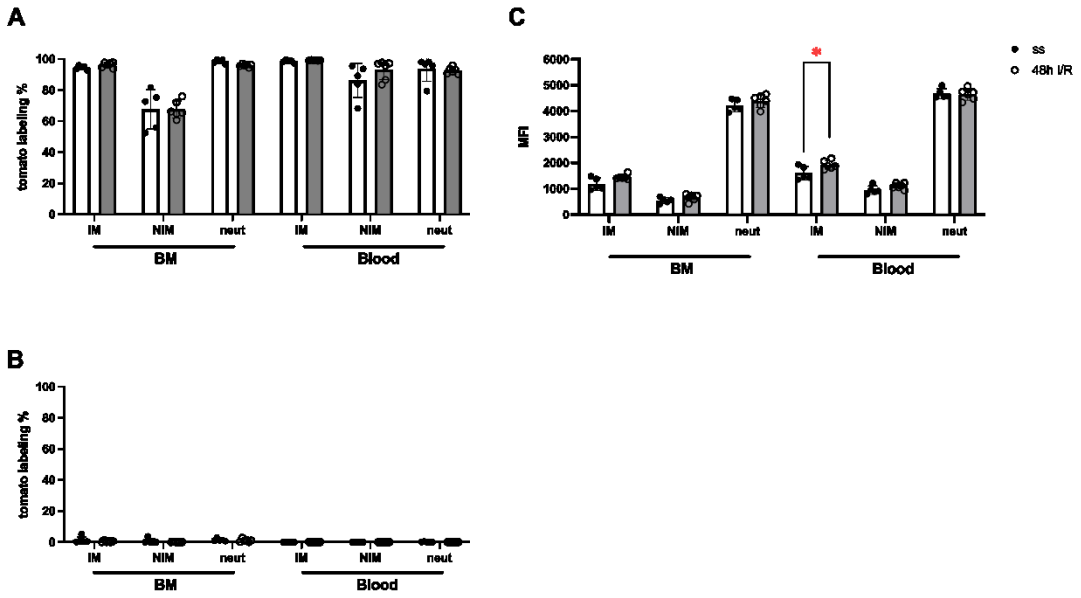

Fig. 3.5.5 No upregulation of C3 by circulating myeloid cells after I/R. Percentage of C3-tdT expression in circulating myeloid cells derived from **A)** CD45.2 donor cells and **B)** non-labelled CD45.1 recipient cells. **C)** Intensity of C3-tdT expression in CD45.2 derived myeloid cells. Steady state is indicated by the abbreviation "ss". Error bar, mean±SD. Unpaired t test between steady state and post-I/R in each population was performed. *p<0.05.

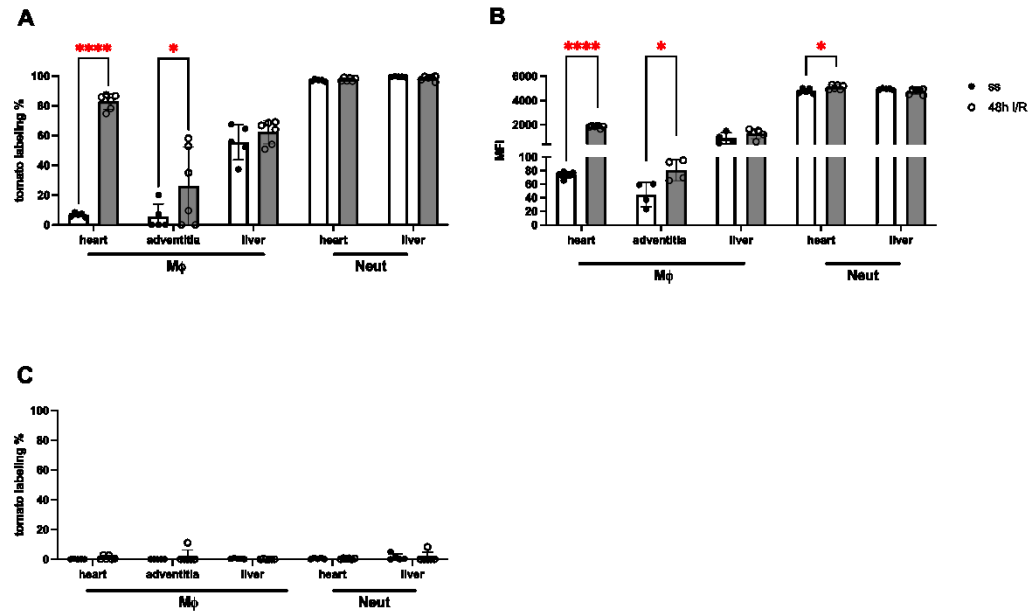

Fig. 3.5.6 Cardiac macrophages produce C3 after I/R. A) Percentage and **B)** intensity of C3-tdT expression in tissue macrophages and neutrophils derived from CD45.2 donor cells; **C)** Percentage of C3-tdT expression in non-labelled CD45.1 recipient derived macrophages and neutrophils. Unpaired t test between steady state and post-I/R in each population was performed. *p<0.05; ****p<0.0001.

Previous studies have shown that cardiac macrophages provide distinct functions and hence can be differentiated into subsets. Further, tissue macrophages can be segregated into two populations based on their distinct origins: BM HSC derived macrophages and YS EMP derived macrophages. Being predominant in the steady-state heart, EMP derived macrophages play a key role in sustaining homeostasis as they execute anti-inflammatory properties. They self-renew by local proliferation and maintain their populations independently of BM HSC. In contrast, BM derived populations are continuously supplemented from circulation and provide their pro-inflammatory functions [26, 28, 75]. Both populations are regarded as tissue resident macrophages after a certain time [76]. In the scenario of BM chimera experiments, mice were sacrificed more than 2 months post-BMT. By that time, some $CD45.2^+$ donor monocytes have populated the heart and contributed to tissue resident macrophages to minor extent, whereas $CD45.1^+$ host macrophages were largely of YS origin. The increase in $CD45.2^+$ cardiac macrophages could be due to monocyte recruitment from blood and further proliferation of monocyte-derived macrophages in the tissue.

Taken together, these results provide important insights into C3 production by circulating myeloid cells independently of extracellular sources. Meanwhile no transfer of C3 took place between myeloid cells in the circulation and in tissues, with and without injury. Recruited monocytes in the injured heart post-I/R could contribute to providing C3 as cardiac macrophages.

3.5.2 C3 generation by tissue myeloid cells

Given that a large proportion of BM derived myeloid cells is capable of producing C3, we asked whether tissue myeloid cells could also generate the complement factor. Therefore, we investigated tomato expression in irradiated C3-tdT reporter mice that were engrafted with BM from *CD45.1* mice. Consequently, tomato labeling would be largely absent in circulating myeloid cells while host derived C3-expressing cells would be tomato positive.

In line with our previous findings, only CD45.2^{+} myeloid cells expressed C3-tdT in steady state, both in the circulation and tin issues. Of note, CD45.1^{+} donor derived cells replaced the recipient BM hematopoiesis and therefore constituted the majority of hematopoietic cells. After mice subjected to I/R, circulating myeloid cells were mobilized from reservoirs and recruited to the injured myocardium as expected. These recruited monocytes differentiated to inflammatory macrophages and phagocytosed apoptotic cells and their debris. However, they did not pick C3-tdT up from serum or from phagocytosing C3-tdT expressing neutrophils either. While CD45.1^{+} tissue macrophages and neutrophils were lacking the tomato signal in steady state, they internalized C3-tdT from surrounding environment, which potentially derived from hepatocytes, when triggered by I/R related inflammation (**Fig. 3.5.7**).

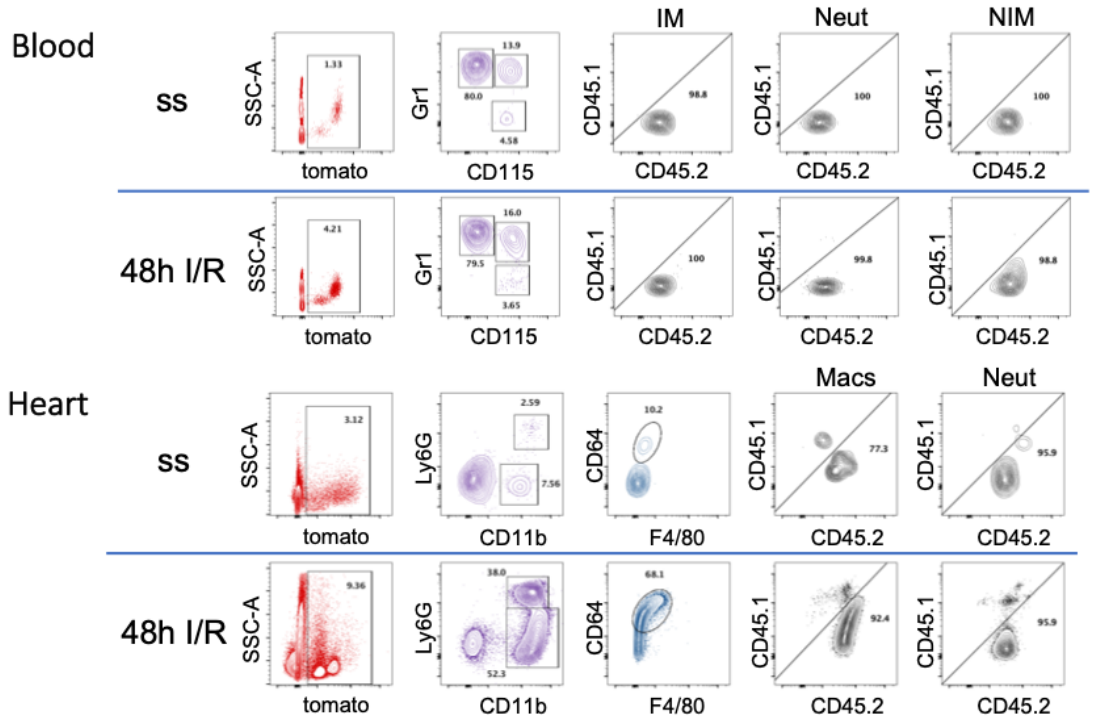

Fig. 3.5.7 Few tissue macrophages and neutrophils uptake C3 from extracellular environment. Tomato^{+} cells were first gated on live cells. Within this population, monocytes and neutrophils were separated by differential expression of Gr1 and CD115 in the blood, macrophages and neutrophils in the heart were defined by CD11b^{+}Ly6GF4/80^{+}CD64^{+} and CD11b^{hi}Ly6G^{+}, respectively. Thereafter, CD45.1 against CD45.2 were gated to determine relative donor and host contributions.

To further examine tissue resident macrophages response after I/R in more detail, we extended analysis as shown in **Fig. 3.5.8**. As assessed by flow cytometry, around 10% of CD45.2^{+} cardiac macrophages expressed tomato in steady state, which was a similar proportion as quantified in non-chimeric *C3-tdT* reporter mice. Moreover, cardiac macrophages increased expression of C3 both in percentage and intensity after 48h I/R injury (**Fig. 3.5.8 A and B**). Since host cardiac macrophages in this chimeric setting were mostly of YS origin, this indicated that tissue-resident macrophages derived from prenatal hematopoiesis could also produce C3, similarly to HSCs. After I/R, only a small proportion of cardiac macrophages derived from CD45.1^{+} cells incorporated C3-tdT from extracellular sources (**Fig. 3.5.8 C**), further indicating that the increase of C3-tdT in CD45.2^{+} cardiac macrophages after 48h reperfusion was due to intrinsic production by resident macrophage. However, an unanticipated finding was shown in the liver, as BM derived CD45.1^{+} liver macrophages and neutrophils picked up C3-tdT not only in steady state but also after I/R, which was distinct from other tissue macrophages (**Fig. 3.5.8 C**). The explanation for this is unknown, however it could be related to the anatomic location of liver macrophages. They reside in the liver sinusoids in close vicinity to hepatocytes, and thus might have directly taken up liver-produced C3.

In the circulation, CD45.2 recipient derived myeloid cells constituted only approximately 5% of whole circulating cells, however the majority of them carried C3-tdT. This signal was not altered by I/R injury (**Fig. 3.5.9 A and B**). Meanwhile, CD45.1 donor derived myeloid cells did not uptake C3 from serum under baseline condition and post-I/R (**Fig. 3.5.9.C**).

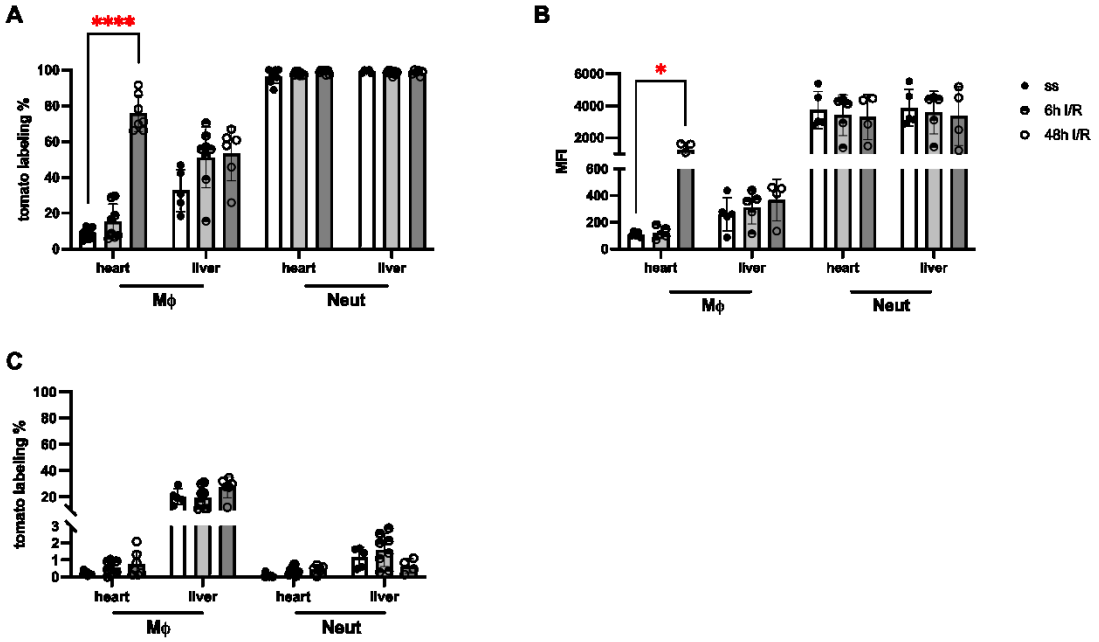

Fig. 3.5.8 Cardiac tissue macrophages produce C3 after I/R. A) Percentage and **B)** intensity of C3-tdT expression in tissue macrophages and neutrophils derived from CD45.2 recipient cells; **C)** percentage of C3-tdT expression in tissue macrophages and neutrophils derived from CD45.1 donor cells. Error bar, mean±SD. One-way ANOVA with multiple comparisons was performed. *p<0.05; ****p<0.0001.

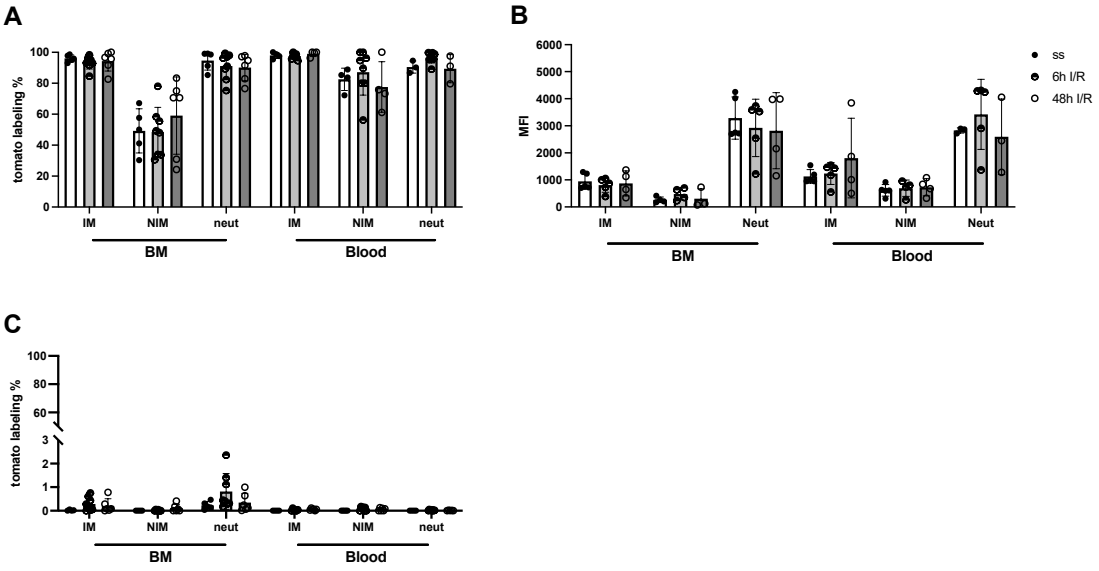

Fig. 3.5.9 No uptake of C3-tdT in myeloid cells from serum. A) Percentage and **B)** intensity of C3-tdT expression in CD45.2 derived circulating myeloid cells; C) percentage of C3-tdT expression in CD45.1 derived circulating myeloid cells under baseline condition and after I/R injury. Error bar, mean±SD. One-way ANOVA with multiple comparisons was performed.

In summary, the experiments conducted in chimeric mice showed that both BM and YS derived macrophages produced C3 and contributed to the upregulation of C3 in cardiac macrophages. The uptake of C3 from extracellular sources was minimal in both steady state or I/R.

3.6 Kinetics of C3 production and of macrophages

As a next step, we measured both the percentage of C3-tdT production in macrophages as well as the absolute quantity of macrophages in the wounded myocardial area following I/R in a time series, to investigate the potential link between C3 production and increased macrophage accumulation in the heart. The absolute number of macrophages strongly increased from 24h post-I/R, remained elevated at high levels for several days, and then normalized after 1 week. Notably, both the fraction of C3-tdT expressing macrophages as well as C3-tdT intensity in individual macrophages, which indicated cellular production, increased 24 hours after I/R. The peak of the C3 signal was reached after 2 days, and then declined after 1 week (**Fig. 3.6.1**).

In summary, the time course analysis indicated that C3 production was triggered in resident macrophages by I/R, leading to increased fraction and intensity of C3 in cardiac macrophages within 24h of ischemic injury. From day 2 post I/R, monocyte-derived macrophages that were recruited in large numbers to the infarct zone contributed to providing C3 in the first week after I/R. As indicated by comparing MFI values at day 7, macrophage C3 production was temporally controlled and restricted to the first week of postischemic inflammation.

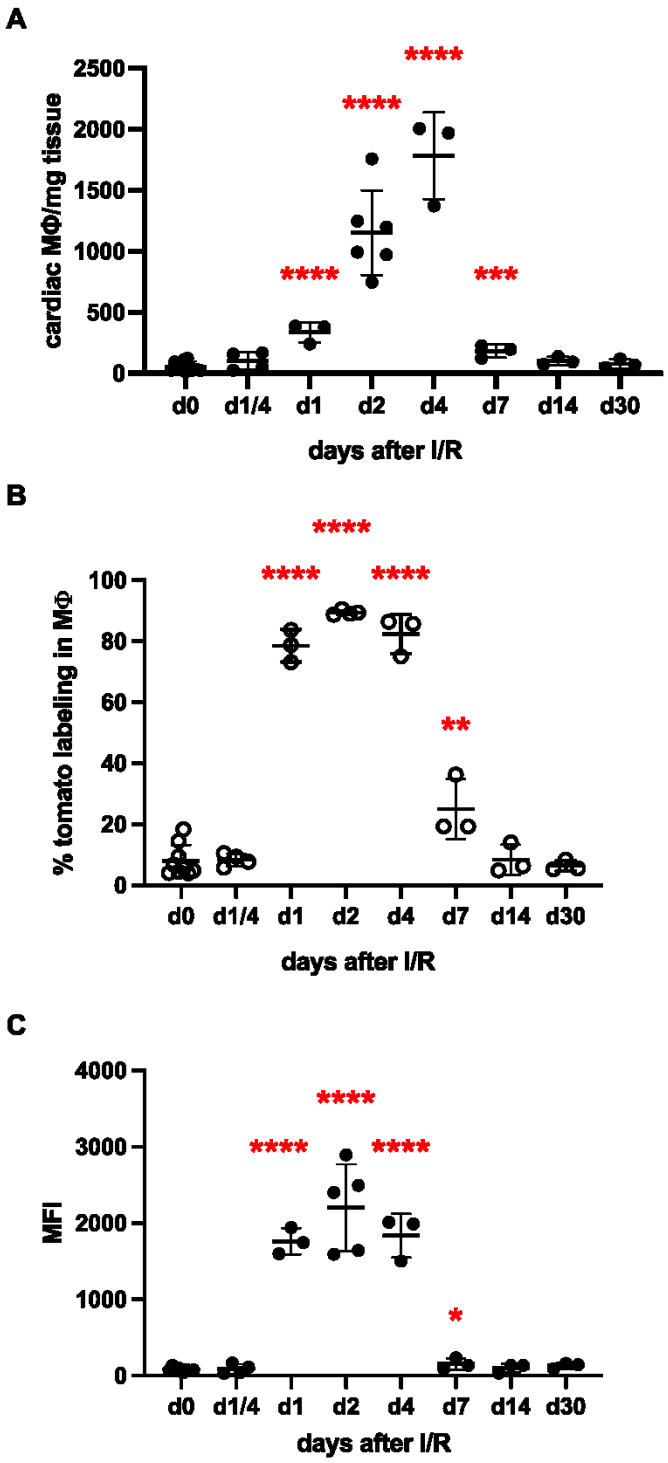

Fig. 3.6.1 Kinetics of C3 production. Percentage **A**) and MFI **B**) of tomato labeling in cardiac macrophages after I/R injury. **C**) Absolute number of cardiac macrophages per mg tissue. Error bar, mean±SD. Unpaired t-test between each time point post-I/R and steady state was performed. *p<0.05; **p<0.01; ***p<0.001; ****p<0.0001.

3.7 Cell specific deletion of C3-tdT

Given that HSC-derived myeloid cells and tissue resident macrophages provided intrinsic C3 in response to inflammation, we next explored whether the complement factor produced by individual cell types had an impact on the extent of myocardial injury and the myocardial healing process. We harnessed the conditional Cre/loxp system to target specific immune cell populations by deletion of loxp-flanked genes in a cre-dependent manner. Thus, we established three different conditional deletion models to deplete C3 in tissue resident macrophages, BM derived myeloid cells, or neutrophils.

Rank (also known as Tnfrsf11a) is a cytokine receptor expressed in tissue macrophages. Studies have demonstrated the efficient labeling of YS EMP-derived resident macrophages in *Rank^{cre}; Rosa26$^{LSL\text{-}YFP}$* mice [60]. LysM (M lysozyme) is expressed in the myeloid lineage of HSC progeny, specifically monocytes/macrophages and neutrophils [77]. Mrp8 strongly marks granulocytes and a small proportion of monocytes, but not tissue macrophages [78-80]. Therefore, we cross mated *Rank^{cre}*, *LysM^{cre}*, and *Mrp8^{cre}* mice with *C3-tdT* reporter mice for several generations. We then employed homozygous *C3-tdT* reporter with heterozygous Cre mice for further experiments. Under the control of specific promoters and Cre activation, C3-tdT was then depleted conditionally in respective cell populations. To characterize the deletion efficacy of C3-tdT in conditional knock-out mice, we conducted flow cytometry and measured the MFI of tomato labeling in target cells, then compared it with *C3-tdT* reporter mice lacking Cre-mediated recombination.

As described before, few tissue resident macrophages produced C3 in steady state, but I/R induced C3 in most cardiac macrophages. Therefore, we applied I/R to *Rank$^{\Delta C3}$* mice, in which expression of C3-tdT remained significantly reduced after cardiac injury (**Fig. 3.7.1**).

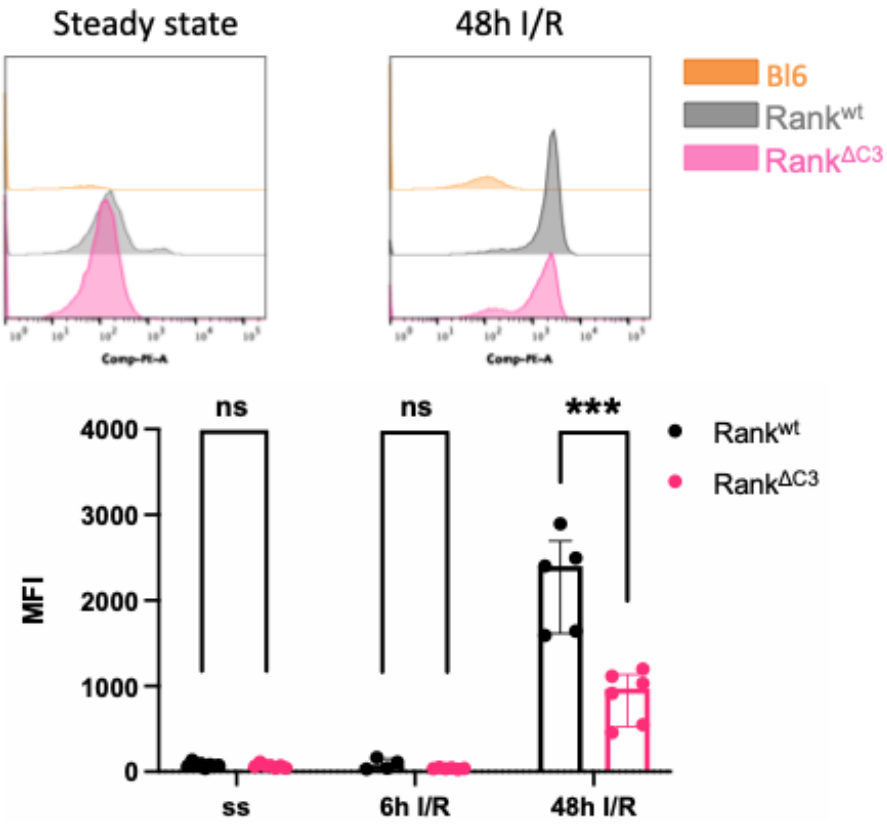

Fig. 3.7.1 Reduction of intracellular C3 in cardiac macrophages in *Rank$^{\Delta C3}$* mice upon I/R injury. Assessment of C3-tdT expression in cardiac macrophages with and without I/R injury by flow cytometry. Error bar, mean±SD. Unpaired t test between *Rank$^{\Delta C3}$* mice was performed. ***p<0.001.

Further, we assessed the deletion efficacy of C3-tdT expression in *LysM$^{\Delta C3}$* and *Mrp8$^{\Delta C3}$* mice. Approximately 50% reduction of C3-tdT was observed in both monocytes and neutrophils in *LysM$^{\Delta C3}$* mice. With regards to *Mrp8$^{\Delta C3}$* mice, C3-tdT production was diminished in the circulating neutrophils as expected. Interestingly, C3-tdT deletion in circulating monocytes was comparable with that of *LysM$^{\Delta C3}$* mice (**Fig. 3.7.2**). We further measured the intensity of C3-tdT in macrophages and neutrophils of cardiac tissue. A significant decrease of C3-tdT expression was found in cardiac macrophages in *LysM$^{\Delta C3}$* mice but not in neutrophils. While *Mrp8$^{\Delta C3}$* mice depleted C3-tdT expression in both circulating monocytes and neutrophils, only cardiac neutrophils displayed reduction of C3-tdT whereas C3 expression in cardiac macrophages was unaltered (**Fig. 3.7.3 and 3.7.4**). Taken together, *LysM$^{\Delta C3}$* mice

provided intermediate deletion efficacy in myeloid cells, whereas *Mrp8*$^{\Delta C3}$ mice efficiently ablated C3 in neutrophils, specifically in cardiac tissue.

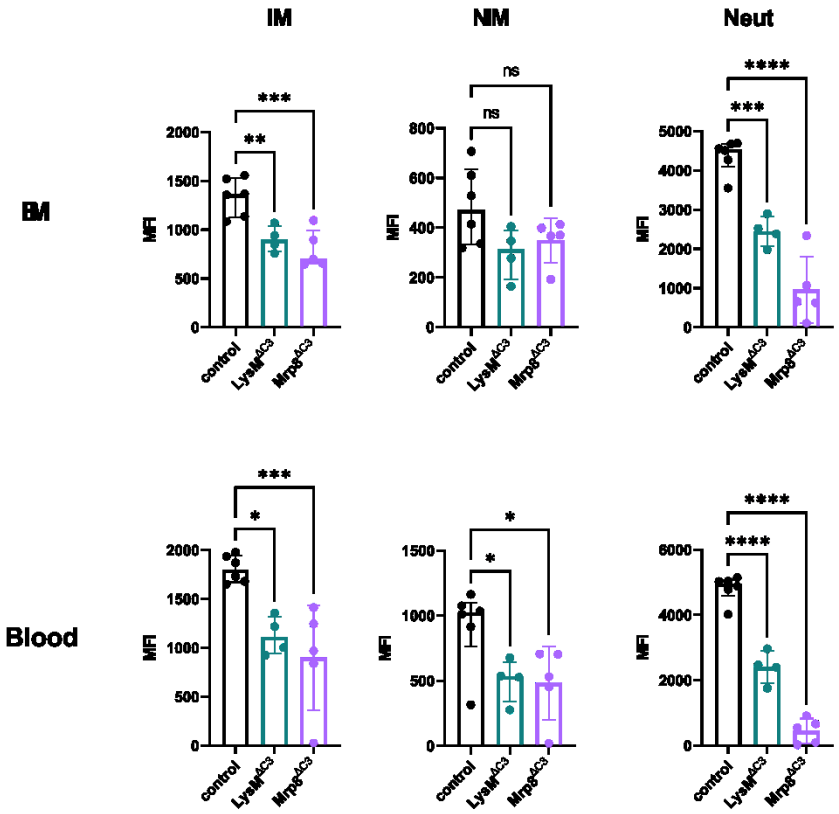

Fig. 3.7.2 Reduction of intracellular C3 in circulating myeloid cells in *LysM*$^{\Delta C3}$ and *Mrp8*$^{\Delta C3}$ mice in steady state. Assessment of C3-tdT expression in circulating myeloid cells in *LysM*$^{\Delta C3}$ (n=4) and *Mrp8*$^{\Delta C3}$ (n=5) mice by flow cytometry. Error bar, mean±SD. One-way ANOVA was performed. *p<0.05; **p<0.01; ***p<0.001; ****p<0.0001.

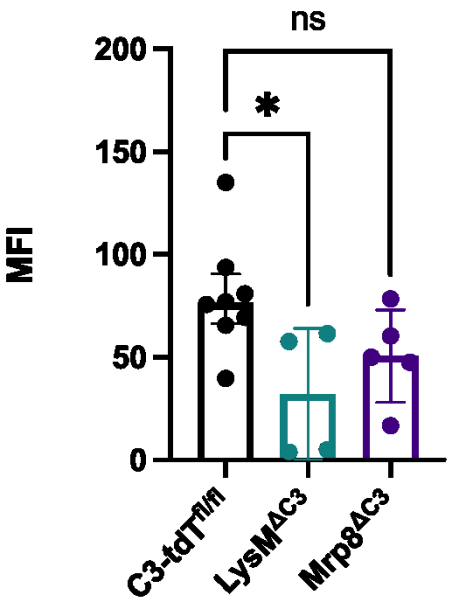

Fig. 3.7.3 Reduction of intracellular C3 in cardiac macrophages in *LysM*$^{\Delta C3}$ and *Mrp8*$^{\Delta C3}$ mice in steady state. Assessment of C3-tdT expression in cardiac macrophages in steady state by flow cytometry. Error bar, mean±SD. One-way ANOVA was performed. *p<0.05.

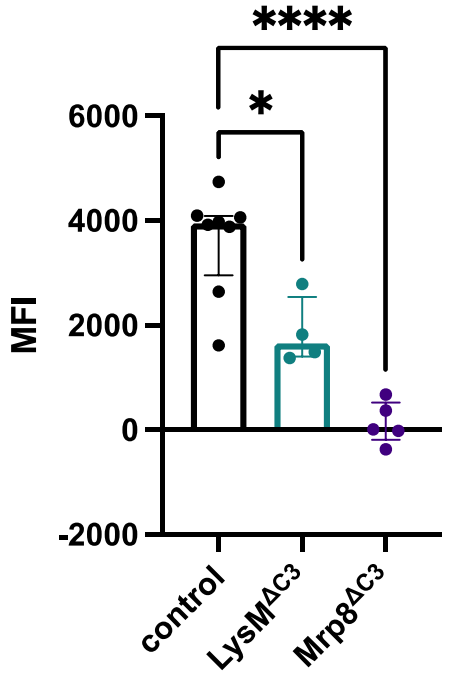

Fig. 3.7.4 Reduction of intracellular C3 in cardiac neutrophils in *LysM*$^{\Delta C3}$ and *Mrp8*$^{\Delta C3}$ mice in steady state. Assessment of C3-tdT expression in cardiac neutrophils in steady state by flow cytometry. Error bar, mean±SD. One-way ANOVA was performed. *p<0.05; ****p<0.0001.

3.7.1 C3 depletion in neutrophils

Since we found identified production of C3 in neutrophils and neutrophil-specific C3 deletion mice successfully reduced C3 expression in both circulating neutrophils as well as cardiac neutrophils, we aimed to determine the role of neutrophil-derived C3 in myocardial injury. First, we subjected *Mrp8*$^{\Delta C3}$ mice to I/R and investigated cardiac remodeling by non-invasive PET imaging at day 6 and day 30 post-I/R. Infarct size was characterized by diminished 18F-FDG uptake and represented by the ratio of extent and severity of hypoperfusion to total myocardial volume. We did not detect any difference in infarct size between control and *Mrp8*$^{\Delta C3}$ mice. In addition, the left ventricular metabolic volume (LVMV) that positively correlates with the increase of cardiac muscle mass, and %ID/g that resembles the ratio of 18F-FDG activity in the myocardium to the activity of radiotracer injected, did not show any difference either (**Fig. 3.7.5**).

We also performed WGA staining to measure myocardial fibrosis after 30 days of I/R. In line with the infarct size collected from PET-CT, we found no difference with regards to the extent of fibrosis (**Fig. 3.7.6**).

Furthermore, cardiac function parameters including EDV, ESV, SV and LVEF were not different between these mice after I/R injury (**Fig. 3.7.7**). And neither infarct size, metabolism, or left ventricular function was altered from day 6 to day 30 (**Fig. 3.7.8**).

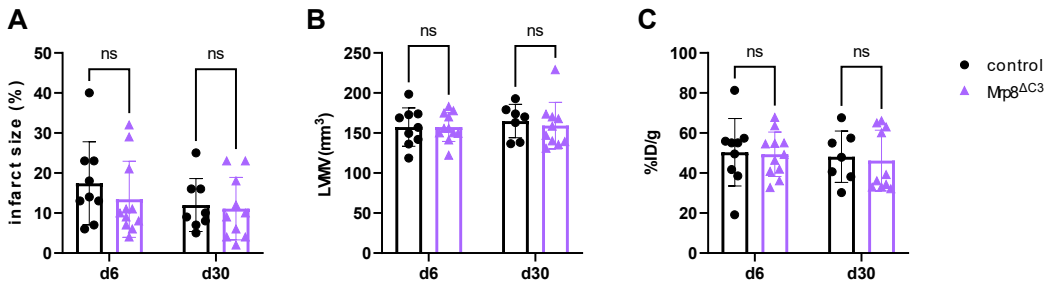

Fig. 3.7.5 Myocardial perfusion parameters in *Mrp8*$^{\Delta C3}$ mice undergoing I/R injury. A) TPD; **B)** LVMV and **C)** cardiac %ID/g in *Mrp8*$^{\Delta C3}$ and control mice was assessed by in vivo PET-CT imaging at day 6 and day 30 post-I/R. Error bar, mean±SD. Multiple unpaired t-tests were performed.

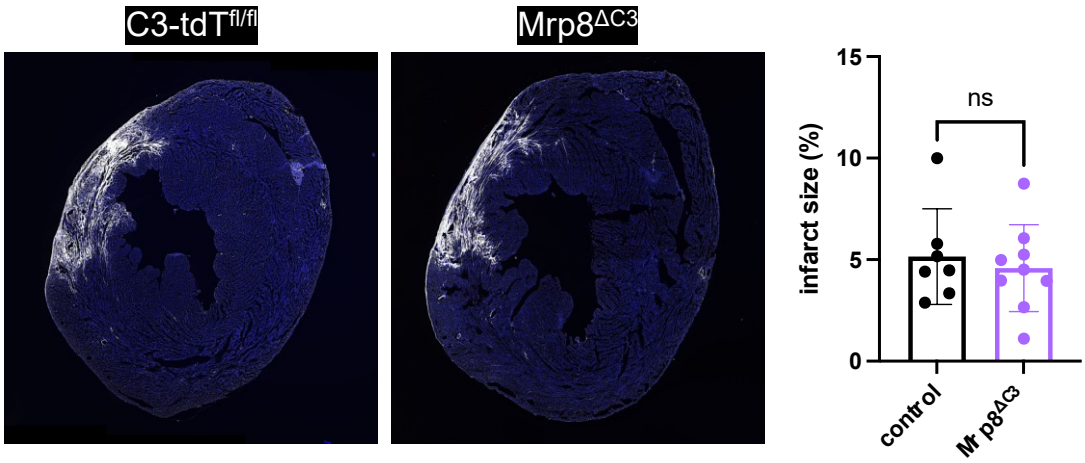

Fig. 3.7.6 Fibrosis in *Mrp8*$^{\Delta C3}$ mice undergoing I/R was evaluated by WGA staining. Left, representative immunofluorescence image obtained from epifluorescence microscope. **Right**, quantification of ratio of fibrotic area to whole heart area, assessed by Image J. Error bar, mean±SD. Unpaired t test was performed.

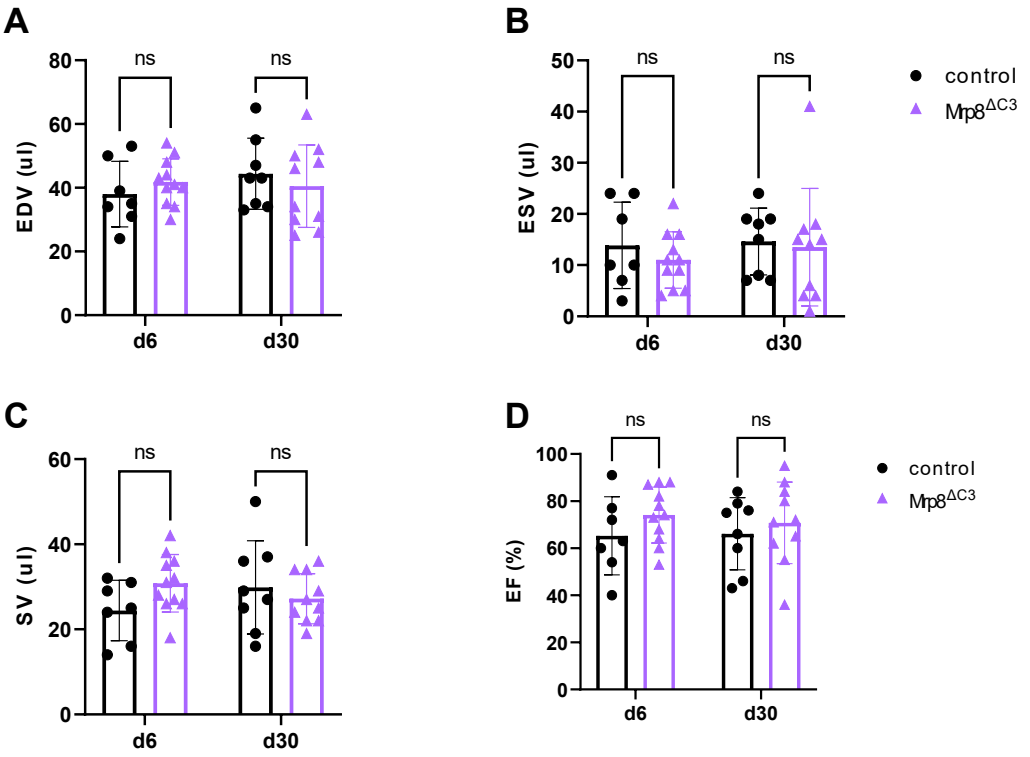

Fig. 3.7.7 Cardiac function parameters in *Mrp8*$^{\Delta C3}$ after I/R. A) EDV; **B)** ESV; **C)** SV and **D)** EF in *Mrp8*$^{\Delta C3}$ and control mice was assessed by in vivo PET-CT imaging

at day 6 and day 30 post-I/R. Error bar, mean±SD. Multiple unpaired t-tests were performed.

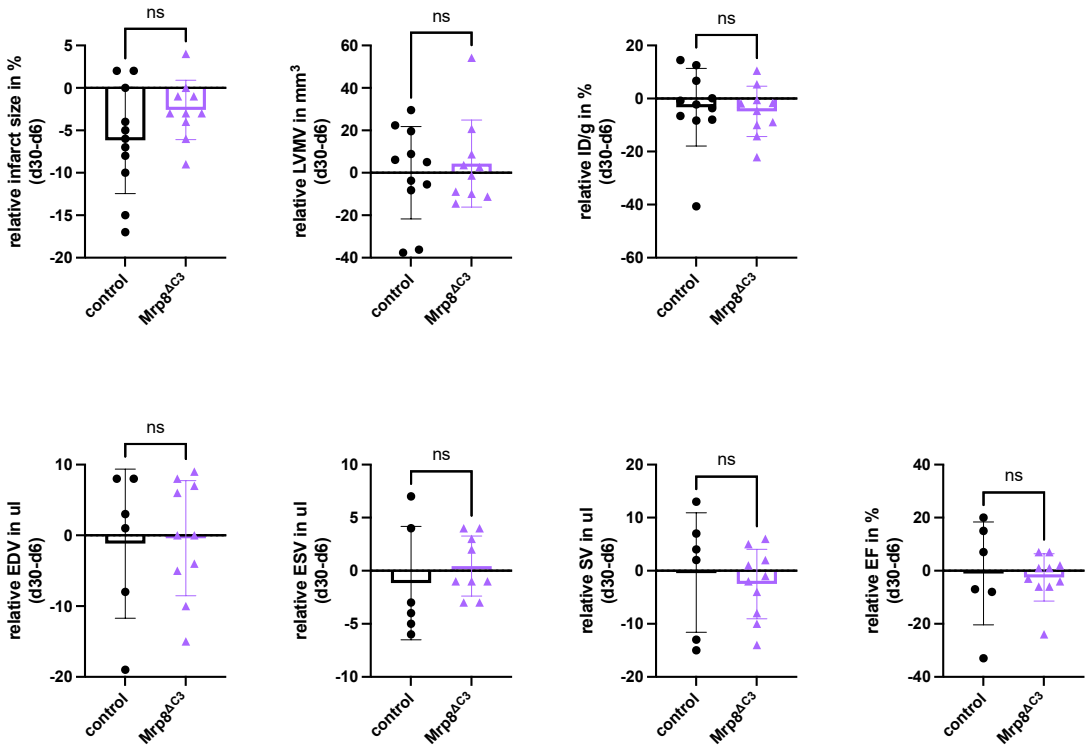

Fig. 3.7.8 Cardiac remodeling in *Mrp8*$^{\Delta C3}$ mice after I/R. Intraindividual change of different parameters in *Mrp8*$^{\Delta C3}$ (n=6-9) and control (n=9) from d6 to d30 after I/R measured with PET-CT. Error bar, mean±SD. Unpaired t-test was performed in each comparison.

To increase the extent of myocardial injury, we performed permanent LAD ligation on neutrophil specific C3 deletion mice to mimick chronic infarction in humans. We did not find difference in infarct size. Contrary to previous studies, cardiac %ID/g was normally heightened in acute phase, there was a significant increase of cardiac %ID/g in *Mrp8*$^{\Delta C3}$ mice in late phase, at day 30 post-MI. This could represent high demand for glucose in *Mrp8*$^{\Delta C3}$ mice even at late phase after injury (**Fig. 3.7.9**).

Associated with perfusion loss, we did not observe difference with regards to cardiac function parameters between neutrophils derived C3-present and C3-absent mice (**Fig. 3.7.10**).

Intraindividual changes of these parameters were also assessed. In parallel to insignificant difference in infarct size and cardiac function between *Mrp8*$^{\Delta C3}$ mice and littermates, there was no influence on cardiac remodeling in neutrophil specific C3

deletion mice from day 6 to day 30 post-MI. Even though we found an extremely increase in cardiac %ID/g in *Mrp8*$^{\Delta C3}$ mice compared to littermates, the relative elevation was not distinctive (**Fig. 3.7.11**).

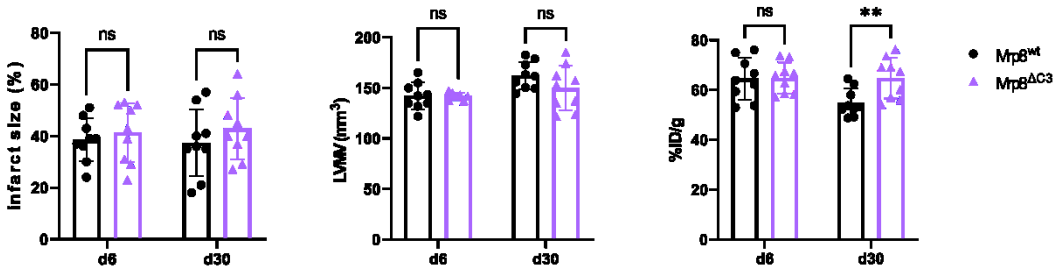

Fig. 3.7.9 Myocardial perfusion parameters in *Mrp8*$^{\Delta C3}$ mice undergoing chronic MI. A) TPD; **B)** LVMV and **C)** cardiac %ID/g in *Mrp8*$^{\Delta C3}$ and *Mrp8*^{wt} littermate mice was assessed by in vivo PET-CT imaging at day 6 and day 30 post-MI. Error bar, mean±SD. Multiple unpaired t-tests were performed. **p<0.01.

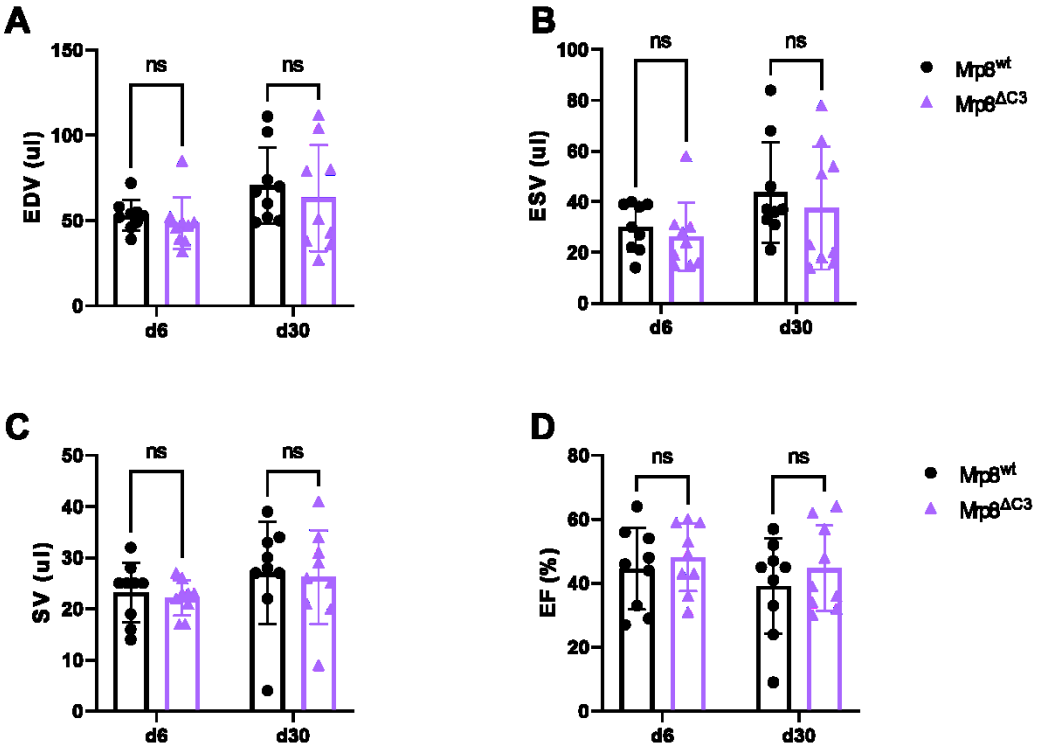

Fig. 3.7.10 Cardiac function parameters in *Mrp8*$^{\Delta C3}$ mice after chronic MI. A) EDV; **B)** ESV; **C)** SV and **D)** EF in *Mrp8*$^{\Delta C3}$ and *Mrp8*^{wt} littermate mice was assessed by in vivo PET-CT imaging at day 6 and day 30 post-MI. Error bar, mean±SD. Multiple unpaired t-tests were performed.

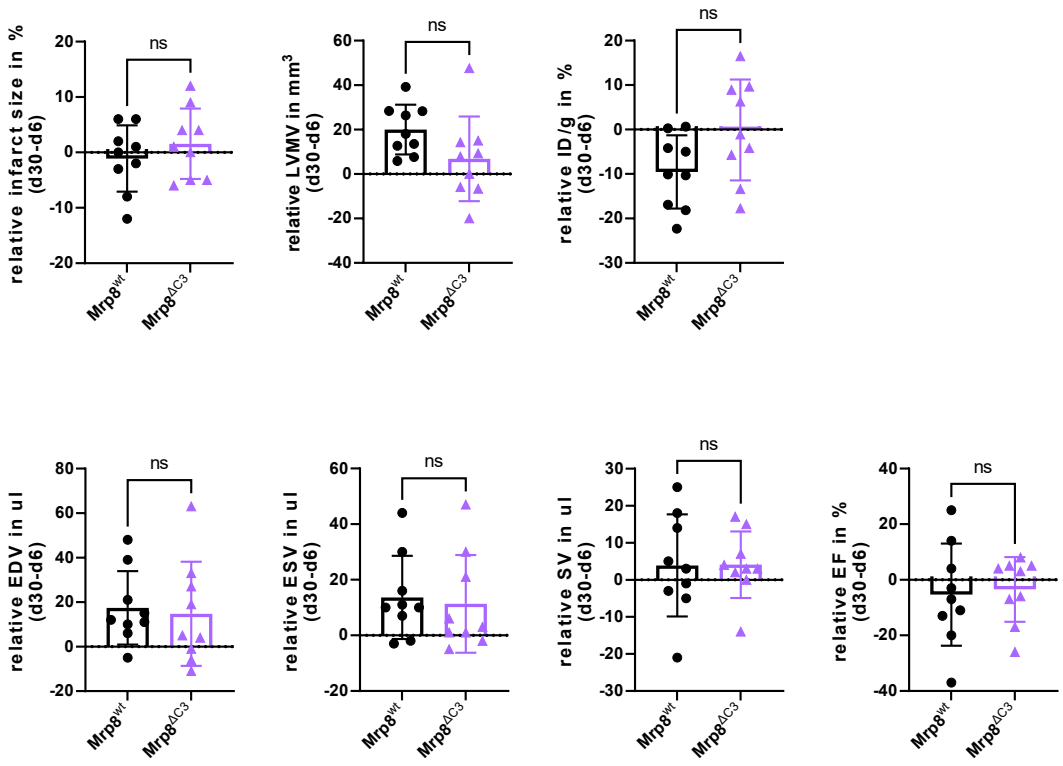

Fig. 3.7.11 Cardiac remodeling in *Mrp8$^{\Delta C3}$* after MI. Intraindividual change of different parameters in *Mrp8$^{\Delta C3}$* (n=9) and *Mrp8^{wt}* littermates (n=9) from d6 to d30 after MI measured with PET-CT. Error bar, mean±SD. Unpaired t-test was performed in each comparison.

Taken together, neutrophil derived C3 provided minor contribution in myocardial injury and cardiac remodeling, even though they have great abundance of C3.

3.7.2 C3 deficiency in BM derived myeloid cells

Then, we aimed to investigate the role of myeloid cell derived C3 during myocardial injury. We therefore assessed cardiac remodeling in I/R and chronic infarction in *LysM$^{\Delta C3}$* mice.

As compared to control mice, the infarct size was not changed in *LysM$^{\Delta C3}$* mice 6 days and 30 days after I/R. Similarly, hypoperfusion volume showed no alteration in *LysM$^{\Delta C3}$* mice. Again, no difference was observed regarding LVMV and cardiac %ID/g between *control* mice and *LysM$^{\Delta C3}$* mice (**Fig. 3.7.12**). Meanwhile, no

difference was found in fibrosis checked by staining WGA in heart sections 30 days after I/R (**Fig. 3.7.13**).

As to be expected from infarct size, cardiac functional analysis showed no differences regarding EDV, ESV, SV, and LVEF between *control* mice and *LysM*$^{\Delta C3}$ mice (**Fig. 3.7.14**).

As regards to relative change from day 6 to day 30 post-I/R, we found no difference in both *LysM*$^{\Delta C3}$ and control mice (**Fig. 3.7.15)**.

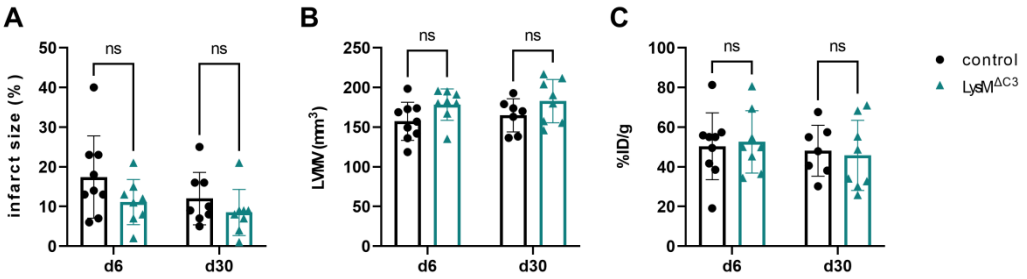

Fig. 3.7.12 Myocardial perfusion parameters in *LysM*$^{\Delta C3}$ mice undergoing I/R. A) TPD; **B)** LVMV and **C)** cardiac %ID/g in *LysM*$^{\Delta C3}$ and control mice was assessed by in vivo PET-CT imaging at day 6 and day 30 post-I/R. Error bar, mean±SD. Multiple unpaired t-tests were performed.

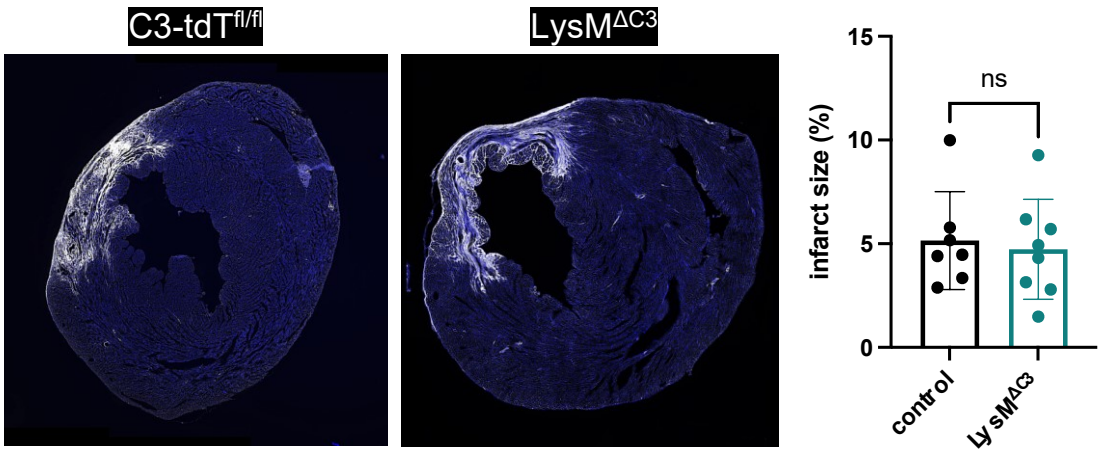

Fig. 3.7.13 Fibrosis in *LysM*$^{\Delta C3}$ undergoing I/R was evaluated by WGA staining. **Left**, representative immunofluorescence image obtained from epifluorescence microscope. **Right**, quantification of ratio of fibrotic area to whole heart area, assessed by Image J. Error bar, mean±SD. Unpaired t test was performed.

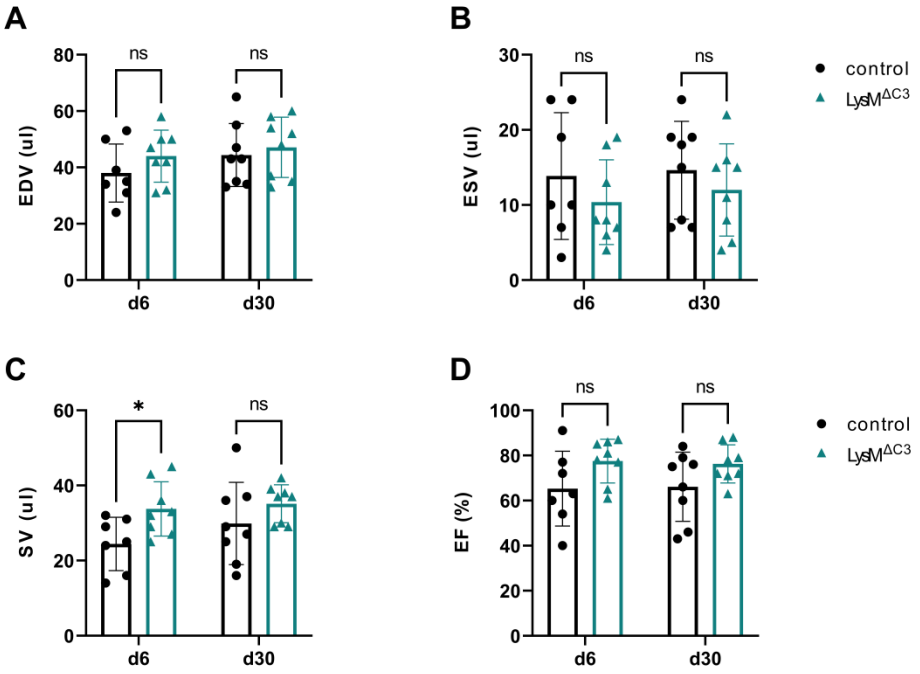

Fig. 3.7.14 Cardiac function parameters in *LysM$^{\Delta C3}$* mice after I/R. A) EDV; **B)** ESV; **C)** SV and **D)** EF in *LysM$^{\Delta C3}$* and control mice was assessed by in vivo PET-CT imaging at day 6 and day 30 post-I/R. Error bar, mean±SD. Multiple unpaired t-tests were performed.

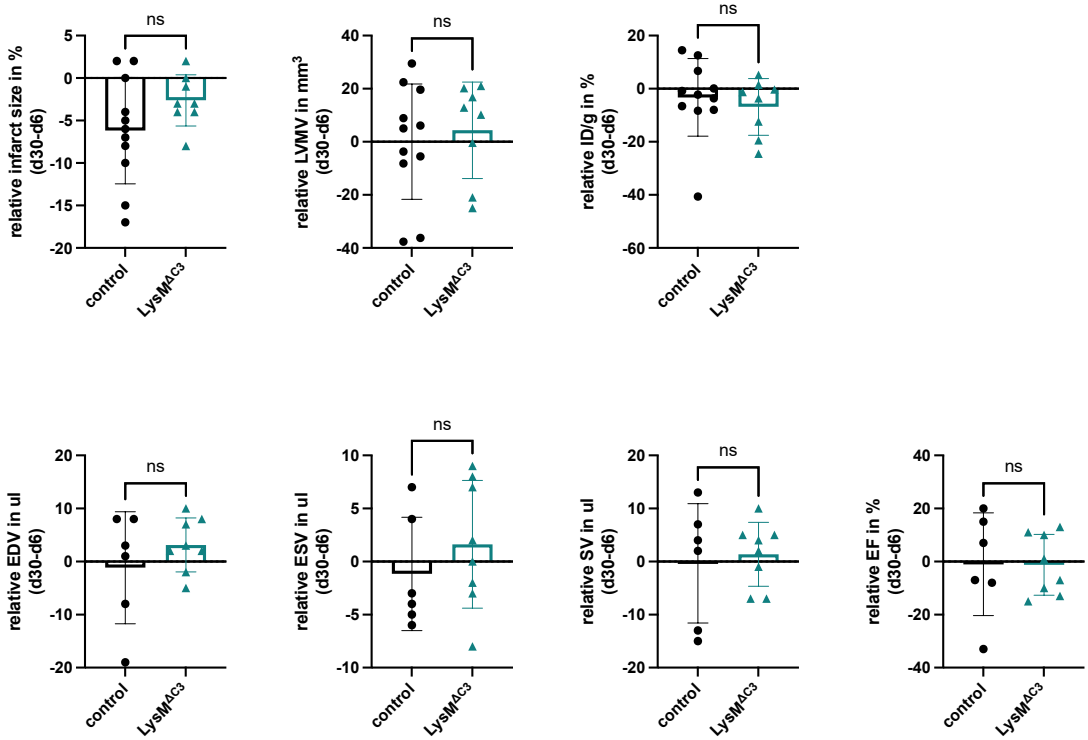

Fig. 3.7.15 Cardiac remodeling in *LysM$^{\Delta C3}$* mice after I/R. Intraindividual change of different parameters in *LysM$^{\Delta C3}$* (n=6-11) and control (n=8) mice from d6 to d30

after MI measured with PET-CT. Error bar, mean±SD. Unpaired t-test was performed in each comparison.

For mice undergoing chronic LAD ligation, there was no difference in infarct size (**Fig. 3.6.16**), cardiac function (**Fig. 3.6.17**) and remodeling (**Fig. 3.6.18**) between *LysM*$^{\Delta C3}$ and *LysM*^{wt} littermate mice post-MI.

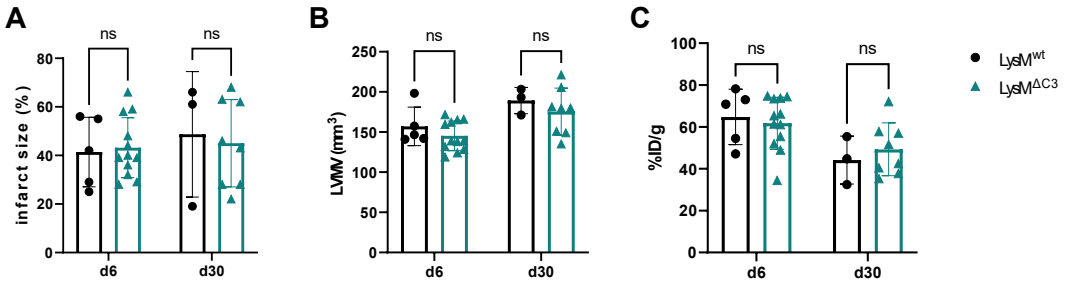

Fig. 3.7.16 Myocardial perfusion parameters in *LysM*$^{\Delta C3}$ mice undergoing chronic MI. A) TPD; **B)** LVMV and **C)** cardiac %ID/g in *LysM*$^{\Delta C3}$ and littermate mice was assessed by in vivo PET-CT imaging at day 6 and day 30 post-MI. Error bar, mean±SD. Multiple unpaired t-tests were performed.

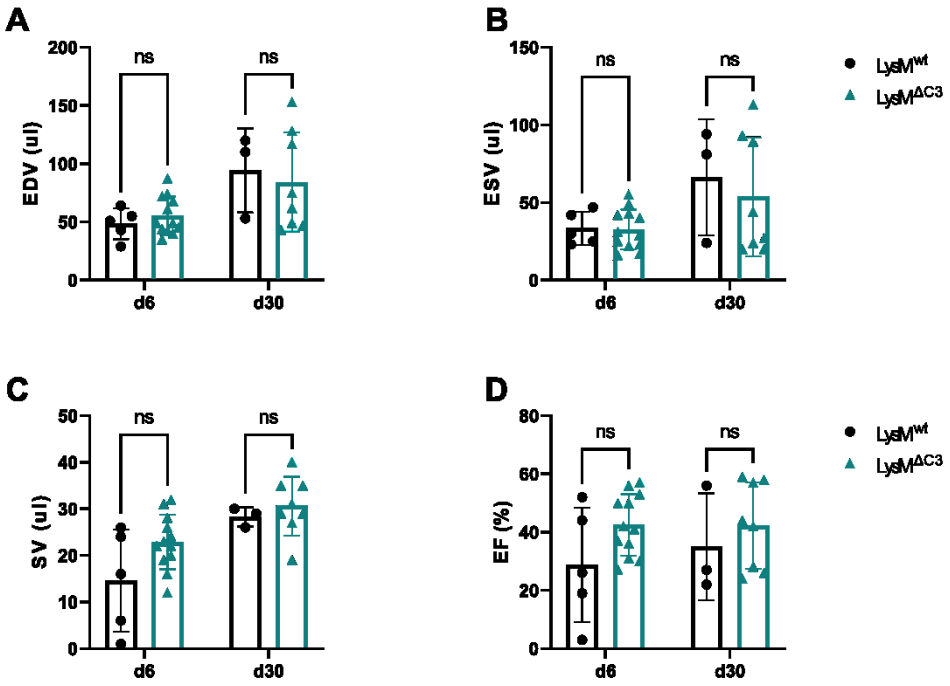

Fig. 3.7.17 Cardiac function parameters in *LysM$^{\Delta C3}$* mice after chronic MI. A) EDV; **B)** ESV; **C)** SV and **D)** EF in *LysM$^{\Delta C3}$* and littermate mice was assessed by in vivo PET-CT imaging at day 6 and day 30 post-MI. Error bar, mean±SD. Multiple unpaired t-tests were performed.

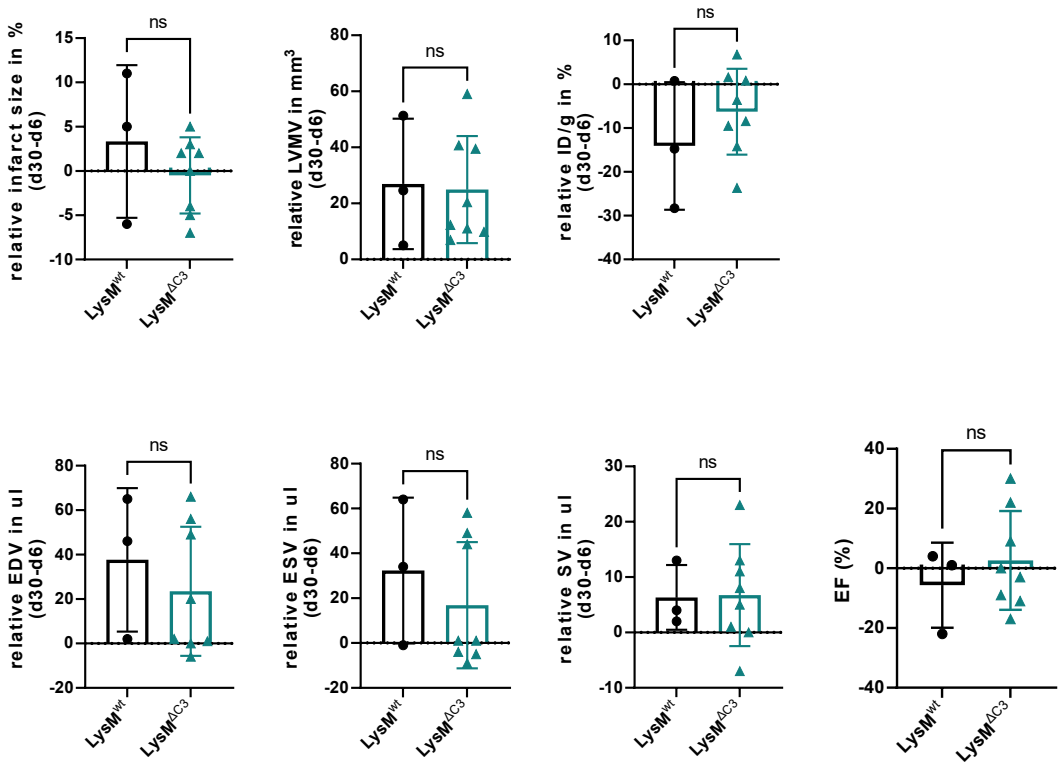

Fig. 3.7.18 Cardiac remodeling in *LysM$^{\Delta C3}$* mice after MI. Intraindividual change of different parameters in *LysM$^{\Delta C3}$* (n=7) and littermates (n=3) from d6 to d30 after MI measured with PET-CT. Error bar, mean±SD. Unpaired t-test was performed in each comparison.

Thus, C3 produced by BM derived myeloid cells was not involved in this ischemia/infarction setting. However, it needs to be further determined with more efficient C3-deletion model.

3.7.3 C3 deletion in tissue resident macrophages

To address the potential role of C3 derived from cardiac macrophages, we further analyzed tissue resident macrophage responses to I/R in *Rank$^{\Delta C3}$* mice compared with control mice. While the number of cardiac resident macrophages in *Rank$^{\Delta C3}$* mice was unchanged in baseline condition, it was significantly reduced after I/R injury (**Fig. 3.7.19**). This could be due to various mechanisms that remain to be determined, such as reduced monocyte recruitment, altered macrophage survival or impaired proliferation of resident macrophages.

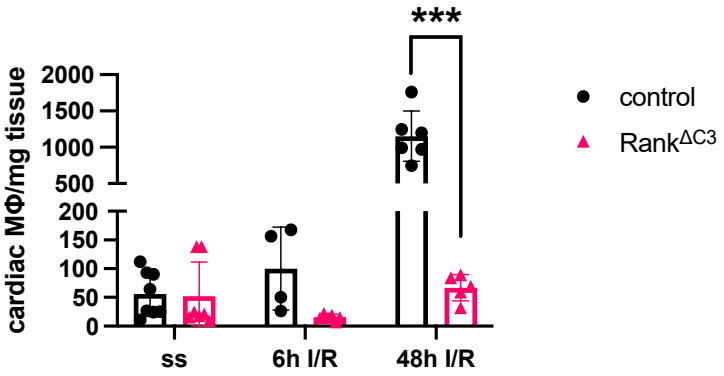

Fig. 3.7.19 Macrophage number is diminished after I/R when C3 is conditionally deleted in tissue resident macrophages. Absolute number of macrophages in ischemic heart tissue after I/R and counterpart area in steady state between *Rank*$^{\Delta C3}$ and control mice. Error bar, mean±SD. Unpaired t test was performed. ***p<0.001.

In analogy to *LysM*$^{\Delta C3}$ and *Mrp8*$^{\Delta C3}$, no significant difference of infarct size could be detected between *Rank*$^{\Delta C3}$ and *control* mice after I/R as measured by both PET-CT and WGA staining (**Fig. 3.7.20 and Fig. 3.7.21**). Consistently, metabolism and cardiac function was unaltered in *Mrp8*$^{\Delta C3}$ mice as compared to control mice (**Fig. 3.7.20 and Fig. 3.7.22**).

Align with no difference in infarct size and cardiac function, cardiac remodeling from day 6 to day 30 post-I/R was similar in both groups. No apparent difference could be identified (**Fig. 3.7.23**).

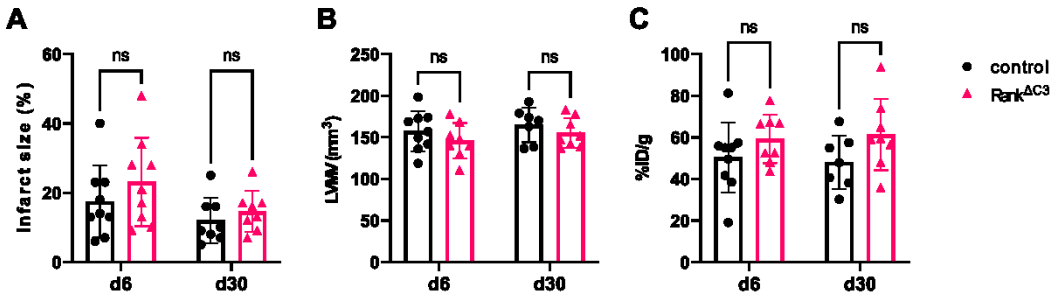

Fig. 3.7.20 Cardiac output in *Rank*$^{\Delta C3}$ mice undergoing transient LAD ligation. A) TPD; **B)** LVMV and **C)** cardiac %ID/g in *Rank*$^{\Delta C3}$ and control mice was assessed by

in vivo PET-CT imaging at day 6 and day 30 post-I/R. Error bar, mean±SD. Multiple unpaired t-tests were performed.

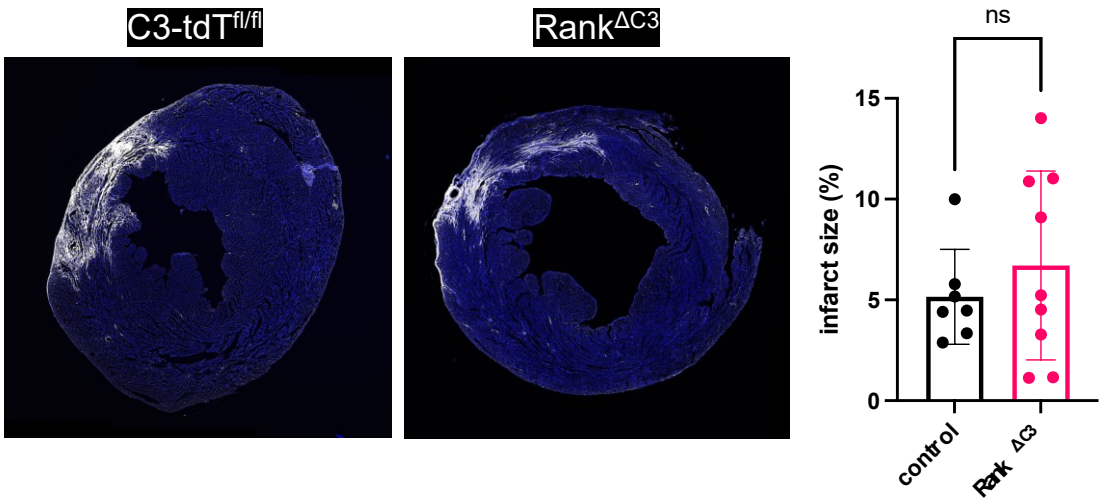

Fig. 3.7.21 Fibrosis in *Rank*$^{\Delta C3}$ and control mice after I/R was evaluated by WGA staining. Left, representative immunofluorescence image obtained from epifluorescence microscope. **Right**, quantification of ratio of fibrotic area to whole heart area, assessed by Image J. Error bar, mean±SD. Unpaired t test was performed.

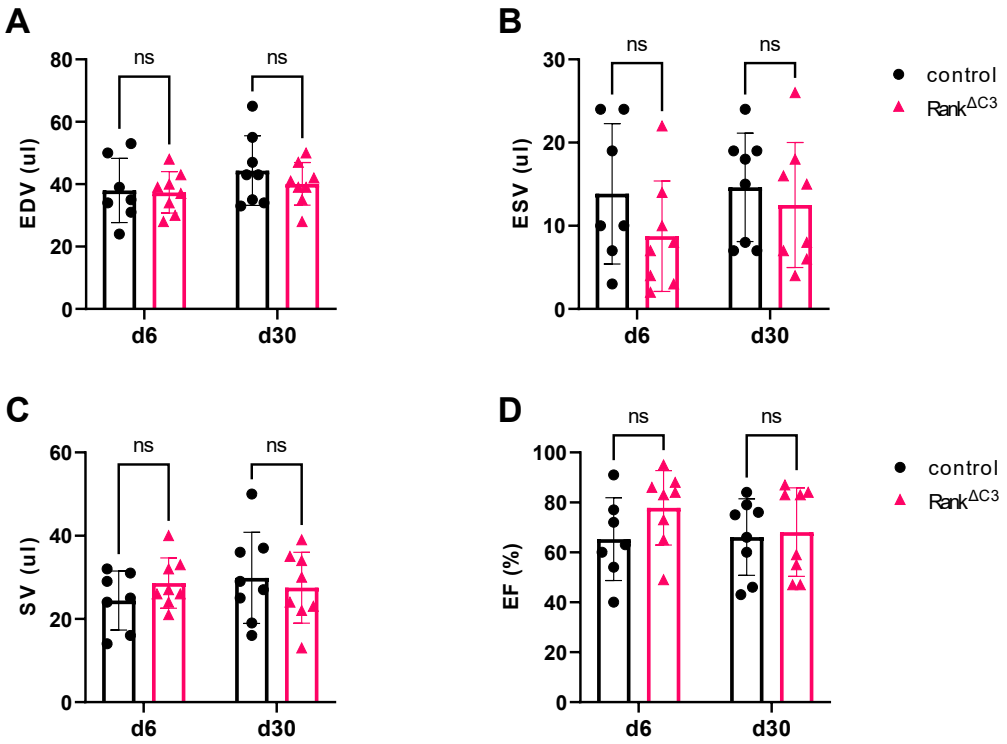

Fig. 3.7.22 Cardiac function parameters in *Rank*$^{\Delta C3}$ mice after I/R. A) EDV; **B)** ESV; **C)** SV and **D)** EF was assessed by in vivo PET-CT imaging at day 6 and day 30 post-I/R. Error bar, mean±SD. Multiple unpaired t-tests were performed.

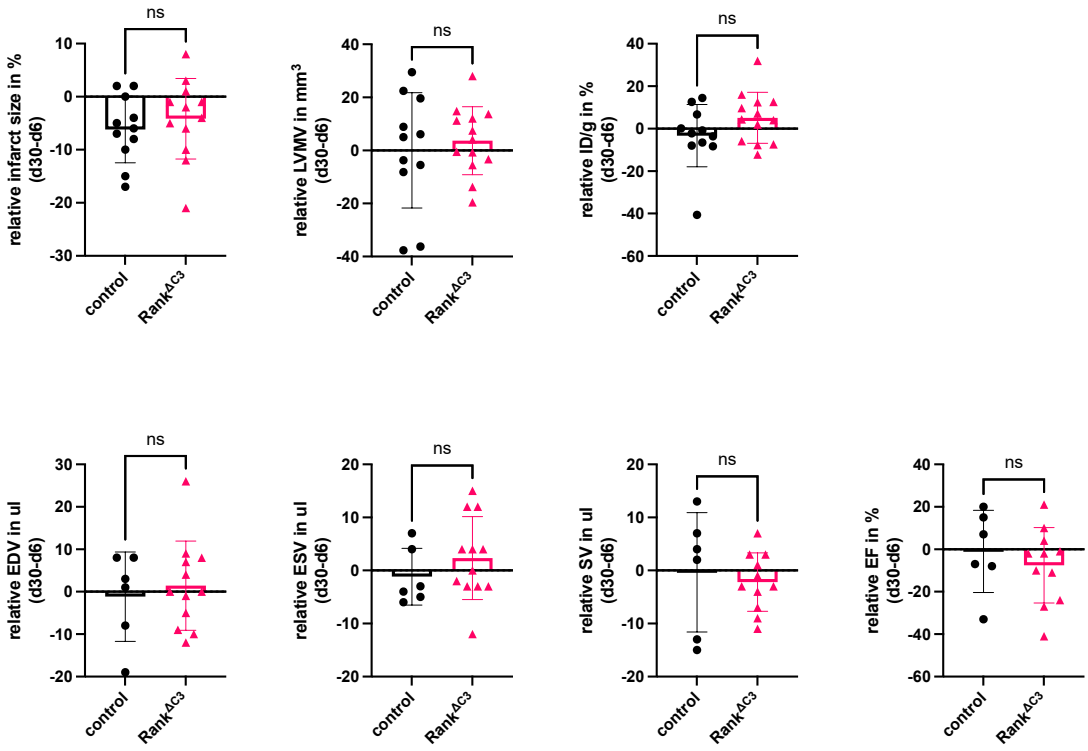

Fig. 3.7.23 Cardiac remodeling in *Rank*$^{\Delta C3}$ after I/R. Intraindividual change of different parameters in *Rank*$^{\Delta C3}$ (n=12) and control (n=11) mice from d6 to d30 after I/R measured with PET-CT. Error bar, mean±SD. Unpaired t-test was performed in each comparison.

As for mice being subjected to MI, we found TPD to be significantly increased in *Rank*$^{\Delta C3}$ 30 days after infarction compared to *Rank*^{wt} mice, while the difference in infarct size was not associated with alterations of LVMV and cardiac %ID/g (**Fig. 3.7.24**).

However, we did not detect any difference regarding EDV and ESV from day 6 to day 30 in *Rank*$^{\Delta C3}$ mice with chronic MI. Governed by both EDV and ESV values, no difference was found regarding SV and EF, indicating cardiac function was to some extent compensated (**Fig.3.7.25**).

Likewise, we compared the relative change from d6 to d30 after MI. In mice with conditional deletion of macrophage-derived C3, we observed increased infarct size indicating adverse cardiac remodeling. Correlated to the perfusion loss, relative LVMV was more pronounced in *Rank*$^{\Delta C3}$ mice, which could be reflected by the increase of EDV and ESV. Further, there was a tendency towards higher EDV and ESV, although parameters did not reach statistical significance in the light of low n numbers (**Fig. 3.7.26**).

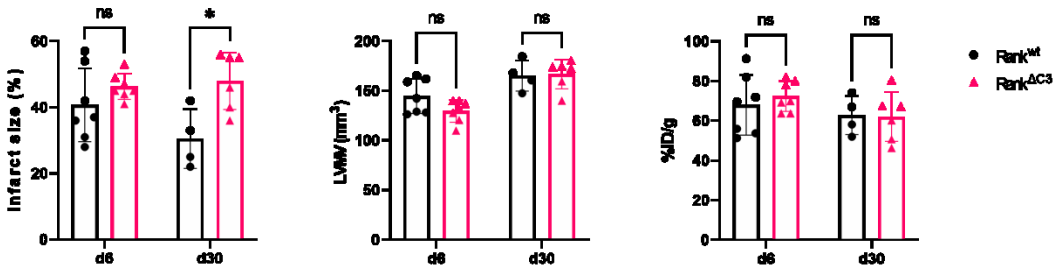

Fig. 3.7.24 Myocardial perfusion parameters in *Rank*$^{\Delta C3}$ mice undergoing chronic MI. A) TPD; **B)** LVMV and **C)** cardiac %ID/g in *Rank*$^{\Delta C3}$ and *Rank*^{wt} littermate mice was assessed by in vivo PET-CT imaging at day 6 and day 30 post-MI. Error bar, mean±SD. Multiple unpaired t-tests were performed. *p<0.05.

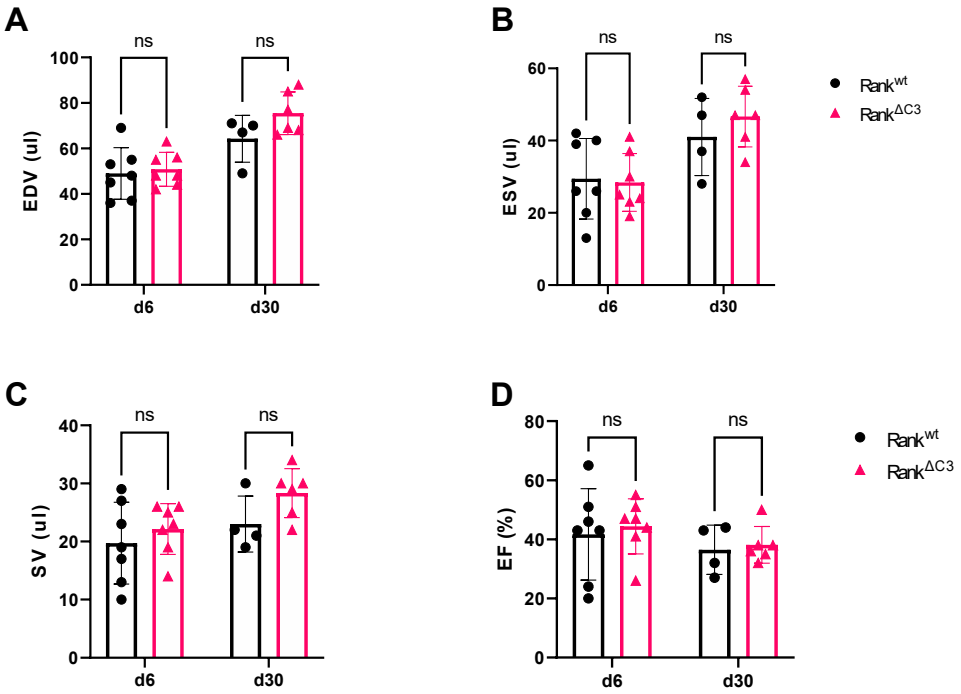

Fig. 3.7.25 Cardiac function in *Rank*$^{\Delta C3}$ mice undergoing chronic MI. A) EDV; **B)** ESV; **C)** SV and **D)** EF in *Rank*$^{\Delta C3}$ and *Rank*^{wt} littermate mice was assessed by in vivo PET-CT imaging at day 6 and day 30 post-MI. Error bar, mean±SD. Multiple unpaired t-tests were performed.

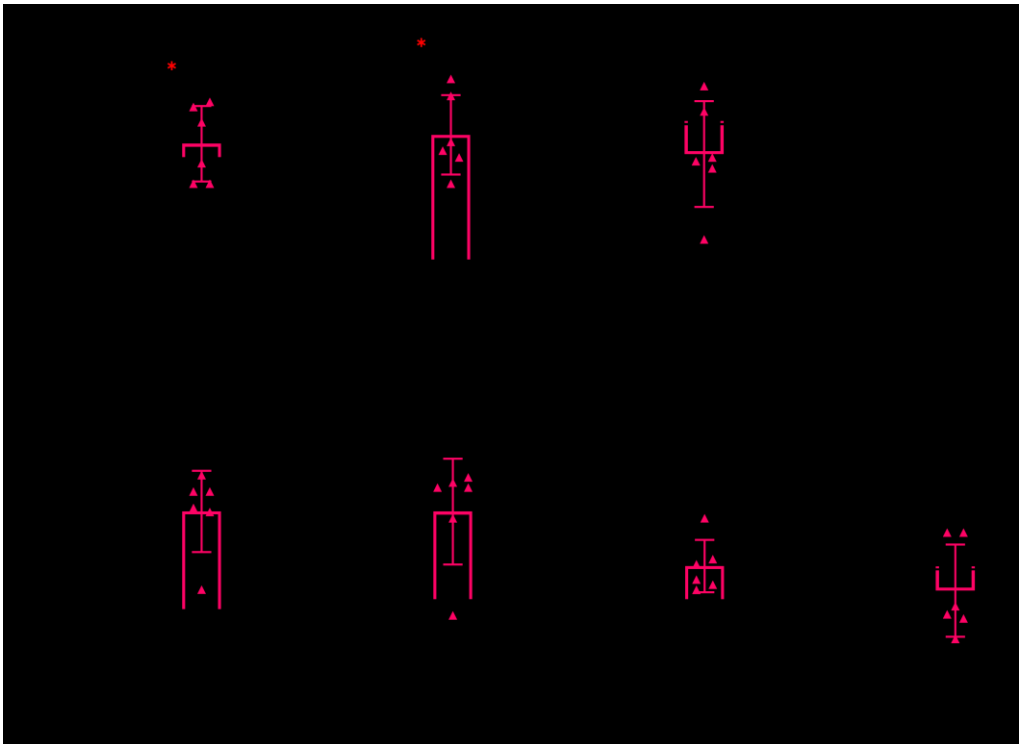

Fig. 3.7.26 Cardiac remodeling in *Rank*$^{\Delta C3}$ after MI. Intraindividual change of different parameters in *Rank*$^{\Delta C3}$ (n=6) and *Rank*^{wt} littermate (n=4) from d6 to d30 after MI measured with PET-CT. Error bar, mean±SD. Unpaired t-test was performed in each comparison. *p<0.05.

To further evaluate the specific role of C3 in myeloid cells in the course of cardiac recovery after chronic MI, we compared the survival rate in cell specific C3 deletion mice and control mice. It turned out tissue resident macrophage derived C3 worsened the outcome in terms of more death rate at early days after MI, which could be a consequence of more cell death or stronger inflammation. This could result in larger infarct size in *Rank*$^{\Delta C3}$ mice at day 30 post-MI. As no improvement or deterioration regarding infarct size and cardiac function occurred in both *LysM*$^{\Delta C3}$ and *Mrp8*$^{\Delta C3}$ mice, the survival rate of mice was also similar between myeloid cell C3 deletion mice and control mice (**Fig. 3.7.27**).

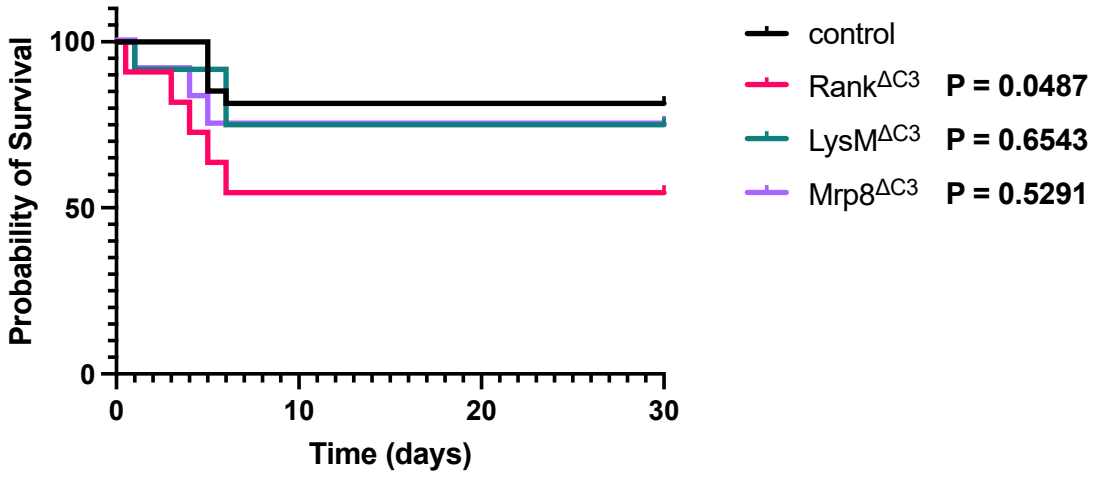

Fig. 3.7.27 Kaplan–Meier curve for cell-specific C3 deletion mice and control mice undergoing chronic MI. Control mice were *C3-tdT* reporter mice without *cre* deletion (n=27). *Rank*$^{\Delta C3}$ (n=11), *LysM*$^{\Delta C3}$ (n=12), and *Mrp8*$^{\Delta C3}$ (n=12) mice were included in the analysis. Long-rank (Mantel-Cox) test was performed.

3.8 C3a/C3aR signaling implicated in the propagation of I/R

3.8.1 C3aR expression on tissue resident macrophages

During myocardial infarction, myocardium damage leads to the activation of complement system. C3 is thereby cleaved into C3a and C3b. C3b promotes the generation of C5, whereas C3a exerts a variety of important functions in inflammation directly. C3a receptor (C3aR) is one of the receptors that C3 binds to, and previous studies has already demonstrated C3aR expression on macrophages. Therefore, C3a produced by myeloid cells or resident macrophages themselves could then bind to C3aReceptor on the surface of macrophages or directly mediated by C3aReceptor on lysosome in the cytoplasm of macrophages (**Fig. 3.8.1**).

We next aimed to decipher the involvement of C3a/C3aR signaling pathway in the development of myocardial injury. We therefore employed C3aR-tdtomato reporter mice (*C3aR-tdT*) as described before and characterized the C3aR expression in immune cells by flow cytometry [59].

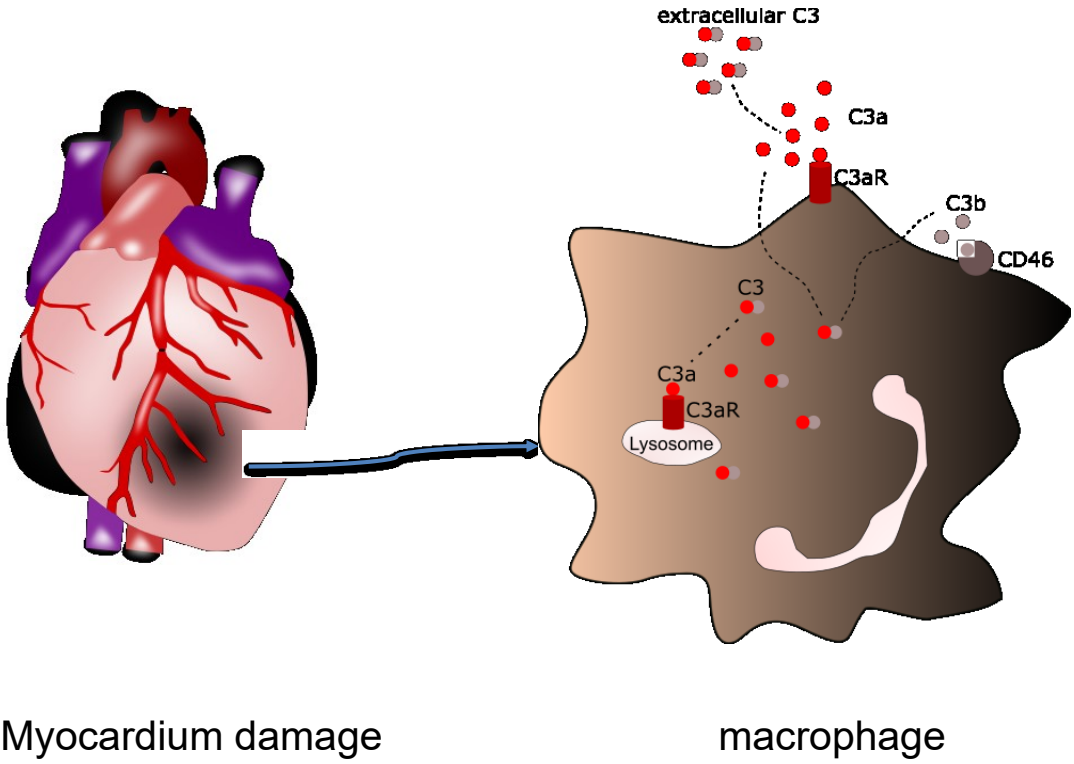

Fig. 3.8.1 Illustration of C3a and C3aR engagement in/on macrophages during MI.

C3aR is expressed in abundance on the surface of macrophages, eosinophils and DCs in many tissues whereas rarely expressed on neutrophils and lymphocytes. In analogy to previous studies, we quantified profound expression of C3aR in tissue macrophages. In contrast, C3aR was barely expressed by neutrophils in steady state (**Fig. 3.8.2 A**). Furthermore, no C3aR expression could be detected in circulating immune cells (**Fig. 3.8.2 B**).

Meanwhile, we performed immunofluorescence staining with heart section obtained from C3aR-tdT mice to further prove the colocalization of macrophages and C3aR. We found nearly all cardiac macrophages were colocalized with C3aR expression (**Fig. 3.8.3**).

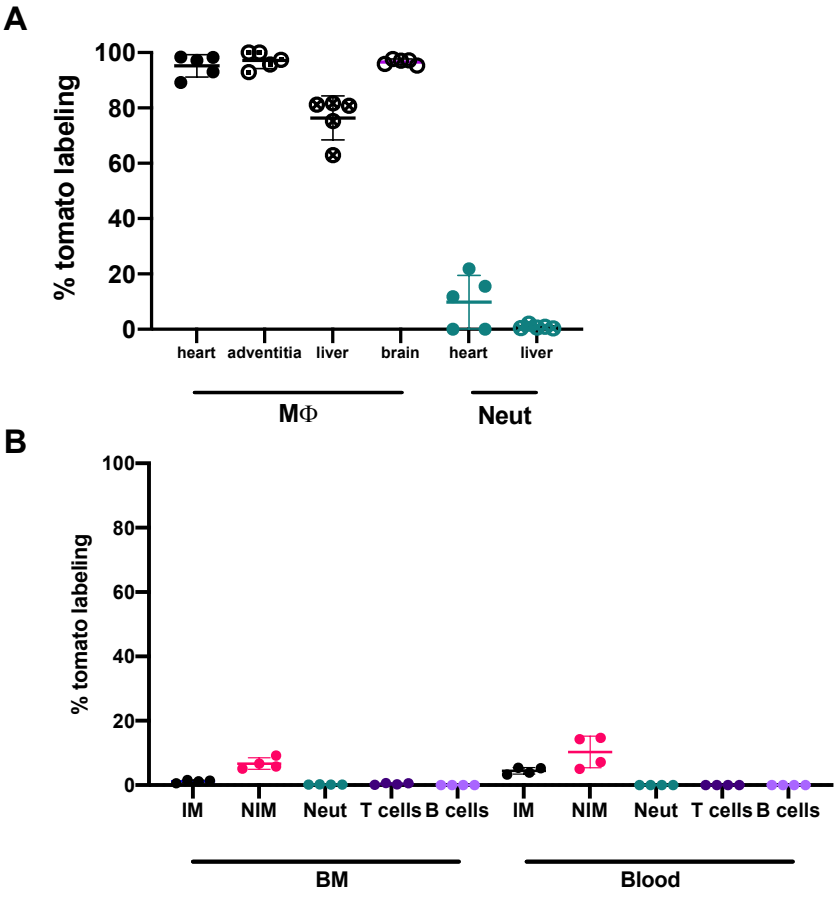

Fig. 3.8.2 C3aR is mainly expressed by tissue resident macrophages in steady state. Percentage quantification of C3aR-tdT expression **A)** in macrophages and neutrophils in different tissues and **B)** in circulating immune cells in *C3aR-tdT* reporter mice checked by flow cytometry. Values shown were mean±SD.

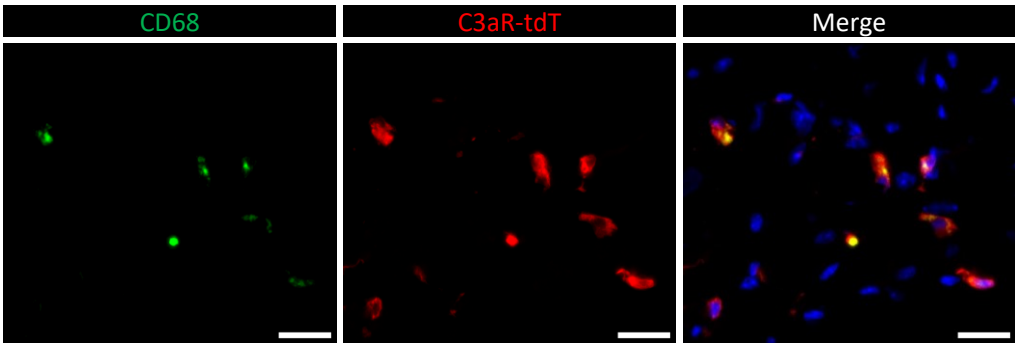

Fig. 3.8.3 Colocalization of macrophage and C3aR. Representative immunofluorescence staining images of cardiac macrophages with C3aR in *C3aR-tdT* mice. Scale bar, 20µM. X40 magnification assessed by epifluorescence microscope.

We further determined whether C3aR is regulated after I/R. Contrary to the induction of C3 in cardiac macrophages after 48h reperfusion, quantification of the percentage of C3aR expression in macrophages was not upregulated after 6h or 48h reperfusion (**Fig. 3.8.4**). However, the intensity of C3aR in cardiac macrophages was downregulated significantly at the time point of 48h, but the increase was abrogated after I/R for 30 days. Meanwhile, there was an unexpected increment in brain microglia at 48h, whereas no induction was found in arterial macrophages and liver macrophages (**Fig. 3.8.5**).

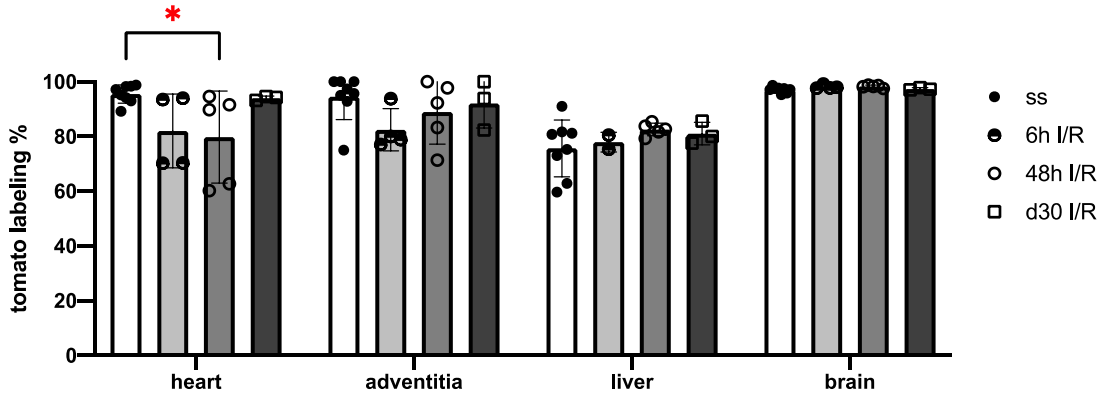

Fig. 3.8.4 Percentage of C3aR-expressing macrophages upon I/R inflammation. Percentage quantification of C3aR-tdT expression in tissue macrophages in *C3aR-tdT* reporter mice in steady state and after I/R injury. Values shown were mean±SD. One-way ANOVA was performed. *p<0.05.

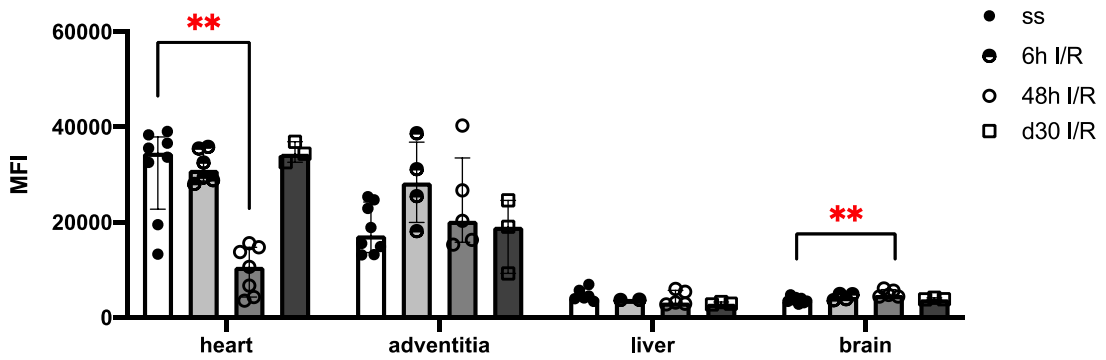

Fig. 3.8.5 C3aR expression on cardiac macrophages was down-regulated after 48h I/R. Median intensity of C3aR-tdT expression in tissue macrophages in *C3aR-tdT*

reporter mice in steady state and after I/R injury. Values shown were mean±SD. One-way ANOVA was performed. **p<0.01.

Furthermore, the downregulation of C3aR expression in cardiac macrophages were mainly presented in MHC II^{high} macrophages (**Fig.3.8.6**), which were regarded as embryo-derived tissue resident macrophages.

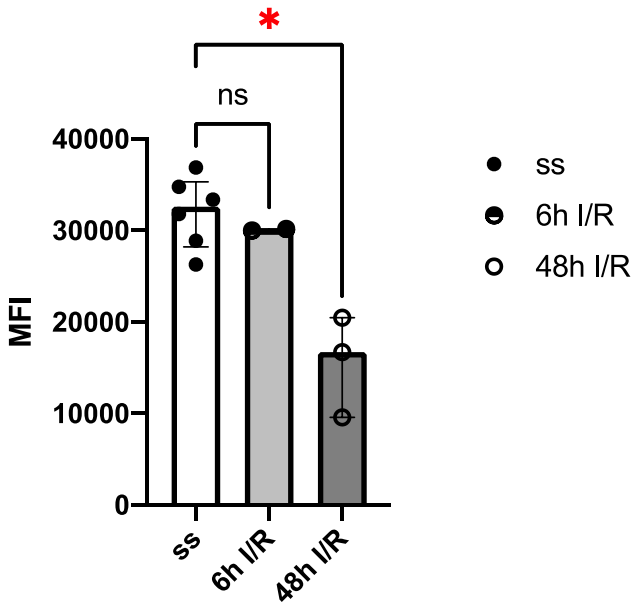

Fig. 3.8.6 MHC II^{high} macrophages down-regulate C3aR expression due to I/R. Median intensity of C3aR-tdT expression in tissue macrophages in *C3aR-tdT* reporter mice in steady state and after I/R injury. Values shown were mean±SD. One-way ANOVA was performed. *p<0.05.

Previous studies found C3aR is not expressed on neutrophils in steady state but could be induced when responds to inflammatory conditions [81, 82]. Thus, we evaluated the expression of C3aR in neutrophils after I/R surgery as well. On the contrary, no increase of C3aR was observed from acute to late inflammation after I/R injury, whereas a slight although not significant reduction was shown in neutrophils after acute injury (**Fig. 3.8.7**).

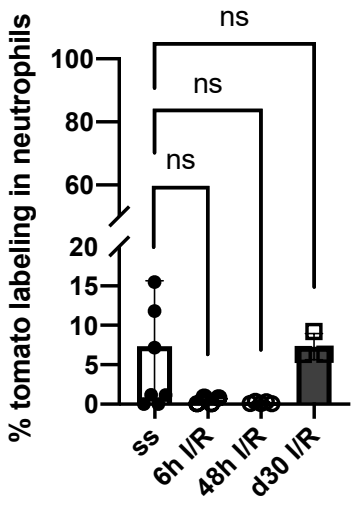

Fig. 3.8.7 Neutrophil C3aR expression was not induced by I/R injury. Percentage quantification of C3aR-tdT expression in cardiac neutrophils in *C3aR-tdT* reporter mice in steady state and after I/R injury. Values shown were mean±SD. One-way ANOVA was performed.

Together, these data indicated the decrease of C3aR in cardiac macrophages after 48h reperfusion mainly own to embryo-derived macrophages down regulate C3aR expression.

3.8.2 C3aR deficiency in tissue resident macrophages

As outlined above, C3aR expression in tissue resident macrophages was significantly reduced when triggered by acute inflammation. We next generated C3aR deletion specifically targeted on YS derived resident macrophages, the $Rank^{\Delta C3aR}$ deletion mice, to solidify the potential engagement of C3a and C3aR on tissue resident macrophages in the process of myocardial injury.

The characterization of C3aR deletion effect was carried out by flow cytometry. Surprisingly, we detected almost complete deficiency of C3aR on tissue resident macrophages in $Rank^{\Delta C3aR}$ mice compared to $Rank^{wt}$ mice, not only in the heart, but also in other tissues (**Fig.3.8.8**). Similar result was also found by immunofluorescence staining, which showed clearly the C3aR expression on cardiac macrophages were absent in $Rank^{\Delta C3aR}$ mice (**Fig. 3.8.9**).

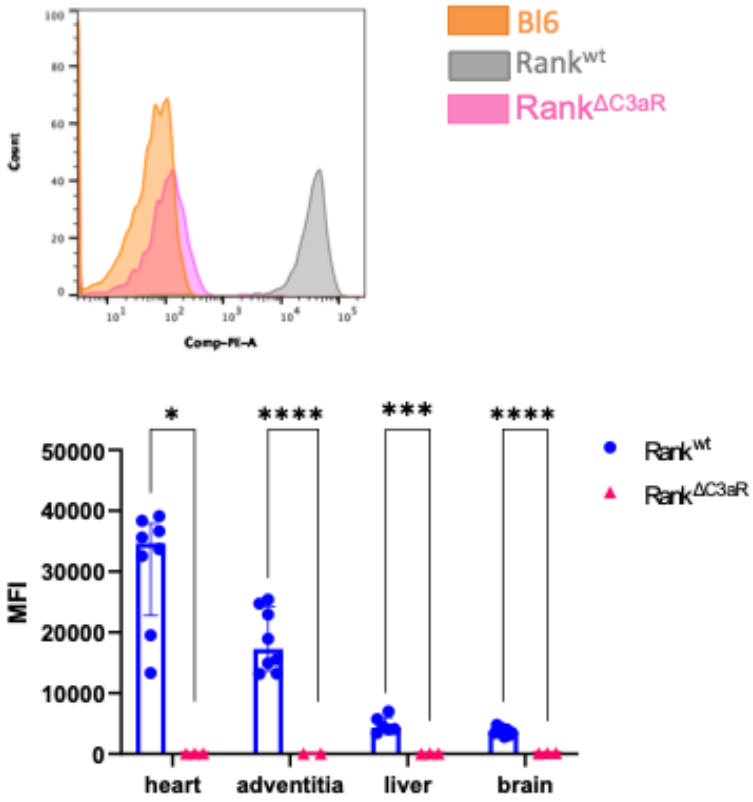

Fig. 3.8.8 Depletion of C3aR on macrophages in *Rank$^{\Delta C3aR}$* mice. C3aR expression was measured by gating on tomato positive population in macrophages by flow cytometry. Histogram (**Upper**) of tomato and Median intensity (**Lower**) of tomato labeling in macrophages in *Rank$^{\Delta C3aR}$* (n=3) and *Rank^{wt}* (n=8) mice. Values shown were mean±SD. Unpaired t test was performed. *p<0.05; ***p<0.001; ****p<0.0001.

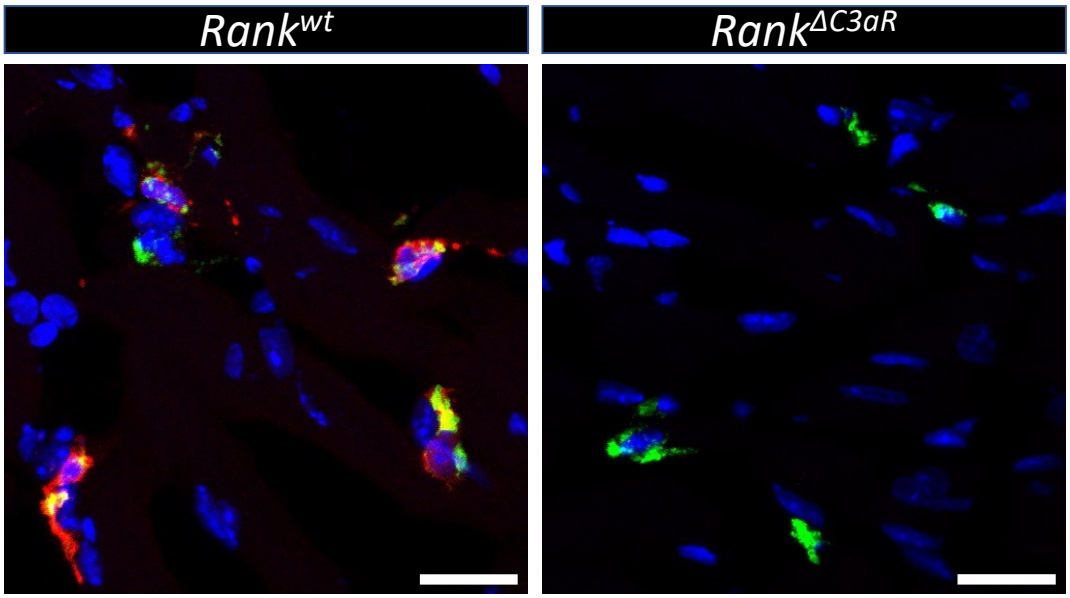

Fig. 3.8.9 Representative image of C3aR deficiency on cardiac macrophages. Fluorescence staining was performed with heart sections in $Rank^{wt}$ (**left**) and $Rank^{\Delta C3aR}$ (**right**) mice. C3aR was determined by tomoto labeling and macrophages were identified by CD68 expression. Scale bar, 20μm. X40 magnification. Image was taken by confocal microscope.

To address whether pathological progress of myocardium damage requires C3aR signaling on macrophages, we next performed I/R injury on $Rank^{\Delta C3aR}$ mice and conducted in vivo cardiac PET-CT imaging to measure cardiac outcome. As a result, we did not find any differences with regards to infarct size and metabolic volume (**Fig. 3.8.10**). In line with this, cardiac function parameters in C3aR deletion mice were unaltered from d6 to d30 (**Fig. 3.8.11**).

Consistently, cardiac remodeling process was also similar from day 6 to day 30 between $Rank^{\Delta C3aR}$ and littermate mice (**Fig. 3.8.12**).

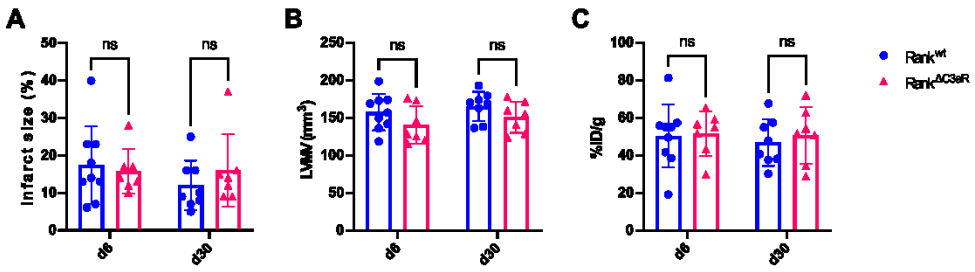

Fig. 3.8.10 Myocardial perfusion parameters of *Rank*$^{\Delta C3aR}$ mice undergoing I/R injury. **A)** TPD; **B)** LVMV and **C)** cardiac %ID/g at day 6 and day 30 post-MI assessed by PET-CT imaging. Error bar, mean±SD. Multiple unpaired t-tests were performed.

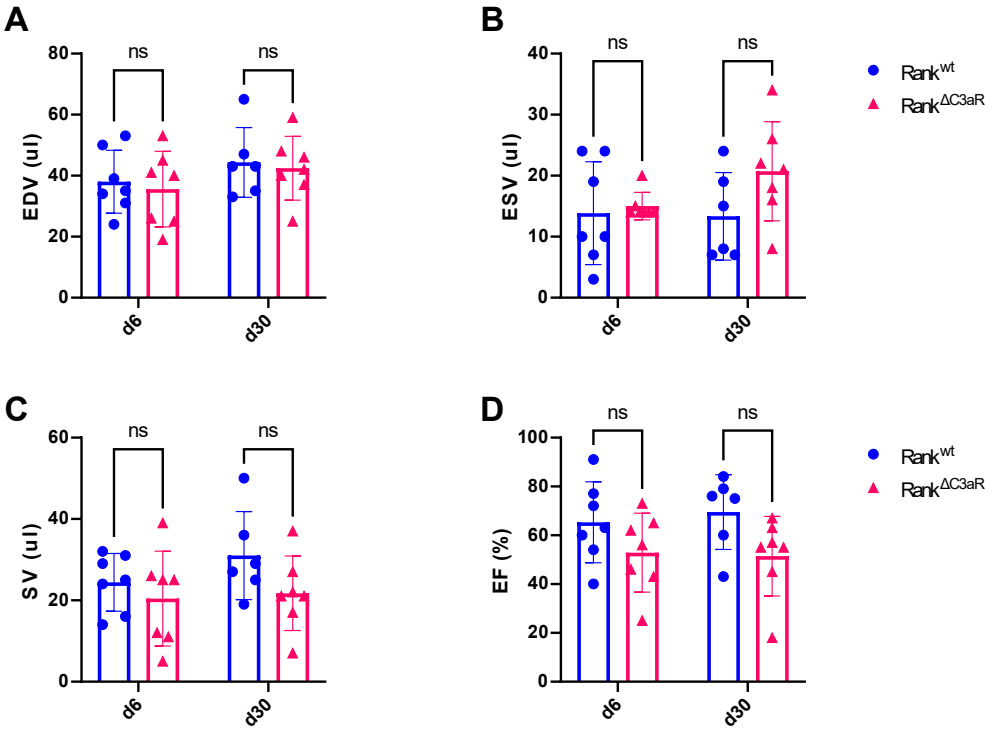

Fig. 3.8.11 Cardiac function parameters of *Rank*$^{\Delta C3aR}$ mice undergoing I/R injury.

A) EDV; **B)** ESV; **C)** SV and **D)** EF at day 6 and day 30 post-I/R. Error bar, mean±SD. Multiple unpaired t-tests were performed.

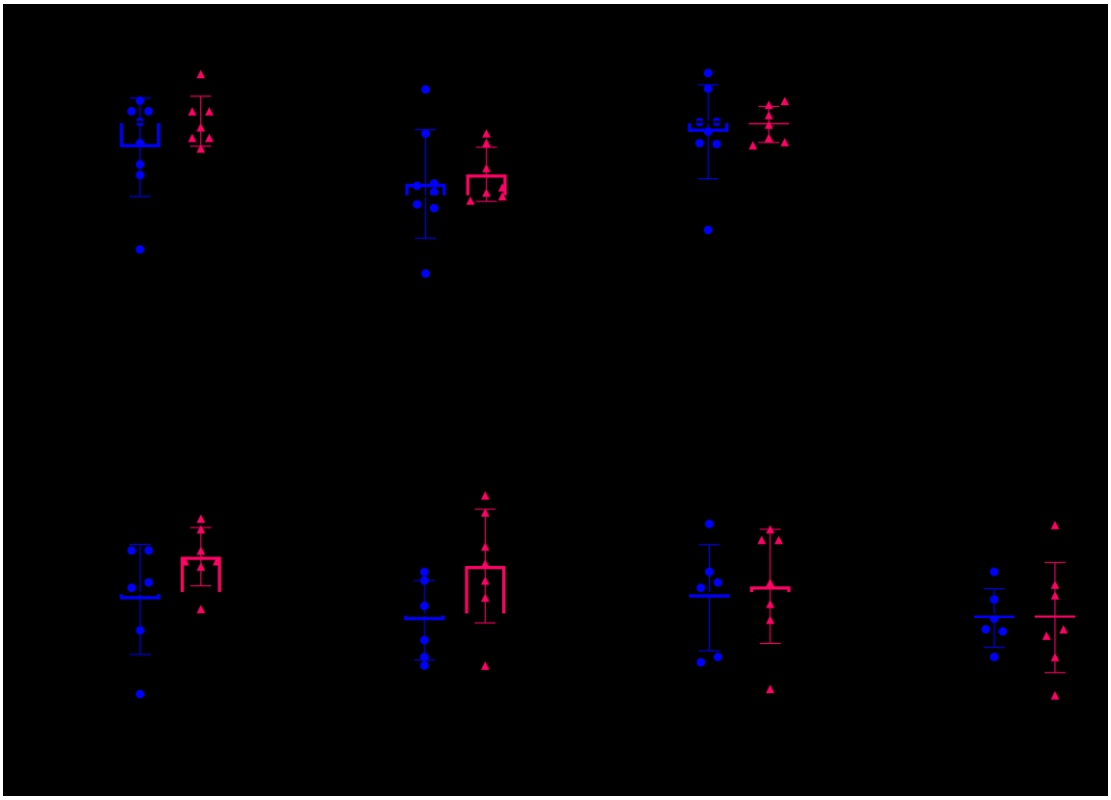

Fig. 3.8.12 Cardiac remodeling in *Rank*$^{\Delta C3aR}$ mice after I/R. Intraindividual change of different parameters in *Rank*$^{\Delta C3aR}$ (n=8) and littermate (n=7) from d6 to d30 after I/R measured with PET-CT. Error bar, mean±SD. Unpaired t-test was performed in each comparison.

Likewise, *Rank*$^{\Delta C3aR}$ mice and their littermates were subjected to permanent LAD ligation as well. We found the infarct size was reduced at day 6 post MI in C3aR deletion mice, but no further increase at day 30. However, there was no metabolism alteration with regards to LVMV and cardiac %ID/g (**Fig. 3.8.13**).

Correlating with the elevated infarct size, we determined a reduction of ESV and better EF at day 6 post-MI. There was also a tendency towards lower EDV at early phase although did not reach significance (p=0.0807). However, align with infarct size, the difference was no longer distinct at day 30 post-MI between *Rank*$^{\Delta C3aR}$ and their littermate mice. This was proximately related to insufficient mouse number due to early death before day 30 measurement in *Rank*^{wt} mice (**Fig. 3.8.14**).

Similarly, we compared the relative change from day 6 to day 30 post-MI in both groups. There was no significant difference in each parameter, which was most likely

driven by the severe variation within groups as well as low mouse number (**Fig. 3.8.15**).

As mentioned above, 8 out of 13 mice died after MI in *Rank*^{wt} group but only 1 out of 8 mice died in *Rank*$^{\Delta C3aR}$ group (**Fig. 3.8.16**). The remarkable survival advantage in *Rank*$^{\Delta C3aR}$ mice was potentially associated with less inflammation in the acute phase, but this hypothesis would need further investigation.

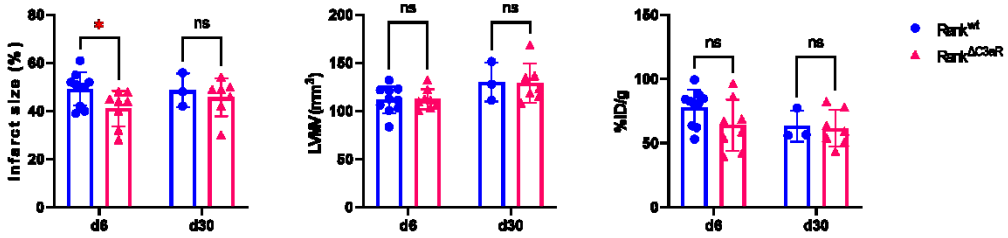

Fig. 3.8.13 Myocardial perfusion parameters of *Rank*$^{\Delta C3aR}$ mice undergoing chronic MI. A) TPD; **B)** LVMV and **C)** cardiac %ID/g at day 6 and day 30 post-MI. Error bar, mean±SD. Multiple unpaired t-tests were performed. *p<0.05.

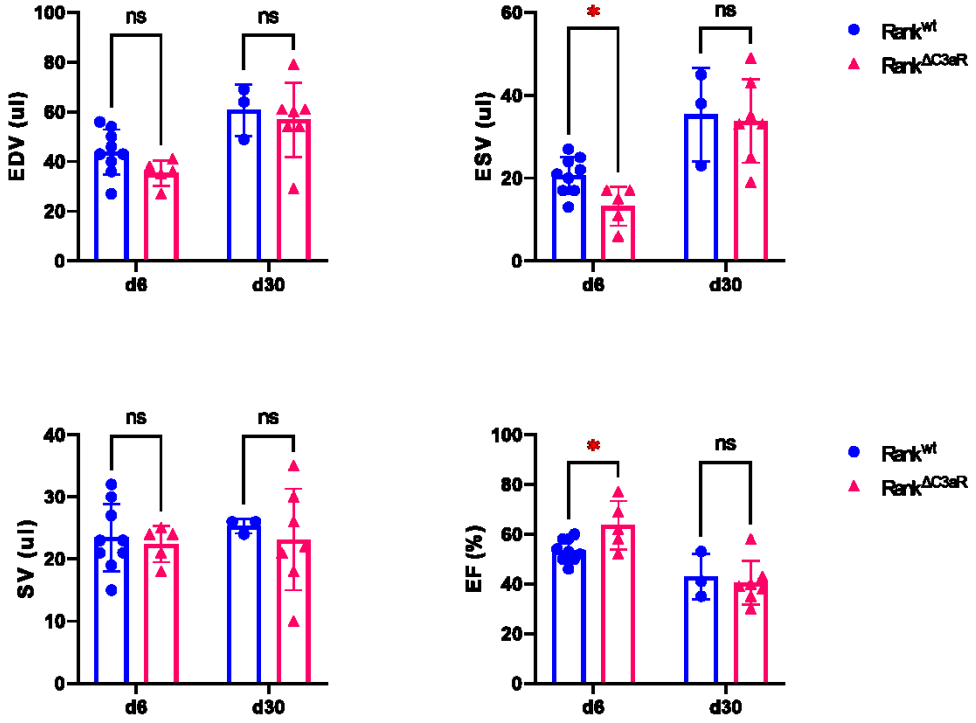

Fig. 3.8.14 Cardiac function parameters of *Rank*$^{\Delta C3aR}$ mice undergoing chronic MI. A) EDV; **B)** ESV; **C)** SV and **D)** EF at day 6 and day 30 post-I/R assessed by

PET-CT imaging. Error bar, mean±SD. Multiple unpaired t-tests were performed. *p<0.05.

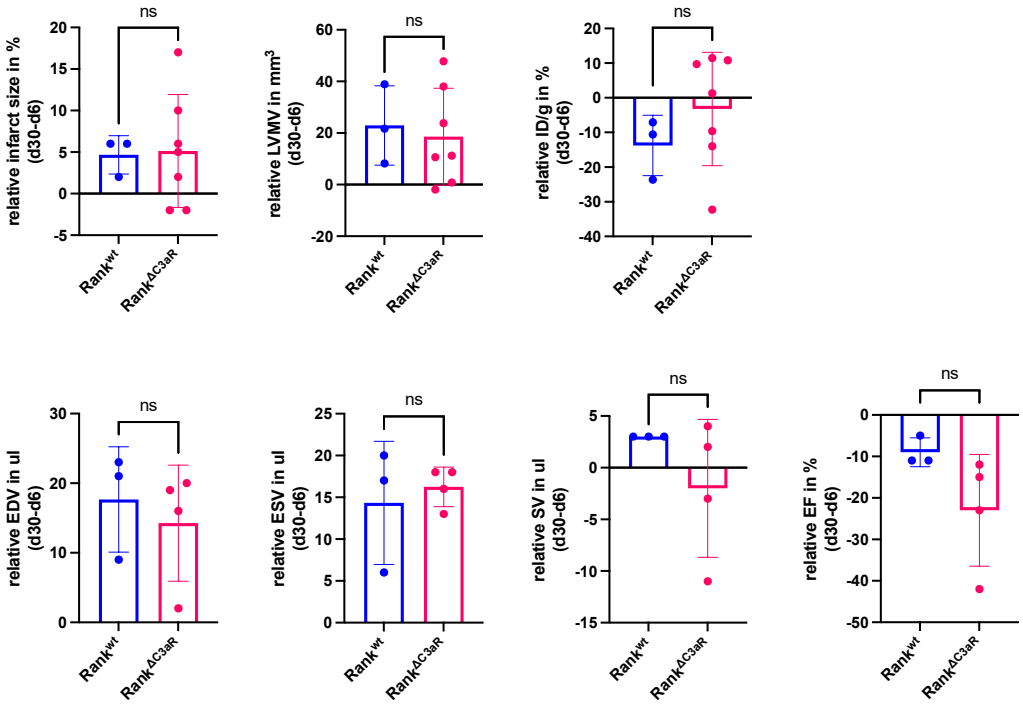

Fig. 3.8.15 Cardiac remodeling in *Rank*$^{\Delta C3aR}$ and littermate mice after MI. Intraindividual change of different parameters in *Rank*$^{\Delta C3aR}$ (n=4-7) and *Rank*^{wt} littermates (n=3) from d6 to d30 after MI measured with PET-CT. Error bar, mean±SD. Unpaired t-test was performed in each comparison.

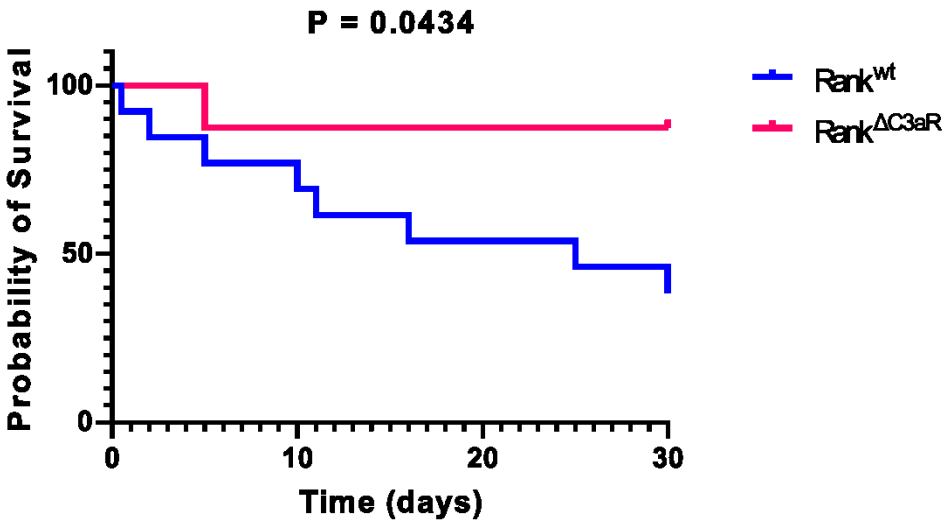

Fig. 3.8.16 Kaplan–Meier curve for *Rank*$^{\Delta C3aR}$ mice undergoing chronic MI. *Rank*$^{\Delta C3aR}$ (n=8) and *Rank*^{wt} littermate (n=13) were included in the analysis. Long-rank (Mantel-Cox) test was performed.

4. Discussion

The engagement of complement and immune cells in the pathological course of MI has long been demonstrated. Complement C3, a major effector of the complement system, interacts with macrophages and neutrophils in response to myocardial injury. Therapeutic strategies broadly targeting on complement effectors and/or immune cells to restrain the severity of damaged myocardium and improve cardiac function post-MI have shown controversial outcomes in animal and clinical trials [43, 83-85]. Recent work has emphasized the importance of autocrine and intracellular C3 in immune cell homeostasis and cellular metabolism. However, very little has been known regarding the features of myeloid cell derived C3 under inflammatory conditions, especially myocardial injury.

In my thesis, I set out to determine the effect of endogenous C3 in myeloid immune cells in response to MI. By using C3-tdtomato reporter mice, we monitored intracellular expression of C3. In steady state, C3 was mainly present in circulating myeloid cells. However, we determined not only BM derived myeloid cells but also resident macrophages originating from embryonic hematopoiesis to produce C3 independently of liver-derived complement. Importantly, C3 was strongly upregulated in cardiac resident macrophages after ischemic injury and impacted on tissue remodeling. Targeted depletion of C3 in macrophages impaired cardiac healing in chronic infarction resulting in reduced cardiac recovery and reduced overall survival.

The intrinsic expression of C3 protein in non-hepatocytes has been subject of ongoing research. Accumulating evidence indicated that intracellular C3 allows for the cooperation of immune system components to provide efficient host defense, but also functions as intracellular regulator for cell survival and metabolism. For instance, *de novo* expression of C3 modulates T cell function and mediates adaptive immunity. [86]. Locally produced C3 by macrophages supports dendritic cell maturation and to induce T cell responses [87]. However, biological expression of C3 varies across cell types and previous studies have mostly focused on C3 production and function within T lymphocytes. Thus, our project characterized C3 protein levels among different

immune cells and provided in-depth information of endogenous C3. This was facilitated by C3-tdTomato knock-in reporter mice, demonstrating that intracellularly generated C3 was present mostly in myeloid cells both in blood circulation and tissues. Over 90% of monocytes and neutrophils expressed C3. As indicated by MFI values, we also found strong expression of C3 in tissue neutrophils in the heart and liver. Regarding tissue macrophages, we detected basal levels of C3 in cardiac macrophages and arterial macrophages, moderate C3 expression in liver Kupfer cells whereas brain microglia were C3 absent. In accordance with a previous report, blood lymphocytes expressed C3 only at low levels [57].

C3 and its fragments are recognized to bind apoptotic cells and mediate opsonization and phagocytosis by tissue macrophages [88-90]. During MI, ischemic cardiomyocytes undergo a process of cell death and thereby release pro-inflammatory cytokines and chemokines. These molecular mediators and damage-associated patterns induce both immune and complement system. In human scenario, patients suffering from MI can be treated with primary PCI to reintroduce blood supply to jeopardized myocardium. The reperfusion of damaged tissue comes at a cost of amplified inflammation, which among others involves radical oxygen species formation and complement cascade activation. This negative effect may cause further tissue damage and exacerbate heart failure.

One of our main findings was the profound induction of C3 in and confined to cardiac macrophages, in line with an increase of macrophage number after I/R injury. Specifically, C3 intensity in cardiac macrophages was increased after 24h along with significant augmented macrophage number. In the first phase after MI, neutrophils and shortly thereafter Ly6C^{high} monocytes infiltrate the myocardium representing the most abundant immune cells at this stage. Both macrophages and neutrophils function as phagocytes and take up extracellular vesicles (EVs) from damaged cardiomyocytes and endothelial cells. Besides, they release proinflammatory cytokines such as TNF-α, IL-1β, IL-6 and chemokines like CXCL1,2,3. Ly6C^{high} monocytes also work in an indirect way by differentiating into Ly6C^{high} macrophages [3, 91]. Consequently, the induction of C3 in cardiac macrophages predominantly derived from Ly6C^{high}

monocytes influx. As neutrophils were recruited significantly to ischemic myocardium as soon as 6h post-I/R whereas C3 began to increase after 24h, in addition, C3 elevation in cardiac macrophages continued till day 7 post-I/R whereas neutrophil number was in the baseline level before day 7, neutrophils recruitment was dispensable for C3 induction in macrophages. This further excluded the potential of C3 from either neutrophils or other origins covalent binding to C3aR in macrophages or on its surface.

Furthermore, cardiac macrophages switch from inflammatory to a reparative phenotype along with the transition of cardiac healing process from inflammatory phase to reparative phase post MI during day 4 to day 7. Here, reparative macrophages dominate the heart and execute its function towards pro-fibrotic and anti-inflammatory, leading to neovasculature generation and collagen deposition [18]. The C3 peaked at day 2 in macrophages while macrophage number was at the highest level at day 4 post-I/R, suggesting monocytes continue to infiltrate myocardium and differentiate into macrophages but without further increase of C3 production. Ly6C^{high} monocytes have a rather short lifespan of approximate 20h, then they differentiate into either inflammatory or reparative macrophages depending on local signals. Ly6C^{low} monocytes that also derive from Ly6C^{high} monocytes mainly patrol along vessels and function as sentinels. They can also give rise to Ly6C^{low} macrophages, although in a much lower numbers and frequencies [27, 92]. Therefore, the induction of C3 in cardiac macrophages could potentially originate from more intrinsic C3 production in resident macrophages and to some extent from Ly6C^{high} inflammatory monocyte/macrophage subsets.

Cardiac resident macrophages surround cardiomyocytes and act as sentinels supporting mitochondrial homeostasis and cardiac function [93]. They have been shown to promote angiogenesis and postinfarct healing [25, 94]. It has also been reported that tissue resident macrophages are responsible for initial neutrophils recruitment when triggered by inflammation [17, 95]. Depletion of neutrophils is associated with reduced Ly6C^{high} monocytes influx and proliferation of macrophages, therefore worsening clearance of necrotic cells and favoring the myocardium towards

more fibrosis [11]. Our data showed C3 depletion in neither circulating myeloid cells nor neutrophils, altered infarct size and cardiac function after I/R or MI injury. Nonetheless, C3 deficiency in tissue resident macrophages had no impact on cardiac recovery after I/R injury, but resulted in larger infarct size and more mortality after chronic MI surgery. One should consider that I/R induced myocardial damage in mice cause only minor ischemic and hypoperfusion area, mice with C3 deficiency do not suffer from severe infarct size and loss of function, either. Therefore, the effect of cell intrinsic C3 in this mild injury may not be visible. Further, perfusion injury could result in excessive aggregation of serum C3 in the damaged myocardium, which then abrogate the function of resident macrophage derived C3. When large-scale damage occurs in the heart, extensive cell death may amplify the response and accumulation of immune cells and complement system. In line with intracellular C3 supporting T cell survival, our data showed deficiency of intracellular generated C3 results in less macrophage number in damaged myocardium after I/R. A recent study also demonstrates that overexpression of intracellular C3 and C3aR in synovial fibroblasts (SF) [96]. C3 expression enhances glycolysis and NLRP3 inflammasome activation and induce release of IL-1β from SF. C3-C3aR axis activation propagate metabolic activity and mediate pathogenic functional change of SF during inflammatory tissue priming in recurrent arthritis. All of these support that there is complement-metabolism-inflammasome communication [96]. Therefore, impaired C3 production in resident macrophages could potentially impact on macrophage metabolism and survival, result in less removal of cell debris and more cell death in the early phase, then later impair anti-inflammatory and pro-fibrotic cytokines production, as compared to the considerate injury. Previous findings also report that macrophage depletion impairs cardiac remodeling and deteriorates heart failure, specifically tissue resident macrophages [97, 98]. The presence of tissue resident macrophages is necessary for cardiac regeneration. In addition, the interaction between macrophages and cardiac resident cells (cardiomyocytes, fibroblasts, and endothelial cells) facilitates angiogenesis and scar formation, thereby regulate cardiac remodeling [92, 99].

Serum C3 has long been recognized to be detrimental during MI and its presence correlates positively with high risk of MI occurrence [100, 101]. Previous studies

were carried out to investigate anti-C3 therapy on MI in both animal models and human. Research using CVF to deplete circulating C3 and fully C3 knock-out mice elucidated the inhibition of complement activation could reduce cell necrosis, accumulation of inflammatory cells, infarct size, and protect from compromised function in I/R injury of diverse organs as well as chronic MI [67, 102, 103]. However, an exception was depicted in Wysoczynski and colleagues' study [51]. They reported that C3 knock-out mice exacerbated myocardium hypertrophy and impaired to preserve cardiac function compared to *WT* mice. Similarly, in our findings, C3 deficiency in tissue resident macrophages worsened cardiac outcome post-MI. Therefore, we speculate that C3 may act as a double-edged sword in the way it is indispensable in the initiation of inflammation but is harmful for reparative process. However, this needs to be further investigated in future studies.

Triggered by ischemia, serum C3 is cleaved by conventional C3 convertase into several products, mainly C3a and C3b. Intrinsic generated C3 can also be processed by cathepsin L (CTSL) into functional homogenous C3a and C3b as external C3 cleavage [55]. C3b therefore binds to other complement components and forms C5 convertase, whereas both internal and external C3a mainly engage with its receptor C3aR on a wide range of cells. C3a, named by its histamine-releasing property, exert its function in many ways, including chemotaxis of leukocytes, increase of vascular permeability, modulation of T cell differentiation, and so forth [104]. C3aR is widely expressed on macrophages in various organs [59]. Similarly, we found almost all tissue macrophages express C3aR in steady state. Worth mentioning, it was undefined whether C3aR we found is expressed on the surface of macrophages or inside the cells since we were detecting on the protein level with flow cytometry. When suffering from I/R injury, C3aR reporter mice showed down-regulation of C3aR expressing on cardiac macrophages after the onset of injury for 48h. In addition, the reduction was mainly attributed to MHC II^{high} macrophages, indicating C3aR were mostly expressed by resident macrophages since macrophages in the injured heart in part developed a MHC II^{high} profile [105]. In previous studies using C3aR-deficient mice, the role of this complement receptor has not been established in full, and some data has even been inconsistent. For example, C3aR-deficient mice exhibited improved lung function in allergic disease [106], and showed reduced microglia activation and

cerebral hypoperfusion injury [107]. In contrast, C3aR played a protective role in atherosclerosis by polarizing macrophages towards reparative phenotype and regulating inflammation-related cytokine secretion [108]. Deficiency of C3aR increased neutrophil influx to ischemic tissue and worsened outcome of intestinal I/R injury [109]. Thus, there is a demanding need for cell specific C3aR deletion model to gain a better perception of the role of C3a/C3aR signaling. We utilized $Rank^{cre}$ mice and cross-mated them with *C3aR-tdT* reporter mice so that we depleted C3aR on tissue resident macrophages. The fully reduction of C3aR on tissue macrophages in $Rank^{\Delta C3aR}$ mice motivated us to perform cardiac injury on them and measure cardiac output after 30 days with in vivo PET-CT imaging. Ablation of C3aR expression on macrophages resulted in smaller infarct size and improved cardiac function, more specifically lower ESV and higher EF, but only at early phase post-MI. However, with the low end-number at day 30 in the littermate $Rank^{wt}$ group due to early death post-MI, the insignificant difference could be underestimated. Consistent with the observation of less infarct area in $Rank^{\Delta C3aR}$ mice, the survival was also more promising. However, we noticed more death in $Rank^{wt}$ (C3aR reporter) mice (8 out of 13) than in C3 reporter mice (5 out of 27), this was most likely by cause of their genotype background. As previously stated, BALB/c mice have more inflammation than C57B6J mice [110, 111]. In addition, the anatomical position of heart in these BALB/c background mice was different from C57B6J background mice, therefore resulting in probably higher ligation of LAD in C3aR reporter mice and larger ischemic area. Nonetheless, $Rank^{wt}$ (C3aR reporter) and $Rank^{\Delta C3aR}$ mice were of same background. The difference we found between these two groups would not be influenced.

Taken together with our findings in $Rank^{\Delta C3}$ mice, the presence of C3 in macrophages is indispensable for cardiac outcome post-MI. We hypothesize that intracellular C3 plays an important role in the function or survival of macrophages therefore impairs cardiac function after injury. Exogenous C3 from alternative origins may bind to cardiac macrophages potentially resulting in exaggerated inflammation that leads to myocardial rupture and early death.

In our study, we focused on functional alterations of the complement system associated with immune cells. This provides a potential target that could be rescued or exacerbated by cell specific generation of C3/C3aR. However, some limitations of our study should be taken into consideration. First, C3 cleavage C3b forms C5 convertase and thereby process C5 into active forms C5a and C5b. The deletion of C3 will not only impair the function of C3 products but also limit the generation of C5 cleavage and MAC. A previous study found reduced production of TNF but heightened secretion of IL-1β instead in LPS-treated macrophages isolated from both C5 knock-out mice and C5aR1 knock-out mice [112]. In analogy, our data of C3 deletion in tissue resident macrophages diminished the recovery of ischemic myocardium following chronic MI, which could potentially be interfered with by the reduction of C5 activation.

In conclusion, targeting macrophage C3 and C3aR may provide novel therapeutic opportunities for the treatment of MI.

Affidavit

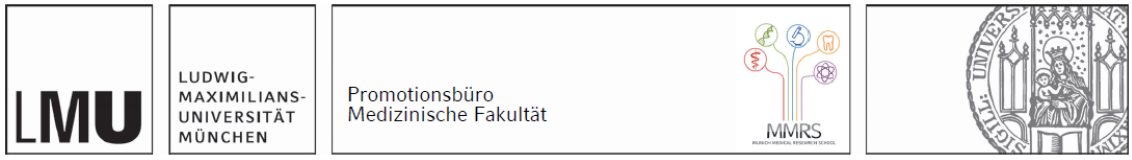

Affidavit

Liu, Lulu

Surname, first name

Marchioninistraße 68

Street

81377, Munich, Germany

Zip code, town, country

I hereby declare, that the submitted thesis entitled:

Macrophage derived complement factor C3 impacts on cardiac remodeling

is my own work. I have only used the sources indicated and have not made unauthorised use of services of a third party. Where the work of others has been quoted or reproduced, the source is always given.

I further declare that the submitted thesis or parts thereof have not been presented as part of an examination degree to any other university.

Munich, 26.07.2023	Lulu Liu
place, date	Signature doctoral candidate

Confirmation of congruency

LMU LUDWIG-MAXIMILIANS-UNIVERSITÄT MÜNCHEN | Promotionsbüro Medizinische Fakultät | MMRS

Confirmation of congruency between printed and electronic version of the doctoral thesis

Liu, Lulu

Surname, first name

Marchioninistraße 68

Street

81377, Munich, Germany

Zip code, town, country

I hereby declare, that the submitted thesis entitled:

Macrophage derived complement factor C3 impacts on cardiac remodeling

is congruent with the printed version both in content and format.

Munich, 26.07.2023

place, date

Lulu Liu

Signature doctoral candidate

References

[1] N. G. Frangogiannis, "The inflammatory response in myocardial injury, repair, and remodelling," *Nature Reviews Cardiology,* vol. 11, no. 5, pp. 255-265, 2014, doi: 10.1038/nrcardio.2014.28.

[2] M. Nahrendorf *et al.*, "The healing myocardium sequentially mobilizes two monocyte subsets with divergent and complementary functions," (in eng), *J Exp Med,* vol. 204, no. 12, pp. 3037-47, Nov 26 2007, doi: 10.1084/jem.20070885.

[3] C. Peet, A. Ivetic, D. I. Bromage, and A. M. Shah, "Cardiac monocytes and macrophages after myocardial infarction," (in eng), *Cardiovasc Res,* vol. 116, no. 6, pp. 1101-1112, May 1 2020, doi: 10.1093/cvr/cvz336.

[4] K. Thygesen, J. S. Alpert, and H. D. White, "Universal definition of myocardial infarction," (in eng), *J Am Coll Cardiol,* vol. 50, no. 22, pp. 2173-95, Nov 27 2007, doi: 10.1016/j.jacc.2007.09.011.

[5] Y. Zhang, W. Wen, and H. Liu, "The Role of Immune Cells in Cardiac Remodeling After Myocardial Infarction," (in eng), *J Cardiovasc Pharmacol,* vol. 76, no. 4, pp. 407-413, Oct 2020, doi: 10.1097/fjc.0000000000000876.

[6] I. Kologrivova, M. Shtatolkina, T. Suslova, and V. Ryabov, "Cells of the Immune System in Cardiac Remodeling: Main Players in Resolution of Inflammation and Repair After Myocardial Infarction," (in eng), *Front Immunol,* vol. 12, p. 664457, 2021, doi: 10.3389/fimmu.2021.664457.

[7] G. Savarese and L. H. Lund, "Global Public Health Burden of Heart Failure," (in eng), *Card Fail Rev,* vol. 3, no. 1, pp. 7-11, Apr 2017, doi: 10.15420/cfr.2016:25:2.

[8] S. D. Prabhu and N. G. Frangogiannis, "The Biological Basis for Cardiac Repair After Myocardial Infarction: From Inflammation to Fibrosis," (in eng), *Circ Res,* vol. 119, no. 1, pp. 91-112, Jun 24 2016, doi: 10.1161/circresaha.116.303577.

[9] N. G. Frangogiannis, "The extracellular matrix in myocardial injury, repair, and remodeling," (in eng), *J Clin Invest,* vol. 127, no. 5, pp. 1600-1612, May 1 2017, doi: 10.1172/jci87491.

[10] F. K. Swirski and M. Nahrendorf, "Cardioimmunology: the immune system in cardiac homeostasis and disease," (in eng), *Nat Rev Immunol,* vol. 18, no. 12, pp. 733-744, Dec 2018, doi: 10.1038/s41577-018-0065-8.

[11] M. Horckmans *et al.*, "Neutrophils orchestrate post-myocardial infarction healing by polarizing macrophages towards a reparative phenotype," (in eng), *Eur Heart J,* vol. 38, no. 3, pp. 187-197, Jan 14 2017, doi: 10.1093/eurheartj/ehw002.

[12] A. Bonaventura *et al.*, "Novel findings in neutrophil biology and their impact on cardiovascular disease," (in eng), *Cardiovasc Res,* vol. 115, no. 8, pp. 1266-1285, Jul 1 2019, doi: 10.1093/cvr/cvz084.

[13] I. Hilgendorf *et al.*, "Ly-6Chigh monocytes depend on Nr4a1 to balance both inflammatory and reparative phases in the infarcted myocardium," (in eng), *Circ Res,* vol. 114, no. 10, pp. 1611-22, May 9 2014, doi: 10.1161/circresaha.114.303204.

[14] C. Auffray *et al.*, "Monitoring of blood vessels and tissues by a population of monocytes with patrolling behavior," (in eng), *Science,* vol. 317, no. 5838, pp. 666-70, Aug 3 2007, doi: 10.1126/science.1142883.

[15] Z. Zhang *et al.*, "New Insights and Novel Therapeutic Potentials for Macrophages in Myocardial Infarction," (in eng), *Inflammation,* vol. 44, no. 5, pp. 1696-1712, Oct 2021, doi: 10.1007/s10753-021-01467-2.

[16] K. Jung *et al.*, "Endoscopic time-lapse imaging of immune cells in infarcted mouse hearts," (in eng), *Circ Res,* vol. 112, no. 6, pp. 891-9, Mar 15 2013, doi: 10.1161/circresaha.111.300484.

[17] W. Li *et al.*, "Heart-resident CCR2(+) macrophages promote neutrophil extravasation through TLR9/MyD88/CXCL5 signaling," (in eng), *JCI Insight,* vol. 1, no. 12, p. e87315, 2016, doi: 10.1172/jci.insight.87315.

[18] H. Shinagawa and S. Frantz, "Cellular immunity and cardiac remodeling after myocardial infarction: role of neutrophils, monocytes, and macrophages," (in eng), *Curr Heart Fail Rep,* vol. 12, no. 3, pp. 247-54, Jun 2015, doi: 10.1007/s11897-015-0255-7.

[19] C. Schulz *et al.*, "A lineage of myeloid cells independent of Myb and hematopoietic stem cells," (in eng), no. 1095-9203 (Electronic).

[20] E. G. Perdiguero and F. Geissmann, "The development and maintenance of resident macrophages," (in eng), *Nat Immunol,* vol. 17, no. 1, pp. 2-8, Jan 2016, doi: 10.1038/ni.3341.

[21] C. Stremmel *et al.*, "Yolk sac macrophage progenitors traffic to the embryo during defined stages of development," *Nat Commun,* vol. 9, no. 1, p. 75, Jan 8 2018, doi: 10.1038/s41467-017-02492-2.

[22] E. Gomez Perdiguero *et al.*, "Tissue-resident macrophages originate from yolk-sac-derived erythro-myeloid progenitors," (in eng), no. 1476-4687 (Electronic).

[23] T. Heidt *et al.*, "Differential contribution of monocytes to heart macrophages in steady-state and after myocardial infarction," (in eng), *Circ Res,* vol. 115, no. 2, pp. 284-95, Jul 7 2014, doi: 10.1161/circresaha.115.303567.

[24] T. Weinberger and C. Schulz, "Myocardial infarction: a critical role of macrophages in cardiac remodeling," (in English), Review vol. 6, no. 107, 2015-April-07 2015, doi: 10.3389/fphys.2015.00107.

[25] K. J. Lavine *et al.*, "Distinct macrophage lineages contribute to disparate patterns of cardiac recovery and remodeling in the neonatal and adult heart," (in eng), *Proc Natl Acad Sci U S A,* vol. 111, no. 45, pp. 16029-34, Nov 11 2014, doi: 10.1073/pnas.1406508111.

[26] S. A. Dick *et al.*, "Self-renewing resident cardiac macrophages limit adverse remodeling following myocardial infarction," (in eng), *Nat Immunol,* vol. 20, no. 1, pp. 29-39, Jan 2019, doi: 10.1038/s41590-018-0272-2.

[27] M. Nahrendorf and F. K. Swirski, "Monocyte and macrophage heterogeneity in the heart," (in eng), *Circ Res,* vol. 112, no. 12, pp. 1624-33, Jun 7 2013, doi: 10.1161/circresaha.113.300890.

[28] G. Bajpai *et al.*, "Tissue Resident CCR2- and CCR2+ Cardiac Macrophages Differentially Orchestrate Monocyte Recruitment and Fate Specification Following Myocardial Injury," (in eng), *Circ Res,* vol. 124, no. 2, pp. 263-278, Jan 18 2019, doi: 10.1161/circresaha.118.314028.

[29] Y. Liu *et al.*, "Complement C3 Produced by Macrophages Promotes Renal Fibrosis via IL-17A Secretion," *Front Immunol,* vol. 9, p. 2385, 2018, doi: 10.3389/fimmu.2018.02385.

[30] R. Lubbers, M. F. van Essen, C. van Kooten, and L. A. Trouw, "Production of complement components by cells of the immune system," (in eng), *Clin Exp Immunol,* vol. 188, no. 2, pp. 183-194, May 2017, doi: 10.1111/cei.12952.

[31] M. K. Liszewski, M. Elvington, H. S. Kulkarni, and J. P. Atkinson, "Complement's hidden arsenal: New insights and novel functions inside the cell," (in eng), *Mol Immunol,* vol. 84, pp. 2-9, Apr 2017, doi: 10.1016/j.molimm.2017.01.004.

[32] P. Gros, F. J. Milder, and B. J. Janssen, "Complement driven by conformational changes," (in eng), *Nat Rev Immunol,* vol. 8, no. 1, pp. 48-58, Jan 2008, doi: 10.1038/nri2231.

[33] M. Kolev and C. Kemper, "Keeping It All Going-Complement Meets Metabolism," *Front Immunol,* vol. 8, p. 1, 2017, doi: 10.3389/fimmu.2017.00001.

[34] D. Ricklin, G. Hajishengallis, K. Yang, and J. D. Lambris, "Complement: a key system for immune surveillance and homeostasis," *Nat Immunol,* vol. 11, no. 9, pp. 785-97, Sep 2010, doi: 10.1038/ni.1923.

[35] M. J. Walport, "Complement. First of two parts," (in eng), *N Engl J Med,* vol. 344, no. 14, pp. 1058-66, Apr 5 2001, doi: 10.1056/nejm200104053441406.

[36] M. W. Lo and T. M. Woodruff, "Complement: Bridging the innate and adaptive immune systems in sterile inflammation," (in eng), *J Leukoc Biol,* vol. 108, no. 1, pp. 339-351, Jul 2020, doi: 10.1002/jlb.3mir0220-270r.

[37] M. Kolev, G. Le Friec, and C. Kemper, "Complement--tapping into new sites and effector systems," *Nat Rev Immunol,* vol. 14, no. 12, pp. 811-20, Dec 2014, doi: 10.1038/nri3761.

[38] M. C. Walsh *et al.*, "Mannose-binding lectin is a regulator of inflammation that accompanies myocardial ischemia and reperfusion injury," (in eng), *J Immunol,* vol. 175, no. 1, pp. 541-6, Jul 1 2005, doi: 10.4049/jimmunol.175.1.541.

[39] A. Panagiotou, M. Trendelenburg, and M. Osthoff, "The Lectin Pathway of Complement in Myocardial Ischemia/Reperfusion Injury—Review of Its Significance and the Potential Impact of Therapeutic Interference by C1

Esterase Inhibitor," (in English), *Frontiers in Immunology,* Review vol. 9, 2018-May-25 2018, doi: 10.3389/fimmu.2018.01151.

[40] V. I. Pavlov, M. O. Skjoedt, Y. Siow Tan, A. Rosbjerg, P. Garred, and G. L. Stahl, "Endogenous and natural complement inhibitor attenuates myocardial injury and arterial thrombogenesis," (in eng), *Circulation,* vol. 126, no. 18, pp. 2227-35, Oct 30 2012, doi: 10.1161/circulationaha.112.123968.

[41] N. Chun *et al.*, "Activation of complement factor B contributes to murine and human myocardial ischemia/reperfusion injury," (in eng), *PLoS One,* vol. 12, no. 6, p. e0179450, 2017, doi: 10.1371/journal.pone.0179450.

[42] C. Farrar, E. Asgari, W. Schwaeble, and S. Sacks, "Which pathways trigger the role of complement in ischaemia/reperfusion injury?," (in English), *Frontiers in Immunology,* Review vol. 3, 2012-November-19 2012, doi: 10.3389/fimmu.2012.00341.

[43] C.-W. Vogel, "The Role of Complement in Myocardial Infarction Reperfusion Injury: An Underappreciated Therapeutic Target," (in English), *Frontiers in Cell and Developmental Biology,* Mini Review vol. 8, 2020-December-23 2020, doi: 10.3389/fcell.2020.606407.

[44] C. W. Vogel, D. C. Fritzinger, B. E. Hew, M. Thorne, and H. Bammert, "Recombinant cobra venom factor," (in eng), *Mol Immunol,* vol. 41, no. 2-3, pp. 191-9, Jun 2004, doi: 10.1016/j.molimm.2004.03.011.

[45] C.-W. Vogel and D. C. Fritzinger, "Cobra Venom Factor: The Unique Component of Cobra Venom That Activates the Complement System," Springer Netherlands, 2017, pp. 345-404.

[46] M. Ing *et al.*, "Absence of a neutralizing antibody response to humanized cobra venom factor in mice," (in eng), *Mol Immunol,* vol. 97, pp. 1-7, May 2018, doi: 10.1016/j.molimm.2018.02.018.

[47] Y. F. Mao *et al.*, "Pre-treatment with Cobra venom factor alleviates acute lung injury induced by intestinal ischemia-reperfusion in rats," (in eng), *Eur Rev Med Pharmacol Sci,* vol. 17, no. 16, pp. 2207-17, Aug 2013.

[48] C. Haihua, W. Wei, H. Kun, L. Yuanli, and L. Fei, "Cobra Venom Factor-induced complement depletion protects against lung ischemia reperfusion injury through alleviating blood-air barrier damage," (in eng), *Sci Rep,* vol. 8, no. 1, p. 10346, Jul 9 2018, doi: 10.1038/s41598-018-28724-z.

[49] W. B. Gorsuch, B. J. Guikema, D. C. Fritzinger, C. W. Vogel, and G. L. Stahl, "Humanized cobra venom factor decreases myocardial ischemia-reperfusion injury," (in eng), *Mol Immunol,* vol. 47, no. 2-3, pp. 506-10, Dec 2009, doi: 10.1016/j.molimm.2009.08.017.

[50] M. N. Busche and G. L. Stahl, "Role of the complement components C5 and C3a in a mouse model of myocardial ischemia and reperfusion injury," (in eng), *Ger Med Sci,* vol. 8, Sep 8 2010, doi: 10.3205/000109.

[51] M. Wysoczynski *et al.*, "Complement component 3 is necessary to preserve myocardium and myocardial function in chronic myocardial infarction," (in eng), *Stem Cells,* vol. 32, no. 9, pp. 2502-15, Sep 2014, doi: 10.1002/stem.1743.

[52] J. Passwell, G. F. Schreiner, M. Nonaka, H. U. Beuscher, and H. R. Colten, "Local extrahepatic expression of complement genes C3, factor B, C2, and C4 is increased in murine lupus nephritis," (in eng), *J Clin Invest,* vol. 82, no. 5, pp. 1676-84, Nov 1988, doi: 10.1172/jci113780.

[53] R. A. Houseright *et al.*, "Cell type specific gene expression profiling reveals a role for complement component C3 in neutrophil responses to tissue damage," (in eng), *Sci Rep,* vol. 10, no. 1, p. 15716, Sep 24 2020, doi: 10.1038/s41598-020-72750-9.

[54] C. Hess and C. Kemper, "Complement-Mediated Regulation of Metabolism and Basic Cellular Processes," *Immunity,* vol. 45, no. 2, pp. 240-54, Aug 16 2016, doi: 10.1016/j.immuni.2016.08.003.

[55] M. K. Liszewski *et al.*, "Intracellular Complement Activation Sustains T Cell Homeostasis and Mediates Effector Differentiation," *Immunity,* vol. 39, no. 6, pp. 1143-1157, 2013, doi: 10.1016/j.immuni.2013.10.018.

[56] G. Arbore and C. Kemper, "A novel "complement-metabolism-inflammasome axis" as a key regulator of immune cell effector function," *Eur J Immunol,* vol. 46, no. 7, pp. 1563-73, Jul 2016, doi: 10.1002/eji.201546131.

[57] M. Kolev *et al.*, "Diapedesis-Induced Integrin Signaling via LFA-1 Facilitates Tissue Immunity by Inducing Intrinsic Complement C3 Expression in Immune Cells," *Immunity,* vol. 52, no. 3, pp. 513-527.e8, 2020, doi: 10.1016/j.immuni.2020.02.006.

[58] M. D. Muzumdar, B. Tasic, K. Miyamichi, L. Li, and L. Luo, "A global double-fluorescent Cre reporter mouse," (in eng), *Genesis,* vol. 45, no. 9, pp. 593-605, Sep 2007, doi: 10.1002/dvg.20335.

[59] K. M. Quell *et al.*, "Monitoring C3aR Expression Using a Floxed tdTomato-C3aR Reporter Knock-in Mouse," *J Immunol,* vol. 199, no. 2, pp. 688-706, Jul 15 2017, doi: 10.4049/jimmunol.1700318.

[60] E. Mass *et al.*, "Specification of tissue-resident macrophages during organogenesis," (in eng), *Science,* vol. 353, no. 6304, Sep 9 2016, doi: 10.1126/science.aaf4238.

[61] N. Haider *et al.*, "Transition of Macrophages to Fibroblast-Like Cells in Healing Myocardial Infarction," (in eng), *J Am Coll Cardiol,* vol. 74, no. 25, pp. 3124-3135, Dec 24 2019, doi: 10.1016/j.jacc.2019.10.036.

[62] J. M. Adrover *et al.*, "A Neutrophil Timer Coordinates Immune Defense and Vascular Protection," (in eng), *Immunity,* vol. 50, no. 2, pp. 390-402.e10, Feb 19 2019, doi: 10.1016/j.immuni.2019.01.002.

[63] S. Elhag *et al.*, "Differences in Cell-Intrinsic Inflammatory Programs of Yolk Sac and Bone Marrow Macrophages," (in eng), *Cells,* vol. 10, no. 12, Dec 17 2021, doi: 10.3390/cells10123564.

[64] A. Orosz, B. Walzog, and A. Mócsai, "In Vivo Functions of Mouse Neutrophils Derived from HoxB8-Transduced Conditionally Immortalized Myeloid Progenitors," (in eng), *J Immunol,* vol. 206, no. 2, pp. 432-445, Jan 15 2021, doi: 10.4049/jimmunol.2000807.

[65] M. Fischer *et al.*, "Cardiac 18F-FDG Positron Emission Tomography: An Accurate Tool to Monitor In vivo Metabolic and Functional Alterations in Murine Myocardial Infarction," (in English), *Frontiers in Cardiovascular Medicine,* Original Research vol. 8, 2021-May-25 2021, doi: 10.3389/fcvm.2021.656742.

[66] H. Gu, J. D. Marth, P. C. Orban, H. Mossmann, and K. Rajewsky, "Deletion of a DNA polymerase beta gene segment in T cells using cell type-specific gene targeting," (in eng), *Science,* vol. 265, no. 5168, pp. 103-6, Jul 1 1994, doi: 10.1126/science.8016642.

[67] M. H. Crawford *et al.*, "Complement and neutrophil activation in the pathogenesis of ischemic myocardial injury," *Circulation,* vol. 78, no. 6, pp. 1449-1458, 1988, doi: doi:10.1161/01.CIR.78.6.1449.

[68] J. E. Jordan, M. C. Montalto, and G. L. Stahl, "Inhibition of mannose-binding lectin reduces postischemic myocardial reperfusion injury," (in eng), *Circulation,* vol. 104, no. 12, pp. 1413-8, Sep 18 2001, doi: 10.1161/hc3601.095578.

[69] S. B. Ong *et al.*, "Inflammation following acute myocardial infarction: Multiple players, dynamic roles, and novel therapeutic opportunities," (in eng), *Pharmacol Ther,* vol. 186, pp. 73-87, Jun 2018, doi: 10.1016/j.pharmthera.2018.01.001.

[70] G. Lemke, "How macrophages deal with death," (in eng), *Nat Rev Immunol,* vol. 19, no. 9, pp. 539-549, Sep 2019, doi: 10.1038/s41577-019-0167-y.

[71] A. R. Pinto *et al.*, "Revisiting Cardiac Cellular Composition," (in eng), *Circ Res,* vol. 118, no. 3, pp. 400-9, Feb 5 2016, doi: 10.1161/circresaha.115.307778.

[72] Y. Katz, O. Nadiv, M. J. Rapoport, and M. Loos, "IL-17 regulates gene expression and protein synthesis of the complement system, C3 and factor B, in skin fibroblasts," (in eng), *Clin Exp Immunol,* vol. 120, no. 1, pp. 22-9, Apr 2000, doi: 10.1046/j.1365-2249.2000.01199.x.

[73] B. P. Morgan and P. Gasque, "Extrahepatic complement biosynthesis: where, when and why?," (in eng), *Clin Exp Immunol,* vol. 107, no. 1, pp. 1-7, Jan 1997, doi: 10.1046/j.1365-2249.1997.d01-890.x.

[74] P. Dutta *et al.*, "Myocardial infarction accelerates atherosclerosis," (in eng), *Nature,* vol. 487, no. 7407, pp. 325-9, Jul 19 2012, doi: 10.1038/nature11260.

[75] T. Weinberger *et al.*, "Ontogeny of arterial macrophages defines their functions in homeostasis and inflammation," (in eng), *Nat Commun,* vol. 11, no. 1, p. 4549, Sep 11 2020, doi: 10.1038/s41467-020-18287-x.

[76] S. Epelman, K. J. Lavine, and G. J. Randolph, "Origin and functions of tissue macrophages," (in eng), *Immunity,* vol. 41, no. 1, pp. 21-35, Jul 17 2014, doi: 10.1016/j.immuni.2014.06.013.

[77] B. E. Clausen, C. Burkhardt, W. Reith, R. Renkawitz, and I. Förster, "Conditional gene targeting in macrophages and granulocytes using LysMcre mice," (in eng), *Transgenic Res,* vol. 8, no. 4, pp. 265-77, Aug 1999, doi: 10.1023/a:1008942828960.

[78] E. Lagasse and I. L. Weissman, "bcl-2 inhibits apoptosis of neutrophils but not their engulfment by macrophages," (in eng), *J Exp Med,* vol. 179, no. 3, pp. 1047-52, Mar 1 1994, doi: 10.1084/jem.179.3.1047.

[79] E. Passegué, E. F. Wagner, and I. L. Weissman, "JunB deficiency leads to a myeloproliferative disorder arising from hematopoietic stem cells," (in eng), *Cell,* vol. 119, no. 3, pp. 431-43, Oct 29 2004, doi: 10.1016/j.cell.2004.10.010.

[80] C. L. Abram, G. L. Roberge, Y. Hu, and C. A. Lowell, "Comparative analysis of the efficiency and specificity of myeloid-Cre deleting strains using ROSA-EYFP reporter mice," (in eng), *J Immunol Methods,* vol. 408, pp. 89-100, Jun 2014, doi: 10.1016/j.jim.2014.05.009.

[81] K. M. Quell *et al.*, "Monitoring C3aR Expression Using a Floxed tdTomato-C3aR Reporter Knock-in Mouse," (in eng), *J Immunol,* vol. 199, no. 2, pp. 688-706, Jul 15 2017, doi: 10.4049/jimmunol.1700318.

[82] S. Guglietta *et al.*, "Coagulation induced by C3aR-dependent NETosis drives protumorigenic neutrophils during small intestinal tumorigenesis," *Nature Communications,* vol. 7, no. 1, p. 11037, 2016/03/21 2016, doi: 10.1038/ncomms11037.

[83] S. E. Pischke *et al.*, "Complement factor 5 blockade reduces porcine myocardial infarction size and improves immediate cardiac function," (in eng), *Basic Res Cardiol,* vol. 112, no. 3, p. 20, May 2017, doi: 10.1007/s00395-017-0610-9.

[84] P. W. Armstrong *et al.*, "Concerning the mechanism of pexelizumab's benefit in acute myocardial infarction," (in eng), *Am Heart J,* vol. 151, no. 4, pp. 787-90, Apr 2006, doi: 10.1016/j.ahj.2005.06.008.

[85] S. Huang and N. G. Frangogiannis, "Anti-inflammatory therapies in myocardial infarction: failures, hopes and challenges," (in eng), *Br J Pharmacol,* vol. 175, no. 9, pp. 1377-1400, May 2018, doi: 10.1111/bph.14155.

[86] P. S. Heeger and C. Kemper, "Novel roles of complement in T effector cell regulation," (in eng), *Immunobiology,* vol. 217, no. 2, pp. 216-24, Feb 2012, doi: 10.1016/j.imbio.2011.06.004.

[87] N. Sándor, D. Pap, J. Prechl, A. Erdei, and Z. Bajtay, "A novel, complement-mediated way to enhance the interplay between macrophages, dendritic cells and T lymphocytes," *Molecular Immunology,* vol. 47, no. 2, pp. 438-448, 2009/12/01/ 2009, doi: https://doi.org/10.1016/j.molimm.2009.08.025.

[88] R. A. Ezekowitz, R. B. Sim, M. Hill, and S. Gordon, "Local opsonization by secreted macrophage complement components. Role of receptors for complement in uptake of zymosan," (in eng), *J Exp Med,* vol. 159, no. 1, pp. 244-60, Jan 1 1984, doi: 10.1084/jem.159.1.244.

[89] L. Baudino *et al.*, "C3 opsonization regulates endocytic handling of apoptotic cells resulting in enhanced T-cell responses to cargo-derived antigens," *Proceedings of the National Academy of Sciences,* vol. 111, no. 4, pp. 1503-1508, 2014, doi: doi:10.1073/pnas.1316877111.

[90] D. Mevorach, J. O. Mascarenhas, D. Gershov, and K. B. Elkon, "Complement-dependent clearance of apoptotic cells by human macrophages," (in eng), *J Exp Med,* vol. 188, no. 12, pp. 2313-20, Dec 21 1998, doi: 10.1084/jem.188.12.2313.

[91] H. B. Sager, T. Kessler, and H. Schunkert, "Monocytes and macrophages in cardiac injury and repair," (in eng), *J Thorac Dis,* vol. 9, no. Suppl 1, pp. S30-s35, Mar 2017, doi: 10.21037/jtd.2016.11.17.

[92] L. Honold and M. Nahrendorf, "Resident and Monocyte-Derived Macrophages in Cardiovascular Disease," (in eng), *Circ Res,* vol. 122, no. 1, pp. 113-127, Jan 5 2018, doi: 10.1161/circresaha.117.311071.

[93] J. A. Nicolás-Ávila *et al.*, "A Network of Macrophages Supports Mitochondrial Homeostasis in the Heart," (in eng), *Cell,* vol. 183, no. 1, pp. 94-109.e23, Oct 1 2020, doi: 10.1016/j.cell.2020.08.031.

[94] A. A. Patel, F. Ginhoux, and S. Yona, "Monocytes, macrophages, dendritic cells and neutrophils: an update on lifespan kinetics in health and disease," (in eng), *Immunology,* vol. 163, no. 3, pp. 250-261, Jul 2021, doi: 10.1111/imm.13320.

[95] J. F. Cailhier *et al.*, "Conditional macrophage ablation demonstrates that resident macrophages initiate acute peritoneal inflammation," (in eng), *J Immunol,* vol. 174, no. 4, pp. 2336-42, Feb 15 2005, doi: 10.4049/jimmunol.174.4.2336.

[96] J. Friščić *et al.*, "The complement system drives local inflammatory tissue priming by metabolic reprogramming of synovial fibroblasts," (in eng), *Immunity,* vol. 54, no. 5, pp. 1002-1021.e10, May 11 2021, doi: 10.1016/j.immuni.2021.03.003.

[97] A. L. Leblond *et al.*, "Systemic and Cardiac Depletion of M2 Macrophage through CSF-1R Signaling Inhibition Alters Cardiac Function Post Myocardial Infarction," (in eng), *PLoS One,* vol. 10, no. 9, p. e0137515, 2015, doi: 10.1371/journal.pone.0137515.

[98] M. J. van Amerongen, M. C. Harmsen, N. van Rooijen, A. H. Petersen, and M. J. van Luyn, "Macrophage depletion impairs wound healing and increases left ventricular remodeling after myocardial injury in mice," (in eng), *Am J Pathol,* vol. 170, no. 3, pp. 818-29, Mar 2007, doi: 10.2353/ajpath.2007.060547.

[99] P. Hitscherich and E. J. Lee, "Crosstalk Between Cardiac Cells and Macrophages Postmyocardial Infarction: Insights from In Vitro Studies," (in eng), *Tissue Eng Part B Rev,* vol. 27, no. 5, pp. 475-485, Oct 2021, doi: 10.1089/ten.TEB.2020.0198.

[100] A. Muscari *et al.*, "Association of serum C3 levels with the risk of myocardial infarction," *The American Journal of Medicine,* vol. 98, no. 4, pp. 357-364, 1995/04/01/ 1995, doi: https://doi.org/10.1016/S0002-9343(99)80314-3.

[101] A. M. Carter, U. K. Prasad, and P. J. Grant, "Complement C3 and C-reactive protein in male survivors of myocardial infarction," (in eng), *Atherosclerosis,* vol. 203, no. 2, pp. 538-43, Apr 2009, doi: 10.1016/j.atherosclerosis.2008.07.007.

[102] Z. Lin, H. Lin, W. Li, Y. Huang, and H. Dai, "Complement Component C3 Promotes Cerebral Ischemia/Reperfusion Injury Mediated by TLR2/NFκB Activation in Diabetic Mice," (in eng), *Neurochem Res,* vol. 43, no. 8, pp. 1599-1607, Aug 2018, doi: 10.1007/s11064-018-2574-z.

[103] G. M. Diepenhorst, T. M. van Gulik, and C. E. Hack, "Complement-mediated ischemia-reperfusion injury: lessons learned from animal and clinical studies," (in eng), *Ann Surg,* vol. 249, no. 6, pp. 889-99, Jun 2009, doi: 10.1097/SLA.0b013e3181a38f45.

[104] D. Ajona, S. Ortiz-Espinosa, and R. Pio, "Complement anaphylatoxins C3a and C5a: Emerging roles in cancer progression and treatment," (in eng), *Semin Cell Dev Biol,* vol. 85, pp. 153-163, Jan 2019, doi: 10.1016/j.semcdb.2017.11.023.

[105] T. Weinberger *et al.*, "Differential MHC-II expression and phagocytic functions of embryo-derived cardiac macrophages in the course of myocardial infarction in mice," (in eng), *Eur J Immunol,* vol. 51, no. 1, pp. 250-252, Jan 2021, doi: 10.1002/eji.202048560.

[106] A. A. Humbles *et al.*, "A role for the C3a anaphylatoxin receptor in the effector phase of asthma," (in eng), *Nature,* vol. 406, no. 6799, pp. 998-1001, Aug 31 2000, doi: 10.1038/35023175.

[107] L. Y. Zhang *et al.*, "Microglia exacerbate white matter injury via complement C3/C3aR pathway after hypoperfusion," (in eng), *Theranostics,* vol. 10, no. 1, pp. 74-90, 2020, doi: 10.7150/thno.35841.

[108] L. L. Wei *et al.*, "Protective Role of C3aR (C3a Anaphylatoxin Receptor) Against Atherosclerosis in Atherosclerosis-Prone Mice," (in eng), *Arterioscler Thromb Vasc Biol,* vol. 40, no. 9, pp. 2070-2083, Sep 2020, doi: 10.1161/atvbaha.120.314150.

[109] M. C. Wu *et al.*, "The receptor for complement component C3a mediates protection from intestinal ischemia-reperfusion injuries by inhibiting neutrophil mobilization," (in eng), *Proc Natl Acad Sci U S A,* vol. 110, no. 23, pp. 9439-44, Jun 4 2013, doi: 10.1073/pnas.1218815110.

[110] M. M. Gueders *et al.*, "Mouse models of asthma: a comparison between C57BL/6 and BALB/c strains regarding bronchial responsiveness, inflammation, and cytokine production," *Inflammation Research,* vol. 58, no. 12, p. 845, 2009/06/09 2009, doi: 10.1007/s00011-009-0054-2.

[111] A. B. Allam, M. von Chamier, M. B. Brown, and L. Reyes, "Immune profiling of BALB/C and C57BL/6 mice reveals a correlation between Ureaplasma parvum-Induced fetal inflammatory response syndrome-like pathology and increased placental expression of TLR2 and CD14," (in eng), *Am J Reprod Immunol,* vol. 71, no. 3, pp. 241-51, Mar 2014, doi: 10.1111/aji.12192.

[112] N. Niyonzima *et al.*, "Mitochondrial C5aR1 activity in macrophages controls IL-1β production underlying sterile inflammation," (in eng), *Sci Immunol,* vol. 6, no. 66, p. eabf2489, Dec 24 2021, doi: 10.1126/sciimmunol.abf2489.

Acknowledgement

First of all, I would like to give my sincere gratitude to Prof. Christian Schulz. I could not thank him enough for offering me this great opportunity to work in this excellent group and do research on this fascinating project. His inspiring ideas, suggestions and wisdom led me to build up the knowledge and broaden my vision for research, let me know how to be a good scientist. His continuous support helped me achieve my doctoral dissertation, let alone his patience and encouraging words whenever I had difficulties. Herein, I would like to thank him again for his invaluable supervision for these 5 years.

Next, I would like to thank my thesis advisory committee members, Prof. Andreas Dendorfer and Prof. Steffen Massberg. With their insightful input and fruitful discussions during my TAC meetings, helped me accelerate the proceeding of my project and gain improvement in many different aspects.

I would also like to express my thankfulness to our helpful and lovely colleagues, Michael Lorenz, Susanne Sauer, Dominic von den Heuvel, who not only taught me how to do research work but also gave me as much support as I need. I also really acknowledge the help from Maximilian Fisher, who indeed put a lot of effort and spent plenty of time on the analysis of PET-CT measurement. Besides, special thanks to Denise Messerer, Julia Winterhalter, Vanessa Schneider, Sara Elhag for welcoming me to the lab, helping me and supporting me both scientifically and emotionally. My deeply thanks go to my Chinese colleagues, they embraced and accompanied me to this foreign country, made my life and work much easier. It is my great pleasure to learn from them and work with all of them. I could not be any luckier to be colleagues with them and working in this amazing group.

I am also grateful for IRTG 914 program for providing so many professional workshops, seminars, retreats and so on, and Dr. Verena Kochan for her kindness and support whenever I come to her.

Moreover, I would like to express my gratitude to our Chinese Scholarship Council for providing me financial support for 4 years. Without it, I would never have the

chance to study abroad and have this unique and everlasting memory for the rest of my life.

I would like to appreciate the support from my friends. Thank Chunfang, Bing and Jincheng for their company, hearing my complaints, and encouraging me every time I was passive. Thank Han, Duan, Fangfang, Wei, Guo for always being there for me and supporting me in various ways.

Last but not least, biggest thanks to my beloved parents, who loved me unconditionally and supported me for every decision I made. I would not have made this success without them. Thank my little brother for being at home, doing what I was supposed to do when our mother was suffering from cancer. Here, I really hope she will get better and away from all the illness.

List of publications

1. Petzold T, Zhang Z, Ballesteros I, Saleh I, Polzin A, Thienel M, **Liu L**, Ul Ain Q, Ehreiser V, Weber C, Kilani B, Mertsch P, Götschke J, Cremer S, Fu W, Lorenz M, Ishikawa-Ankerhold H, Raatz E, El-Nemr S, Görlach A, Marhuenda E, Stark K, Pircher J, Stegner D, Gieger C, Schmidt-Supprian M, Gaertner F, Almendros I, Kelm M, Schulz C, Hidalgo A, Massberg S. Neutrophil "plucking" on megakaryocytes drives platelet production and boosts cardiovascular disease. Immunity. 2022 Dec 13;55(12):2285-2299.e7. doi: 10.1016/j.immuni.2022.10.001. Epub 2022 Oct 21. PMID: 36272416; PMCID: PMC9767676.

2. Elhag S, Stremmel C, Zehrer A, Plocke J, Hennel R, Keuper M, Knabe C, Winterhalter J, Gölling V, Tomas L, Weinberger T, Fischer M, **Liu L**, Wagner F, Lorenz M, Stark K, Häcker H, Schmidt-Supprian M, Völker U, Jastroch M, Lauber K, Straub T, Walzog B, Hammer E, Schulz C. Differences in Cell-Intrinsic Inflammatory Programs of Yolk Sac and Bone Marrow Macrophages. Cells. 2021 Dec 17;10(12):3564. doi: 10.3390/cells10123564. PMID: 34944072; PMCID: PMC8699930.

3. Weinberger T, Esfandyari D, Messerer D, Percin G, Schleifer C, Thaler R, **Liu L**, Stremmel C, Schneider V, Vagnozzi RJ, Schwanenkamp J, Fischer M, Busch K, Klapproth K, Ishikawa-Ankerhold H, Klösges L, Titova A, Molkentin JD, Kobayashi Y, Engelhardt S, Massberg S, Waskow C, Perdiguero EG, Schulz C. Ontogeny of arterial macrophages defines their functions in homeostasis and inflammation. Nat Commun. 2020 Sep 11;11(1):4549. doi: 10.1038/s41467-020-18287-x. PMID: 32917889; PMCID: PMC7486394.